

**FINITE ELEMENT SIMULATION OF DURELLI'S  
PHOTOELASTIC STRESS MINIMIZATION METHOD FOR SHAPE  
OPTIMIZATION**

by  
**Vu Thua Nguyen, B.E.**

**Thesis submitted to Victoria University of Technology  
in fulfilment of the requirement for the Degree of  
Master of Engineering**



**SCHOOL OF THE BUILT ENVIRONMENT  
FACULTY OF ENGINEERING AND SCIENCE  
VICTORIA UNIVERSITY OF TECHNOLOGY  
AUSTRALIA**

**1999**

FTS THESIS

620.118 NGU

30001005536968

Nguyen, Vu Thua

Finite element simulation of  
Durelli's photoelastic  
stress minimization method

## *Acknowledgements*

The study was performed at the School of the Built Environment, Faculty of Engineering and Science, Victoria University of Technology (VUT), Melbourne, Australia, under the supervision of Dr. Danh Tran, who has been a tremendous source of inspiration and guidance. The author would like to thank Dr. Tran for his tireless assistance. I am also grateful to Associate Professor Jimin He who acted as my supervisor during the six months when Dr. Tran was on a sabbatical leave in the United States of America.

I would like to express my appreciation to Victoria University of Technology for its financial support given in the form of a VUT Postgraduate Scholarship, and to the School of the Built Environment and Faculty of Engineering and Science for providing resources and equipment for the study.

The support of the School of the Built Environment staff is greatly appreciated. I would like to thank Associate Professor Michael Sek - Head of the School for his advice and encouragement. I would also like to thank Professor Geoffrey Lleonart for his time spent on reading and editing the final manuscript of the thesis. Thanks are also due to Mr. Tien Do – Computer Administrator and my postgraduate colleague David Ip for their help in the days when I learnt how to login to the network and how to search for a document using telnet.

Finally, I would like to thank my parents and my family wholeheartedly for their encouragement and full support throughout the course of my study.

*Vu Thua Nguyen*

# CERTIFICATE OF RESEARCH

This is certified that except where specific reference to other investigation is made, the work described in this thesis is the result of the candidate's own investigations.

Candidate



Vu Thua Nguyen

Principal supervisor

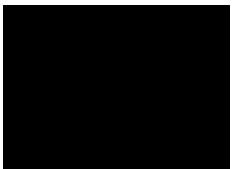


Dr. Danh Xuan Tran

## DECLARATION

This thesis contains no material which has been previously accepted for the award of any other degree or diploma in any university or institution. To the best of the author's knowledge, it contains no material previously published or written by any other person, except where due reference is made in the text.

Candidate



Vu Thua Nguyen

August 1999

## SUMMARY

The Finite Element Method (FEM) was used to simulate the Photoelastic Stress Minimization (PSM) method developed by Durelli to solve the problem of finding the optimal stress raiser profiles in isotropic and advanced composite structures. In Durelli's method, material in lowly stressed regions of the design domain is removed so as to make the sections of the discontinuity boundary become isochromatics of the same Tresca stress. The process of material removal was simulated by iterative deleting of elements lying on the stress raiser boundary, followed by smoothing and remeshing subroutines. The criterion proposed for element "removal" was to select only a number of elements having lower stresses among those that are in the design domain and on the current boundary. This number was set by a removal rate and controlled to get smaller as the optimization proceeds. The process was terminated when the stress distribution on the boundary became uniform or the number of elements to be removed reached the predefined minimum value.

It was shown that the proposed FEM simulation could be applied to solve various stress minimization problems involving isotropic materials. Investigations of the effects of parameters controlling the optimization process on the convergence and the final results were carried out. By taking into account the existence of isotropic points of zero stress, which could lead to the divergence from the optimal profile, the proposed FEM simulation proved to be capable of handling more general classes of stress minimization problems.

The FEM simulation was further extended to search for optimal stress raiser profiles for structures made of advanced composite materials.

# CONTENTS

	<b>Page</b>
<b>Summary</b>	iv
<b>Contents</b>	v
<b>Notations</b>	ix
<b>List of figures</b>	xii
<b>Chapter 1 Introduction</b>	1
1.1 Introduction	1
1.2 Aims	2
1.3 Research approach	3
1.4 Thesis outlines	4
<b>Chapter 2 Literature review</b>	6
2.1 Introduction to structural optimization	6
2.2 Literature review in shape optimization	8
2.2.1 Mathematical programming methods	10
2.2.2 Calculus of variations and optimality criteria methods	10
2.2.3 Pattern transformation methods	13
2.2.4 Methods coupled with the boundary element method	13
2.2.5 Biological growth methods	14
2.2.6 Solid-Empty element methods	16
2.2.7 The homogenization method	17

2.2.8 The photoelasticity stress minimization method and its simulation	18
2.2.9 Shape optimization of cutouts in composite laminates	19
2.3 Recent development of FEM simulation of PSM	22
<b>Chapter 3 Finite element simulation</b>	<b>26</b>
3.1 Introduction	26
3.2 FEM simulation of PSM with boundary smoothing and remeshing subroutines	26
3.2.1 Boundary smoothing	30
3.2.2 FEM mesh generation	32
3.2.3 Design of the FEM model	34
3.2.4 FEM simulation algorithm	39
3.2.4.1 Main features of the algorithm	39
3.2.4.2 Definition of parameters used in the flowchart	42
3.2.4.3 Flow of the algorithm	45
3.3. Case study - a plate with a hole under biaxial tensions	49
3.3.1 Description of the structure	50
3.3.2 Optimal hole profile when $S_r = 1.5$	52
3.3.3 Effects of the minimum number of elements removed at the fine tuning stage [ $\min \{nmin(K)\}$ ]	57
3.3.4 Effects of element size ( <i>esize</i> ) on the optimal solution	58
3.3.5 Effects of the initially set element removal rate [ <i>remrate(0)</i> ] on the optimal solution	59
3.3.6 Effects of stress ratio ( $S_r$ ) on the optimal solution	60
3.4. Concluding remarks	62



<b>Chapter 6 Conclusions and recommendations for future works</b>	113
6.2 Conclusions	113
6.3 Recommendations for future works	116
<b>References</b>	118
<b>Appendix A</b>	138
<b>Appendix B</b>	141

## NOTATIONS

$\sigma_1, \sigma_2$	stress components in the 1-2 reference axes
$\nu_{12}$	Poisson ratio in plane 1-2
$\tau_{12}$	the shear component in plane 1-2
$(\tau_{12})_{\text{ult}}$	the ultimate in-plane shear strength (in plane 1-2)
$\sigma_{\text{max}}$	the maximum equivalent or Tresca stress occurring on the hole boundary
$\sigma_{\text{mean}}$	the mean value of equivalent or Tresca stress distribution occurring on the hole boundary
$\sigma_{\text{min}}$	the minimum equivalent or Tresca stress occurring on the hole boundary
$\sigma_x$	applied stress along X-axis
$\sigma_y$	applied tensile stress along Y-axis
$(\sigma_1^T)_{\text{ult}}$	the ultimate longitudinal tensile strength (direction 1)
$(\sigma_1^C)_{\text{ult}}$	the ultimate longitudinal compressive strength (direction 1)
$(\sigma_2^T)_{\text{ult}}$	the ultimate transverse tensile strength (direction 2)
$(\sigma_2^C)_{\text{ult}}$	the ultimate transverse compressive strength (direction 2)
$\theta$	angular coordinate
$\sigma$	applied tensile stress
CAO	Computer-Aided shape Optimization
CPU	Central Processing Unit
D	hole diameter

$D_i$	the distance from $P_k$ to the $i^{\text{th}}$ node lying on the boundary (Figure A.1)
ESO	Evolutionary Structural Optimization
$E_1$	longitudinal Young's modulus
$E_2$	transverse Young's modulus
<i>esize</i>	the smallest element size used to mesh the area along the boundary, distance from $P_k$ to $Q_k$ (Figure 3.5)
<i>Ext_elem</i>	the set of external elements currently lying on the stress raiser boundary within the design domain.
FEM	Finite Element Method
<i>finetune</i>	a flag indicating the status of the cutting stage of the process
$G_{12}$	shear modulus
$i, j, k$	indices
$I, J, K$	loop indices
$k_{\text{biax}}$	stress concentration factor under biaxial stress state
$K_{\text{tg}}$	stress concentration factor based on the gross cross section
$K_{\text{tn}}$	stress concentration factor based on the minimum net cross section
$L$	plate length
$m_r$	the ratio of the accumulative removed area to the original hole area
$N$	the number of nodes lying on the the $k^{\text{th}}$ section of the boundary
<i>n_ext_elem</i>	the total number of elements of the set <i>Ext_elem</i>
<i>n_ext_elem(J)</i>	the number of external elements lying on the stress raiser boundary, counted at the $J^{\text{th}}$ iteration.
NE	the number of elements to be reduced in each step of the $K$ loop
<i>nmin(K)</i>	the number of elements removed at the $K^{\text{th}}$ step of the $K$ loop
<i>nrem</i>	the number of selected elements that have lower equivalent or Tresca

stresses (isotropic material), or Tsai-Wu indices (advanced composite material) among elements of the set *Ext\_elem*

PSM	Photoelastic Stress Minimization method
$P_k$	the $k^{\text{th}}$ primary control point (Figures 3.5, A.1)
$Q_k, R_k$	the $k^{\text{th}}$ secondary control points (Figure 3.5)
<i>remrate(I)</i>	the element removal rate at the $I^{\text{th}}$ step of the <i>I</i> loop
SEPC	the structural percentage error in energy norm
SKO	Soft Kill Option
$S_r$	applied stress ratio, $S_r = \sigma_y/\sigma_x$
STDV	standard deviation
T	plate thickness
$T_b$	distance from $P_k$ to $R_k$ (Figure 3.5)
TF	tuning factor
W	plate width
$X_i, Y_i$	Cartesian coordinates of the $i^{\text{th}}$ node lying on the boundary
$X_{P_k}, Y_{P_k}$	Cartesian coordinates of $P_k$

## LIST OF FIGURES

	<b>Page</b>
Figure 2.1: Flowchart of a simple FEM simulation	23
Figure 3.1: Finest cuts by PSM and FEM simulation	29
Figure 3.2: Primary control points on the boundary	31
Figure 3.3a: Boundaries after removing 16 elements and after being smoothed	33
Figure 3.3b: Boundaries after removing 1, 3 elements and after being smoothed.	33
Figure 3.4: The design element concept (Braibant and Fleury 1985)	35
Figure 3.5: Design of the FEM model	36
Figure 3.6a: Meshing boundary with triangular shape elements	37
Figure 3.6b: Boundaries after removing 1 element with different possibilities and after being smoothed.	37
Figure 3.7: a typical quarter FEM model of a square plate containing a circular hole	38
Figure 3.8: Flowchart of the FEM simulation	41
Figure 3.9: Description of the problem	51
Figure 3.10: The FEM model	52
Figure 3.11: Initial Tresca stress distribution in the plate, $S_r = 1.5$	53
Figure 3.12: Tresca stress distribution in the plate at iteration 41(optimal), $S_r = 1.5$	54
Figure 3.13: Hole shapes at iteration 0 (initial), 10, 20, and 41 (optimal), $S_r = 1.5$	55

Figure 3.14: Tresca stress distribution along the hole boundary at iteration 0 (initial), 41 (optimal) and theoretical optimal stress distribution, $S_r = 1.5$ .	55
Figure 3.15: Optimization history, $S_r = 1.5$	56
Figure 3.16: Effects of stress ratio, $S_r = 1.5$	61
Figure 3.17: Effects of stress ratio, $S_r = 2.0$	61
Figure 3.18: Effects of stress ratio, $S_r = 2.5$	62
Figure 4.1: Initial Tresca stress distribution, $S_r = -1$	66
Figure 4.2a: Tresca stress distribution in the plate at iteration 38, $S_r = -1$	68
Figure 4.2b: Stress distribution along the hole boundary versus angular position at iteration 38, $S_r = -1$	68
Figure 4.3: Flowchart of the improved FEM simulation algorithm	71
Figure 4.4: Tresca stress distribution at iteration 42 (optimal), $S_r = -1$ .	72
Figure 4.5: Hole shapes at iterations 0(initial), 10, 20 and 42 (optimal), $S_r = -1$	73
Figure 4.6: Optimization history, $S_r = -1$	73
Figure 4.7: Optimal hole profile, $S_r = -1.5$	75
Figure 4.8: Optimal hole profile, $S_r = -2.0$	75
Figure 4.9: Various optimal hole profiles with different negative stress ratios, where $D$ is the diameter of the initial circular hole	76
Figure 4.10: Problem description	77
Figure 4.11: $K_{tg}$ and $K_{tn}$ versus $D/W$	78
Figure 4.12: FEM model ( $D/W=0.837$ )	79
Figure 4.13: Initial Tresca stress distribution in the plate ( $D/W = 0.837$ )	80
Figure 4.14: Hole shapes at iterations 0(initial), 10, 20, 30, 47 (optimal) ( $D/W = 0.837$ )	81
Figure 4.15: Optimization history ( $D/W = 0.837$ )	82

Figure 4.16: Optimal hole profile, case $D/W = 0.140$	84
Figure 4.17: Optimal hole profile, case $D/W = 0.250$	84
Figure 4.18: Optimal hole profile, case $D/W = 0.377$	85
Figure 4.19: Optimal hole profile, case $D/W = 0.518$	85
Figure 4.20: Optimal hole profile, case $D/W = 0.650$	86
Figure 4.21: Optimal hole profile, case $D/W = 0.775$	86
Figure 4.22: Optimal hole profile, case $D/W = 0.837$	87
Figure 4.23: Variation of $K_{tn}$ versus $D/W$ for circular hole and optimal hole profile	87
Figure 4.24: Variation of $K_{tn}$ versus $D/W$ for circular hole and optimal hole profile	88
Figure 5.1: A laminate formed by four unidirectional plies	92
Figure 5.2: Flowchart of the FEM simulation algorithm for laminated composite plates	96
Figure 5.3: Stacking sequence of the laminate $[0^0, \pm 45^0, 90^0]_s$	98
Figure 5.4: Description of the problem	99
Figure 5.5: The FEM model	99
Figure 5.6: Tsai-Wu index distribution at iteration 0 (initial), $S_r = 1.5$	101
Figure 5.7: Tsai-Wu index distribution at iteration 45 (optimal), $S_r = 1.5$	102
Figure 5.8: Tsai-Wu index distribution along the profile versus angular positions at iteration 0 (initial) and iteration 45 (optimal), $S_r = 1.5$	102
Figure 5.9: Hole shapes at iterations 0(initial), 15, 30 and 45 (optimal), $S_r = 1.5$	103
Figure 5.10: Optimization history, $S_r = 1.5$	104
Figure 5.11: Tsai-Wu index distribution at iteration 74 (optimal), $S_r = 2.0$	105
Figure 5.12: Tsai-Wu index distribution at iteration 97 (optimal), $S_r = 2.5$	105

Figure 5.13: Tsai-Wu index distribution at iteration 0 (initial), $S_r = -1$	107
Figure 5.14: Tsai-Wu index distribution at iteration 71 (optimal), $S_r = -1$	108
Figure 5.15: Tsai-Wu index distribution along the profile versus angular positions at iteration 0 (initial) and iteration 71 (optimal), $S_r = -1$	108
Figure 5.16: Hole profiles at iterations 0(initial), 20, 40, 60 and 71 (optimal), $S_r = -1$	109
Figure 5.17: Optimization history, $S_r = -1$	110
Figure 5.18: Tsai-Wu index distribution at iteration 119 (optimal), $S_r = -1.5$	111
Figure 5.19: Tsai-Wu index distribution at iteration 140 (optimal), $S_r = -2.0$	111
Figure A.1: Diagram of minimization of $\sum_{i=1}^N D_i^2$	138
Figure B.1a: FEM mesh produced by the optimization program	144
Figure B.1b: FEM mesh after mesh refinement	144
Figure B.2a: Optimal Tresca stress distribution before mesh refinement	145
Figure B.2b: Optimal Tresca stress distribution after mesh refinement	145
Figure B.3a: FEM mesh produced by the optimization program	146
Figure B.3b: FEM mesh after mesh refinement	146
Figure B.4a: Optimal Tresca stress distribution before mesh refinement	147
Figure B.4b: Optimal Tresca stress distribution after mesh refinement	147
Figure B.5a: FEM mesh produced by the optimization program	148
Figure B.5b: FEM mesh after mesh refinement	148
Figure B.6a: Optimal Tsai-Wu index distribution before mesh refinement	149
Figure B.6b: Optimal Tsai-Wu index distribution after mesh refinement	149

# *Chapter 1*

## **INTRODUCTION**

### **1.1 Introduction**

Failures in mechanical parts most frequently occur at discontinuities such as holes, fillets, grooves, and notches. These features disturb stress distributions, often creating high stress concentrations, which ultimately promote failure, Durelli and Rajaiah (1981). Minimizing stress concentrations occurring at discontinuities in a structure therefore increases the strength and life of the structure under comparable working conditions.

For minimization of the stress concentration effect, one can either add or remove materials. For instance, material can be added to reinforce hole edges to maintain the strength of the structure. On the other hand, the geometry of stress raisers can be improved to reduce stress concentrations by changing their shapes. In the second approach, an elegant method has long been developed by photoelasticians, notably Heywood (1969), Durelli *et al.*

(1968, 1978, 1979, and 1981).

Durelli's Photoelasticity Stress Minimization method (PSM) is an experimental technique that focuses on a systematic procedure to achieve optimized shapes of components or structures. By gradually removing material from the lowly stressed regions, the geometry of stress raisers converges toward the optimum. As a result, the optimized structure will be lighter and have less stress concentration under the specified loading conditions.

Shape optimization by PSM requires a model of the structure. The model is usually made of transparent polymeric materials. Tresca stress distribution is determined by observing its contours or isochromatic fringes through a polariscope. However, PSM is practically restricted to the Tresca criterion involving plane stress problems with simple geometry, loading and restraints.

This study explores an effective simulation procedure of Durelli's PSM by the finite element method (FEM) so that it can be applied to structures of more complicated geometry, boundary conditions, and/or of more complex material properties. The investigation has shown that the FEM simulation can be applied to a wide range of stress concentration problems including structures made of laminated composite materials.

## **1.2 Aims**

The aim of this study is to develop an effective algorithm based on FEM to simulate Durelli's PSM to search for optimal shapes of stress raiser profiles in structures made of homogeneous isotropic and advanced composite materials.

### **1.3 Research approach**

The algorithm can be effected by existing commercial finite element analysis software to perform optimization tasks. Specifically, the following approach will be taken:

- Firstly, the PSM procedure will be examined and an equivalent simulation algorithm based on FEM developed. The optimization procedure by FEM simulation is controlled by a number of parameters. It is proposed to study the effects of these parameters on the convergence to the optimal shapes.
- Secondly, the effects of different external loading conditions on the optimal profiles will be investigated.
- Finally, the proposed FEM simulation procedure will be extended to search for optimal stress raiser profiles in structures made of composite materials.

ANSYS 5.3 finite element software developed by ANSYS, Inc. is employed throughout the study. Programs are written using the parametric design language, which is available in ANSYS 5.3. In this study, all programs were run within the ANSYS environment. All errors occurring during the optimization process could be monitored and reported.

Computer facilities used include DEC ALPHA 200/233 (Unix base) and Pentium II-350 (Windows NT service pack 3, 128 Megabyte physical memory) workstations. All the reported running times are based on the Pentium II-350 (Windows NT) workstation for

consistency.

All investigations performed were under static boundary conditions. It was assumed that all materials behaved linearly and elastically during the optimization processes.

#### **1.4 Thesis outlines**

The thesis consists of six chapters, a list of references and appendices.

- Chapter 1 introduces the significance, aims and scope of the study. The content presented in each chapter is summarized in the thesis outlines section (Section 1.4).
- Chapter 2 provides a literature review on shape optimization, with an emphasis on boundary shape optimization and stress minimization problems including shape optimization in advanced composite material structures.
- Chapter 3 presents the algorithm developed to simulate the characteristics of PSM. A large plate with a hole made of homogeneous isotropic materials under the biaxial tensile stress is optimized. The results are then compared with established solutions to validate the feasibility of the proposed algorithm.

The FEM simulation employs a number of parameters to control the optimization process. The effects of these control parameters on the speed of convergence and final results are also investigated. A homogeneous isotropic plate containing an initial central circular hole under biaxial tensile stress is optimized with different set values

of control parameters to study these effects.

- Chapter 4 presents various optimal stress raiser profiles containing isotropic points of zero stress. They represent the optimal solutions that result in profiles having sections under compression and tension. These characteristics are commonly found in general and technically interesting problems. Two typical examples are given: (i) a large plate with a hole in structures made of homogeneous isotropic materials under various biaxial tensile-compressive stress ratios; (ii) a finite width plate with initial circular holes of different diameters under uniaxial tensile stress.
- Chapter 5 presents the application of FEM simulation in optimizing a quasi-isotropic carbon-epoxy laminated composite plate  $[0^0/\pm 45^0/90^0]_s$ , containing an initial central circular hole under various biaxial stress states employing the Tsai-Wu criterion and the first ply failure theory.
- Chapter 6 summarizes the findings of the study. Some recommendations for future works are also given.
- A list of references and appendices. Appendix A presents the analytical solution for determining a control point such that the sum of squares of the distances from it to a given set of nodes is minimized. Appendix B provides the checks of some of the optima with finer meshes: cases  $S_r$  of 1.5, -1 for isotropic material; and  $S_r$  of 1.5 for composite material.

## ***Chapter 2***

### **LITERATURE REVIEW**

#### **2.1 Introduction**

Structural optimization aims to reduce weight or to improve the performance of structures while satisfying certain requirements. Although the early development of mathematical optimization began after the introduction of calculus by Newton and Leibniz during the latter part of the seventeenth century, Venkayya (1993a), the first analytical work in structural optimization was by Maxwell in 1869, followed by a well known work of Michell (1904).

Structural optimization has now become a broad multidisciplinary field, which finds applications in aeronautical, civil, mechanical, nuclear and off-shore engineering, as well as in space technology. Reviews on the structural optimization field can be found in Venkayya (1978, 1993a), Vanderplaats (1982), Olhoff and Taylor (1983), Topping (1983), Haftka and Grandhi (1986), Ding (1986), Rozvany *et al.* (1995), and Seireg and

Rodriguez (1997). Structural optimization problems are commonly classified into three important classes: sizing optimization, topology optimization and shape optimization problems:

- **Sizing optimization problems**

In sizing optimization problems, the geometry (nodal coordinates) and topology (member connectivities) of structures are kept unchanged during the course of optimization. Sizing design variables may include cross-sectional areas, moments of inertia, plate/shell element thickness. They may include material properties such as Young's modulus and/or Poisson's ratio as in the optimization of composite structures.

- **Topology optimization problems**

Topology optimization is an optimization problem in which the pattern of element connectivity to nodes is to be determined. Topology optimization of skeletal structures seeks the number and spatial sequence of elements, joints and supports. During topology optimization elements can be removed from the structure and hence parameters which describe the presence or absence of each element, can be design variables. When nodal positions are allowed to change, the nodal coordinates are also design variables. Topology optimization of continuum structures involves creation of internal holes.

- **Shape optimization problems**

The term *shape optimization* is often used in a narrow sense to refer only to the optimum design of the shape of the boundary of two and three-dimensional structural components. It is proposed in this study to use the term *boundary shape optimization* to identify such problems. Design variables in boundary shape optimization problems can be nodal co-ordinates related to the finite element model and may also include sizing variables.

However, in a broad sense the term *shape optimization*, Haftka and Gürdal (1992), or *generalized shape optimization*, Rozvany *et al.* (1995), is used for any problem where the positions of nodes of the finite element model or the patterns of element connectivity to nodes need to be changed. Thus, the broad usage of shape optimization includes also topology optimization and geometrical optimization of skeletal structures (frames and trusses) where member sizes and joint locations are design variables.

The study described in this thesis is related to shape optimization involving both isotropic and laminated fibrous composite materials. Consequently, a review on solutions for shape optimization including isotropic and advanced composite materials is given in the next section.

## **2.2 Literature review in shape optimization**

Boundary shape optimization problems are more complex than sizing optimization problems since the shapes are continuously changing in the design process

resulting in a number of problems.

The first problem is mesh distortion. As the shape of the structure changes, the finite element model is continuously changed. Highly distorted finite element meshes will result in the loss of the accuracy in stress and sensitivity derivative calculations. It is therefore difficult to ensure that the accuracy of the finite element analysis remains adequate throughout the optimization process. This problem can be alleviated by a proper selection of design variables, suitable boundary representation using the design element concept and by employing the automatic mesh generator with adapted mesh refinement capabilities, Haftka and Grandhi (1986) and Ding (1986).

Another problem is the existence or creation of internal boundaries or holes. In many problems the optimal design will have internal cavities. According to Haftka and Gürdal (1992), it is impossible to generate these cavities with a standard optimization approach without prior knowledge of their existence. One approach to deal with this problem is to assume that the material is not homogeneous, but has a microstructure with microcavities in the material, Haftka and Gürdal (1992) and Rozvany *et al.* (1995). Some methods were proposed to avoid remeshing problems and to allow internal cavities as outlined in sections 2.2.6 and 2.2.7.

The methods used for solving shape optimization problems range from the calculus of variations to the simulation of structural forms found in nature or experimental techniques. The main approaches to shape optimization problems can be summarized as follows.

### **2.2.1 Mathematical programming methods**

Mathematical programming offers a general tool for solving structural optimization problems. Many shape optimization techniques were based on employing mathematical programming methods coupled with the finite element method, Haftka and Grandhi (1986), and Ding (1986). They include linear programming, penalty function method, feasible direction method, sequential linear programming and sequential non-linear approximate optimization, Vanderplaats (1993). These methods require calculation of derivatives of the objective and constraint functions with respect to all design variables. This is referred to as sensitivity analysis, Arora and Haug (1979) and Adelman and Haftka (1986). Repeated finite element analyses are often performed to carry out sensitivity analysis, which is very costly for large problems. Many approximation methods and techniques have been developed and employed to improve the efficiency of the sensitivity analysis and optimization algorithms, Kamat (1993), Rozvany *et al.* (1995).

### **2.2.2 Calculus of variations and optimality criteria methods**

One dimensional shape optimization problems are often solved by the calculus of variations. For example, Curtis and Walpole (1982) maximized torsional rigidity of axisymmetrical hollow shafts. Plant and Olhoff (1983) used the calculus of variations to obtain the optimal forms of shallow arches for vibration and stability requirements.

While the classical methods used in structural optimization such as differential calculus or calculus of variations provide analytical solutions, optimality criteria methods can be considered as numerical methods that mimic the classical solution process. These

methods can be very efficient when the number of constraints is small compared to the number of design variables, Fleury (1980) and Haftka and Gürdal (1992).

Optimality criteria methods consist of two complementary ingredients. The first is the stipulation of the optimality criteria, which can be intuitive or rigorous. The second ingredient is the algorithm used to reshape the structure so that the optimality criterion is satisfied. A robust mathematical algorithm may be used to achieve satisfaction of the optimality criterion, whereas an ad-hoc method may be adopted where optimality criteria cannot be derived mathematically. The division into intuitive and rigorous methods is usually made on the basis of the chosen optimality criterion rather than of the reshaping algorithm. Typical applications and developments of optimality criteria methods can be found in Venkayya (1978, 1993b), Khot (1981), Berke and Khot (1988), Haftka and Gürdal (1992) and Rozvany *et al.* (1995).

The intuitive hypothesis may assume that uniform strain energy density in a structure is an optimality criterion. In problems of boundary shape optimization, one may stipulate that the best shape is the one that gives rise to stress or strain energy density of constant magnitude over the sections of the boundary. Baud (1934) investigated 'Fillet Profiles for Constant Stress' by means of photoelasticity techniques. He concluded 'The most economical contour from the material and stress point of view is one in which the stress is constant for the entire contour, and is equal to the average stress across the section'. Durelli and Murray (1943) studied the stress distribution around an elliptical discontinuity, of which the major axis was twice the length of the minor axis, under various biaxial stress ratios by means of photoelasticity and brittle coatings. They found that when the applied stress in the direction of the major axis was twice that of the other

applied stress, the stress distribution around the elliptical hole boundary became uniform and the stress concentration factor was minimized. They also reviewed and expanded the theoretical work of Inglis (1913) to confirm these results. Weck and Steinke (1983-1984) assumed that a uniform tangential stress was the optimality condition for boundary shape optimization problems.

A rigorous optimality criterion can be derived mathematically, for instance, to satisfy Kuhn-Tucker conditions, Haftka and Gürdal (1992). Dems and Mroz (1978) and Dems (1980) used the principle of virtual work and a boundary perturbation analysis to derive optimality criteria for attaining a minimum of mean elastic compliance. The optimal design was obtained by iteratively solving the optimality conditions using a finite element representation of the equations.

Banichuk (1976) formulated the problem of selecting the optimum shape of a cross-section for a shaft to maximise its torsional stiffness with a given amount of material. The problem was solved analytically. Banichuk (1989) employed classical tools and derived many rigorous optimality conditions for shape optimization problems in a planar solid.

Richards and Bjorkman (1980, 1982) demonstrated that it is possible to leave the geometry of an opening unspecified and invert the standard problem in elasticity to solve analytically for shapes which achieve an optimum design condition – the harmonic field condition - on the final stress state. The strategy was applied to determine the optimum shape for the extreme case of a rigid inclusion in a biaxial field, and to the problem of reinforced holes to determine optimum liner shape and stiffness properties.

Dhir (1981, 1983) used a procedure based on first developing analytical boundary stress expression as functions of the hole geometry, plate material, amount of reinforcement and specified load. The integral of the square of the stress around the opening boundary was assumed to be a reasonable objective function and was minimized analytically. He concluded that a uniform tangential stress along the opening boundary would lead to the minimum stress concentration.

### **2.2.3 Pattern transformation methods**

The pattern transformation method, Oda and Yamazaki (1977, 1979), Oda (1977) is a technique that transforms the shape of the boundary based on the stress ratio in the boundary finite elements. In the first step, the stress ratio in the boundary finite elements is calculated. In the second step, the size of the boundary elements is scaled up or down based on the stress ratio. Umetani and Hirai (1978) used the same stress ratio approach, whereas Hemada (1980) employed the strain energy ratio approach to obtain the optimal shape.

### **2.2.4 Methods coupled with the boundary element method**

Because the boundary element method requires only discretizing the boundary, it seems to be ideally suited for boundary shape optimization. In dealing with FEM, besides the difficulties involved in sensitivity derivatives stemming from inaccurate boundary representation, it is necessary to refine and regenerate the mesh in order to ensure the accuracy of the analysis in the course of changing the boundary of the structure. Soares *et al.* (1984) obtained the optimal shapes of shafts using the boundary element method. They discretized only the boundary of the structure and the optimization problem was solved by

Pshenichny's linearization method.

Tada *et al.* (1991) exploited the fact that a structure optimized for a given set of loading is not optimal for other sets. They then proposed a shape determination method by boundary element method for structures under uncertain loads. The authors also made the assumption that the optimal shape would be obtained when values of the strain energy densities are uniform on every boundary element.

However, optimization techniques coupled with the boundary element method are still not as reliable as FEM, especially when modeling structures made of complex property materials such as those of composite materials.

### **2.2.5 Biological growth methods**

Biological growth structures such as bones and trees, which change their own shape by growth and atrophy to adapt to external loads for reducing stress peaks, provide a natural and simple example for shape optimization.

Mattheck and Burkhardt (1990) developed a Computer-Aided shape Optimization (CAO) algorithm by simulating tree growth to optimize mechanical engineering structures. The method was based on the assumption that in all structures considered, a state of constant stress at the surface of the biological 'component' was always given for the natural loading case applied. This technique is therefore equivalent to a procedure in which material is added at overloaded places in the structure and is not added (or even removed) at places with stresses below the reference stress until the optimal shape obtained.

Baumgartner *et al.* (1992) proposed an optimization algorithm called Soft Kill Option (SKO) to find optimal structural topology based on simulation of adaptive bone mineralization by varying the Young's modulus according to a calculated stress distribution. The optimal topology obtained then can be used to generate a new finite element model for a subsequent shape optimization with CAO to smooth the contours and to reduce remaining stress concentration as described by Mattheck and Burkhardt (1990).

Chen and Tsai (1993) extended simulated biological growth approaches with a fictitious temperature loading to minimize stress concentration subjected to area constraint or to minimize area (weight) subjected to stress constraint.

Tekkaya and Güneri (1996) noted that the application of the biological growth method was based on a heuristic approach and studied systematically the effects of parameters, which control the optimization process, on the optimization procedure when minimizing stress concentration of a square plate containing initial circular hole under biaxial tensions.

Recently, Le Riche and Cailletaud (1998) proposed a mixed evolutionary/heuristic approach to solve shape optimization problems. Biological growth was considered an efficient heuristic for improving designs by reducing stresses in localized regions, but might not yield global optimal shapes. Evolutionary or genetic algorithms, Hajela (1990), Jenkins (1991), Rajeev and Krishnamoorthy (1992), on the other hand can handle non-convex problems and search for the global optimum but their computation cost may be high when dealing with large problems. Thus, a mix of evolutionary search and biological growth was expected to achieve a reliable, global optimization at a low computational

cost. The results were in good agreement with the expectation of Le Riche and Cailletaud.

### **2.2.6 Solid-Empty element methods**

One possibility for overcoming difficulties arising from the changing of the shape description, remeshing and creation of cavities, is to rely on the entire finite element mesh chosen for the initial design domain. The shape of the structure is obtained by an element removal procedure (i.e. material is removed from structures) based on appropriate criteria for element removal. Thus, the term “Solid-Empty element” used here, indicates solid stages where elements are retained, and empty stages where elements are removed. Maier (1973) proposed a ‘zero-one programming’ to try the idea of element removal. Rodriguez-Velazquez and Seireg (1985), Seireg and Rodriguez (1997) applied this technique and found optimal designs for various mechanical elements and structures.

Atrek (1989) introduced a program -SHAPE- for shape optimization of continuum structures. The program can find optimal shapes of solid, shell or plane-stress systems for multiple load cases, with multiple constraints such as stress, displacement, and stiffness. A linear maximization sub-problem, employing Lagrange multipliers has to be solved to identify the optimal locations for removing elements.

Xie and Steven (1993), (1994), (1997) proposed a simple approach for shape and layout optimization, called Evolutionary Structural Optimization (ESO). The original idea of ESO stated that an optimal shape of a structure could be obtained by systematically removing lowly stressed elements from the structure. The method has been extended for frequency optimization problems and finding optimal shapes of cutouts in composite panels. The final design by ESO however requires a post processing tool to extract the

structure from the final model and to smooth the boundary, employing conventional boundary shape optimization methods, Hinton and Sienz (1995).

### **2.2.7 The homogenization method**

An important shape optimization method is the homogenization method proposed by Bendsøe and Kikuchi (1988). In this approach a structure is represented by a model of finite elements containing microvoids i.e. a micro rectangular hole is included in each element. By changing the sizes of the rectangular hole, the element can become a complete void or solid, as well as a generalized porous medium. The hole's orientation is also an important aspect. Thus, the sizes and orientation of the microscale rectangular holes are design variables, which characterize the porosity of the porous medium. The objective is to minimize the mean compliance of the structure subjected to equilibrium equations and a volume constraint. An optimality criteria method is used to derive the optimal porosity of such a porous medium. The problem then can be considered as an optimal distribution of material. Many successful applications based on this method can be found in Bendsøe and Kikuchi (1988), Suzuki and Kikuchi (1993), Bendsøe (1995), Jiang and Papalambros (1996) and Thierauf (1996).

Generally, homogenization-based strategies for topology optimization (including shape optimization) avoid problems of boundary descriptions and remeshing. However, there are limitations specific to homogenization: when a non-porous material is used, it is necessary to post-process the result of the optimization in order to remove intermediate porosities. Finally, certain boundary conditions such as pressure cannot be imposed when homogenization is used, Le Riche and Cailletaud (1998).

### **2.2.8 The photoelasticity stress minimization method and its simulation**

In the design of plate and shells, minimization of stress concentration due to the presence of holes and/or other discontinuities such as fillets, grooves, notches, is an important task. Some photoelasticians have attempted to optimize the shape discontinuities experimentally.

Shape optimization by PSM requires a two-dimensional model of the structure. The model is usually made of transparent polymeric materials, Durelli (1968) and Heywood (1969). Tresca stress distribution is determined by observing its contours or isochromatic fringes through a polariscope.

The geometry of stress raisers is optimized by removing material from lowly stressed regions. A portable router can initially speed up the removal of large amounts of material, while a file should be used to remove small amounts of material during the fine tuning stage. A stress raiser has optimal shape when its tensile and compressive stresses are approximately constant along boundary sections of the discontinuity.

Durelli and his associates performed a series of experiments and obtained many interesting results. Typically, Durelli *et al.* (1968) optimized a slot end configuration in a finite plate subjected to a uniformly distributed load. Durelli *et al.* (1978) presented results obtained in optimization of (i) the tip of the several rays of stars in perforated solid propellant grains used for rocket propulsion, (ii) the transition between the blade and the dove-tail joint in a turbine, (iii) the inside boundary of a circular ring subjected to diametral compression, and (iv) the boundary of a hole in a rectangular plate subjected to axial load in the case when the hole diameter to plate width ratio is 0.6. Durelli and

Rajaiah (1979) optimized hole shapes in plates of finite width subjected to uniaxial load for a large range of ratios of hole diameter to plate width. Durelli *et al.*(1981) obtained optimal shapes of central holes in square plates under uniaxial uniform compression load. The study was conducted for a large range of hole diameters to plate width ratios.

Schnack (1979) and Schnack and Spörl (1986) developed a numerical optimization procedure equivalent to the photoelastic stress minimization technique with applications to load-free notch surfaces of bodies made of a linear-elastic homogeneous isotropic materials. Schnack (1979) exploited works by Baud (1934), Wheeler (1976), and the notch stress theory of Neuber (1958) to generate the optimality criteria for more general cases of stress minimization problems. The finite element method was employed for calculating the displacement and stress field of the structure. An increment procedure was introduced for determining the displacement field of boundary nodal positions after every iterative step.

### **2.2.9 Shape optimization of cutouts in composite laminates**

Designing with laminated composites has become a challenge because a wide range of parameters can be varied and because of the complex behaviour of these structures, Gürdal and Haftka (1993), Hoa (1995). Finding an efficient composite structural design that meets the requirements of a certain application can be achieved not only by sizing the cross-sectional areas and member thickness, but also by global or local tailoring of the material properties through selective use of orientation, number and stacking sequence of plies. The increase in the number of design variables, on the one hand, gives designers more control to fine-tune the structure, but on the other hand,

challenges them to select design variables effectively.

Bäcklund and Isby (1988) used a point stress criterion with Tsai-Hill index at a distance of 1 mm from the hole's edge to determine the stress field in the vicinity of the cutout in composite panels. The hole was defined using spline curves and these were allowed to change with the objective of minimizing the weight without increasing the maximum Tsai-Hill index.

In the case of a given loading, laminated construction and elliptical cutout area, Vellaichamy *et al.* (1990) used linear analysis to search for the aspect ratio and orientation of the ellipse such that the value of the maximum failure criterion around the circumference of the hole was a minimum. The effect of the hole on the critical buckling load was also studied. The analysis demonstrated that the ellipse configuration was the optimum, since it had a maximum failure criterion value which was substantially lower than that of the equivalent circular hole. The variation of the buckling factor with respect to the ellipse orientation was not very significant. The reduction in the buckling factor with respect to that in the plate area, due to the presence of the hole, bore a linear relationship but the variation of the buckling factor with respect to the aspect ratio was not linear, with the result that the lower the aspect ratio, the better buckling strength would be obtained. Hyer and Lee (1991) used a fibres placement technique to optimize the buckling strength of composite panels containing central circular holes.

Han and Wang (1993) investigated composite panels with a circular or an elliptical hole. The objective was to find the best hole location, size and orientation so as to minimize the maximum tangential strain along the circumference of the hole. The

problem was treated as a shape optimization problem, and the hole boundary parameterization method was developed in order to maintain the required hole shape. The parameterized relationship was further utilized to transform the sensitivity data. The optimization problem was solved iteratively using P-method finite element analysis and linear programming. The results indicated that substantial reduction in the maximum tangential strain was achieved by adjusting the size, location and orientation of circular and elliptical holes.

Pedersen (1993) optimized the shape of fillets in orthotropic plates by minimizing the “maximum energy density” at the points along the boundary. The approach was based on semi-analytical sensitivity analysis and linear programming. Falzon *et al.* (1996) adapted the ESO procedure which was developed by Xie and Steven (1993) to optimize the shape of the interior cutout in composite panels made of carbon-epoxy laminates  $[\pm 45^\circ/0^\circ/90^\circ]_S$ . In this approach, an initial small cutout was introduced into each finite element model and elements were removed from around this cutout based on a pre-defined rejection criterion. The Tsai-Hill failure index was used to determine the limiting ply within each plate element around the cutout. Plate elements with values below the product of the average Tsai-Hill number and a rejection ratio (RR) were subsequently removed. This process was repeated until a steady state was reached and the RR was then increased by an evolutionary rate (ER). The above steps were repeated until a cutout of a desired area was achieved.

Recently, Sivakumar *et al.* (1998) investigated the free vibrational response of composite plates with an elliptical cutout. Orientation of the ellipse with respect to the

reference axis, aspect ratio of the cutout, orientation of plies, thickness of plies and material of plies were used as design parameters with a constraint on natural frequencies. A genetic algorithm was employed to locate the optimum.

### **2.3 Recent development of FEM simulation of PSM**

As previously discussed in Section 2.2.8, Durelli's PSM has been successfully used to solve the optimization problem of finding optimal stress raiser profiles. Solutions obtained by PSM are explicit and have been used as benchmarks for a number of researchers, for example Schnack (1979), Schnack and Spörl (1986) and Tran and Nguyen (1999).

However, PSM is practically limited to plane elastic problems involving simple geometry and boundary conditions. These limits are imposed by the nature of the photoelasticity technique, i.e. difficulties in making models as well as simulating the same boundary conditions of loading and restraints on the models. A successful FEM simulation can extend Durelli's PSM method to solve optimization problems involving complicated geometry, boundary conditions and/or structures made of materials of more complex behavior. Recently, Tranxuan (1998) investigated the simulation of the concept of gradual removal of material of PSM by a FEM procedure, in which lowly stressed elements are removed without remeshing the model. The FEM procedure consists of the following steps:

Step 1: Specifying the design objective, design domain, creating a FEM model of the structure with the same loading and boundary conditions of restraints. Fine mesh should be used in the design domain.

Step 2: Analysing the structure by utilising solution and post processing phases.

Step 3: Monitoring if the optimality criterion is satisfied. If it is satisfied then the process stops and results are output, otherwise the process goes to step 4.

Step 4: Specifying criterion for element removal, selecting elements in the design domain satisfying the removal criterion.

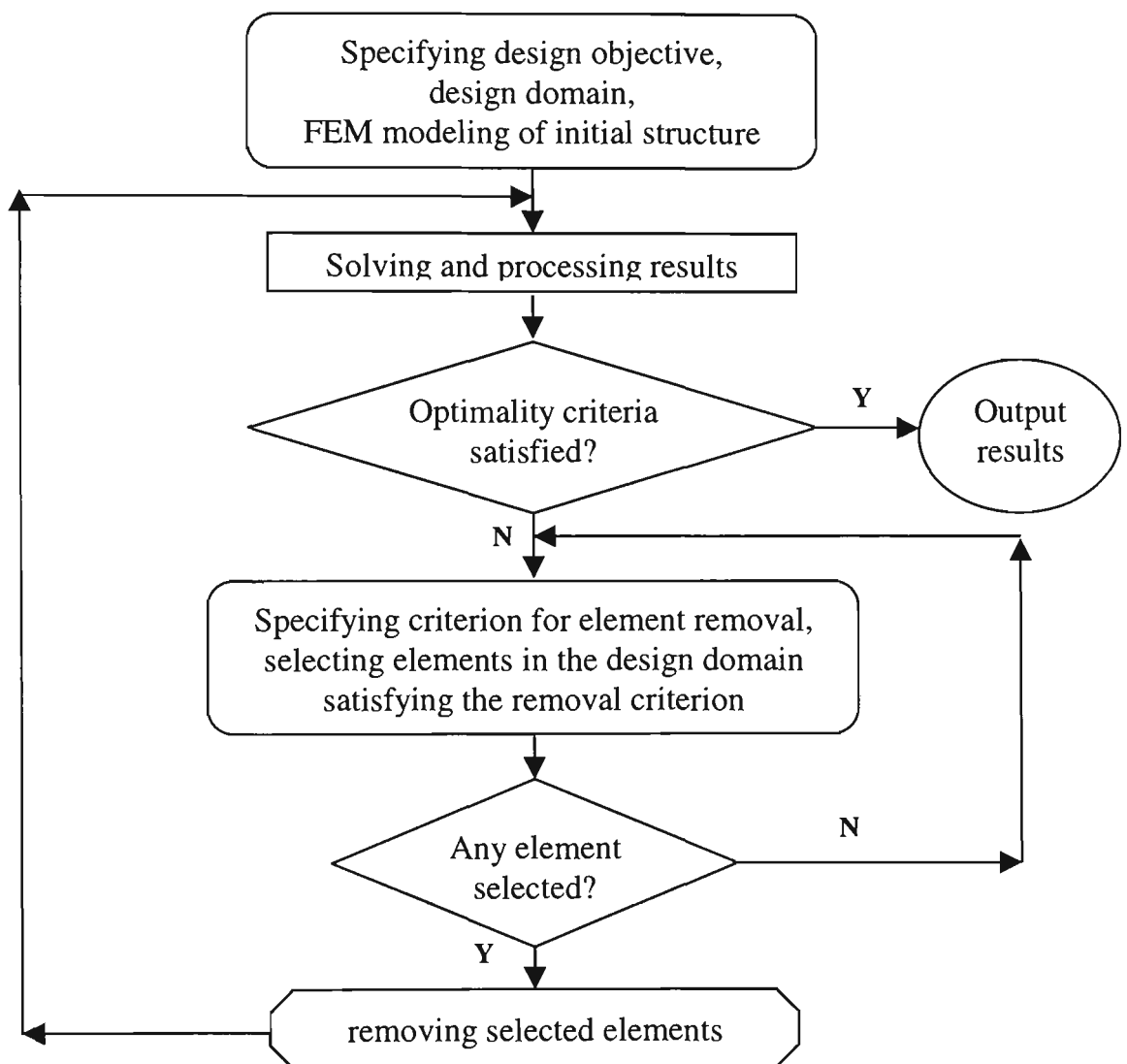


**Figure 2.1:** Flowchart of a simple FEM simulation

Step 5: Checking if the number of selected elements is larger than zero. If it equals zero, then the process goes back to step 4, otherwise the process goes to step 6.

Step 6: Removing selected elements then going back to step 2.

The simple simulation is presented by a flowchart as shown in Figure 2.1. The design objective is to minimize stress concentration as in the PSM technique. Step 1 is very straightforward in FEM modelling. In step 2, stress patterns in a FEM model can be produced, which is equivalent to observing isochromatic fringe orders in a photoelastic model through a polariscope. Step 3 stands for the observation of stress distribution along the modified boundary to see whether it is uniform or not in the PSM. Finally, steps 4, 5, 6 simulate the process of removing lowly stressed materials performed in the experimental procedure. Element removal in FEM simulation can be implemented by actually deleting elements or by removing them numerically, i.e. by simply not incorporating these elements' stiffness matrix into the model structural stiffness matrix.

In the above simulation, the original meshing is retained throughout the optimization procedure. It allows internal holes created during the course of optimization and also avoids problems of boundary description and remeshing. However, a consequence of removing elements of finite sizes will result in a new jagged shape boundary that introduces 'notch effects' or local stress concentration effects, as reported by Tranxuan (1998). These effects cause 'pseudo-minimum stress' and 'pseudo-maximum stress' phenomena, giving extremely high stress at the root of the notch and practically zero stress at shoulders near the root of the notch.

There are problems, in which the genuine isotropic points of zero stress always exist as shown in Chapter 4, the introduced pseudo-minimum elements of very small or in fact zero stress would result in quick false spreading of these pseudo-minimum elements,

unless smoothing is effected after every iteration (Tranxuan 1998). Furthermore, the pseudo-maximum stress will terminate the optimization process early or the resulting shape is still far from the optimal one due to the increase of the maximum equivalent stress observed. Certainly, the final jagged profile can be smoothed in the final stage but the 'notch effect' still prevents it from simulating PSM accurately. Moreover, in problems involving stress minimization or boundary shape optimization, the boundary description is required. Consequently, a FEM simulation of PSM with boundary smoothing and remeshing subroutines is desirable.

More recently, Tran and Nguyen (1999) have addressed the problem of the notch-effects by slowly removing lower stressed elements within an intra-layer of external elements lying on the discontinuity boundary, followed by smoothing and remeshing subroutines. Using the example of a finite width plate with a hole under uniaxial tensile stress, they showed that the results obtained by the FEM simulation gained some further improvements over the results produced by PSM reported in Durelli and Rajaiah (1979).

The above technique, however, requires a number of internal iterations to remove elements within an intra-layer, thus increasing the computation cost. A FEM simulation procedure with boundary smoothing effected after each element removal, followed by remeshing, consequently avoids the notch-effect problems, yet saves the computation cost. Furthermore, the proposed FEM simulation avoids sensitivity analysis, thus is easily extended to minimize stress concentrations in laminated composite structures. It is investigated and presented in the following chapters.

## *Chapter 3*

### **FINITE ELEMENT SIMULATION**

#### **3.1 Introduction**

In this chapter, a FEM simulation procedure of PSM with boundary smoothing and remeshing subroutines after each step of element removal is proposed.

Stress minimization of a large elastic plate with a hole under biaxial tensile stress is investigated. This problem is chosen since its closed-form analytical solution is available. The effects of parameters controlling the optimization process are also examined.

#### **3.2 FEM simulation of PSM with boundary smoothing and remeshing subroutines**

The concept of gradual removal of lowly stressed material of PSM can be simulated by a simple FEM procedure as presented in Section 2.4. A closer look at the mechanism of removing material of Durelli's PSM, however, indicates that it has the

following specific characteristics:

- (i) PSM removes only materials within the design domain from the boundary to be optimized.
- (ii) Isochromatics are continually observed to guide the cut and to terminate the process as the boundary becomes coincident with an isochromatic fringe order.
- (iii) The cut should provide a smooth transition from the current boundary to the next boundary.
- (iv) Material is removed in steps, rough cuts may be used first, finer cuts should be used in later stages to fine-tune the boundary.

The above characteristics play important roles in the success of the PSM, however the difference between photoelastic models and the equivalent FEM models requires further development for a successful simulation.

In order to implement the first characteristic of PSM, only elements lying on the boundary of the discontinuity and within the design domain, can be considered as candidates for element removal in a FEM simulation. The thickness of the cut can not be deeper than *esize*, where *esize* is the element size used to mesh the boundary of interest as shown in Figure 3.3.

The second characteristic suggests that stress patterns should be observed continually during the optimization process. It can be seen that the PSM analyst needs to observe not only within the lowly stressed region but needs to have a global view of the stress distribution and direction of the boundary and the nearby isochromatics. This observation is related to both field values and the gradient. The cut is guided further by

the direction of the boundary and that of its nearby isochromatics. Thus the PSM material removal does not mechanically focus on regions of low stress confined between isochromatics but, if possible, makes a trans-isochromatics cut with the objective of making the boundary becoming an isochromatic.

In a PSM procedure, as the optimization task proceeds, it is expected that the Tresca stress distribution along the boundary becomes more uniform after each boundary modification, resulting in a decrease of the maximum Tresca stress. Hence, instead of observing the uniformity of stress distribution, maximum Tresca stresses on the boundary are monitored and their reduction can be considered as the indicator of a convergence toward the optimum. Such an observation is very significant in a FEM simulation due to the saving in computing effort, as it does not require the calculation of the standard deviation, which measures the uniformity of Tresca stress distribution along the boundary at each iteration. However, the standard deviation should be employed to check if the final output result satisfies the optimality requirement.

The third characteristic, whilst can be easily exercised in a PSM procedure, is greatly affected by finite sizes and shapes of elements in a FEM simulation. For example, a finest cut can be simulated by removing only one element, which creates a new boundary far different from a PSM cut as illustrated in Figure 3.1, resulting in notch effects as previously mentioned in Section 2.3. However, notch effects can be avoided by smoothing the jagged boundary and remeshing the structure after element removal as reported by Tran and Nguyen (1998b), (1999). The task of the boundary smoothing is to create a new boundary, which is based on the geometry of the jagged boundary after element removal.

The final characteristic results in materials being removed as much as possible and thus speeds up the convergence to the optimal contour. In FEM simulation, this can be implemented in such a way that large amounts of elements should be removed in initial iterations then smaller quantities are removed in subsequent iterations. A monitoring scheme should be put in place to ensure that no over-cutting occurs. Over-cutting happens when the cut is too rough or too many elements are removed in one iteration making the maximum stress on the boundary increase. This procedure, while improving convergence rate, still ensures the satisfaction of the optimality criteria.

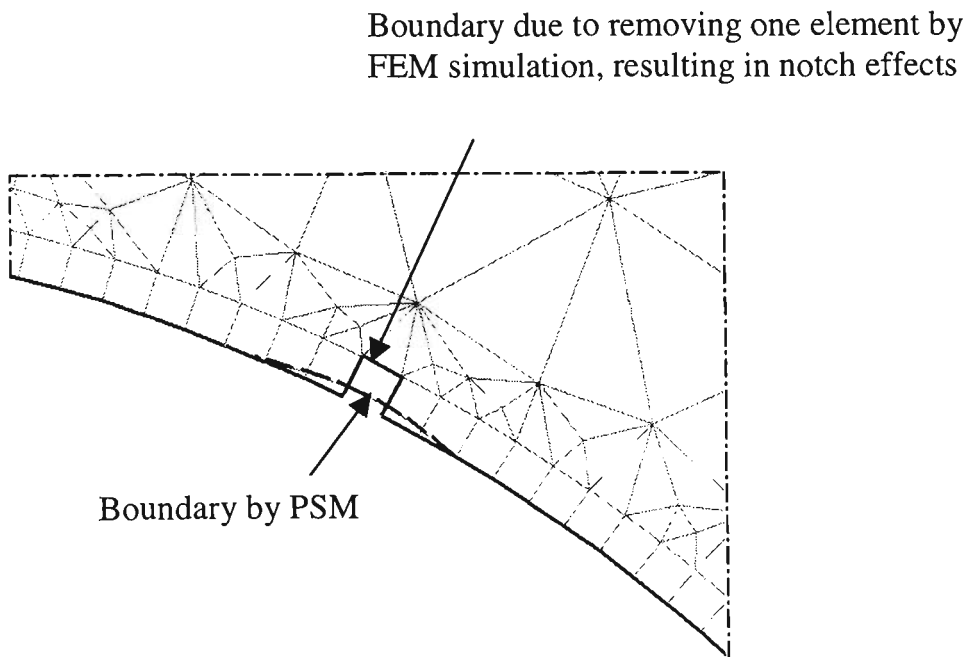


**Figure 3.1:** Finest cuts by PSM and FEM simulation

Before constructing the FEM algorithm for simulating the above characteristics of PSM, problems related to boundary smoothing, mesh generation and design of the FEM model are discussed.

### **3.2.1 Boundary smoothing**

In order to avoid notch effects created by jagged boundary after element removal a boundary smoothing subroutine is essential. The smoothing task is based on the pattern of external boundary nodes to create a new smooth boundary. The way used to describe the shape of the boundary is one of the key elements in the process of attaining the optimum shape. Common shape representations found in the literature include polynomials and splines. The use of polynomials with control nodes to describe the boundary, however, can result in an oscillatory boundary shape for the boundary shape of higher order polynomials due to the numerical instability with higher order curves, Haftka and Grandhi (1986), Ding (1986).

In a PSM procedure, the shape of the boundary only changes at positions where materials are removed and is kept unchanged at others. To simulate this characteristic, the FEM simulation demands a smooth curve that only changes its shape at locations where elements are removed without affecting the remaining parts of the boundary. Thus, B-splines would be the most appropriate curves that should be employed to smooth the jagged shape boundary after element removal. Furthermore, B-splines support local control and additional points can be introduced without increasing the degree of the curve, Braibant and Fleury (1984).

In the FEM simulation, an external layer of elements associated with the boundary of the discontinuity can be divided into a number of even length sections. Each section is represented by a primary control point, which is associated with external nodes lying on the boundary of that section as shown in Figure 3.2. After element removals, only primary control points at sections that have elements removed are redefined. The control

points are redefined following the least square rule, i.e. the sum of squares of the distances between a new primary control point to external nodes lying on the boundary of that section is minimized.

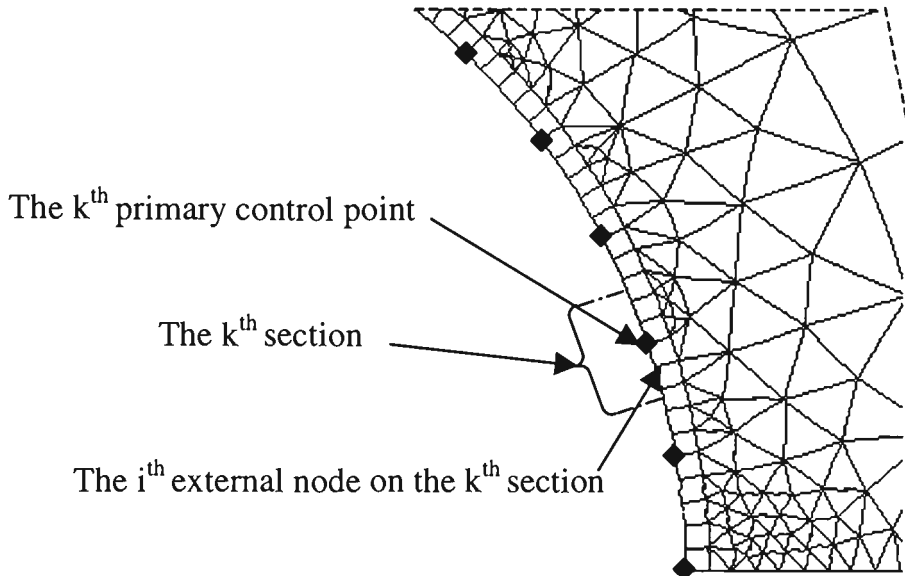


**Figure 3.2:** Primary control points on the boundary

It has been shown in Appendix A that the  $k^{\text{th}}$  control point,  $P_k$ , of the  $k^{\text{th}}$  boundary section containing  $N$  external nodes that satisfies the least square condition is determined by:

$$x_{P_k} = \frac{1}{N} \sum_{i=1}^N x_i \quad (3.1)$$

$$y_{P_k} = \frac{1}{N} \sum_{i=1}^N y_i \quad (3.2)$$

Where,

$x_{P_k}$   $y_{P_k}$  are Cartesian coordinates of  $P_k$ .

$x_i$   $y_i$  are Cartesian coordinates of the  $i^{\text{th}}$  node

Figures 3.3a and 3.3b illustrate the boundaries after element removal and after

being smoothed. It can be seen that:

- (i) The more elements are removed, the deeper and longer is the change in boundary.
- (ii) The less elements are removed or the smaller *esize* is used, the finer the cut that can be simulated.

Therefore, this smoothing scheme simulates PSM material removal more accurately than a procedure in which elements are removed leaving a new jagged boundary.

### **3.2.2 FEM mesh generation**

Before the advent of automatic mesh generators and adaptive mesh refinement techniques, in most cases the meshing of a finite element model was a manual rather than an automated process, Haftka and Grandhi (1986). The analyst used judgement and experience to generate the mesh. A trial and error process was often facilitated by user-interface facilities. This manual approach is tedious and inadequate for shape optimization problems, in which the analyst needs to remesh for a series of structures with unpredictable shapes. In order to overcome this difficulty, an automated mesh generation should be employed. However, badly distorted elements may be created during automated mesh generating processes, which reduce the accuracy of the stress evaluation.

An important tool to avoid mesh distortion is adaptive mesh refinement. Information from an analysis with a trial mesh is used to identify regions which need

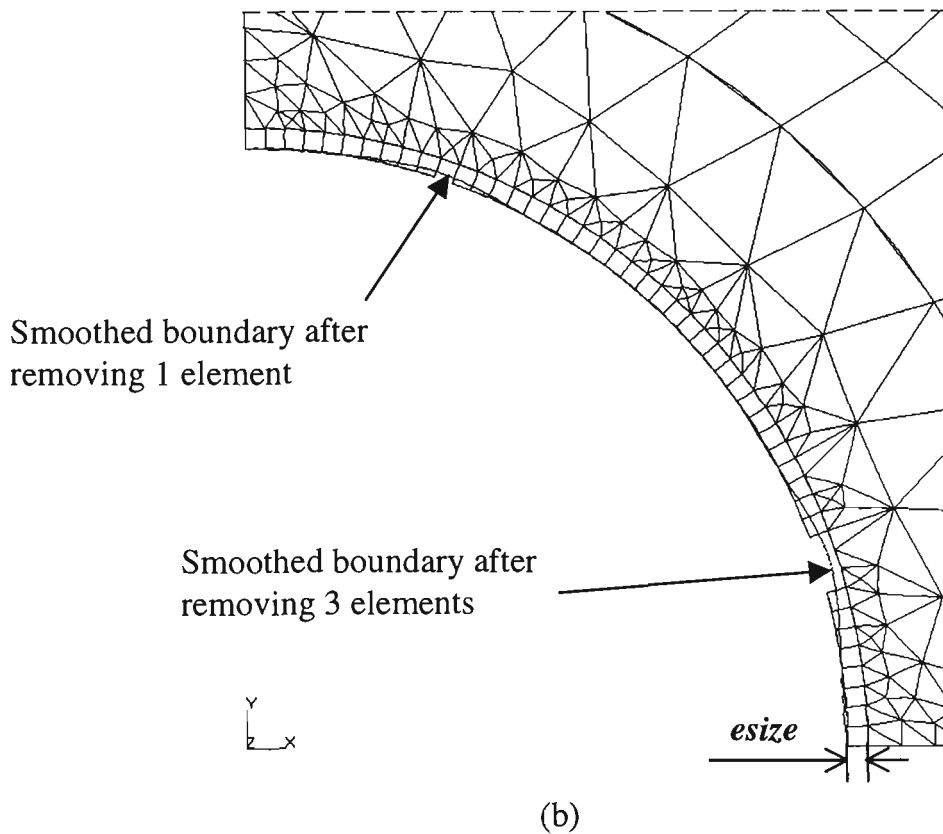
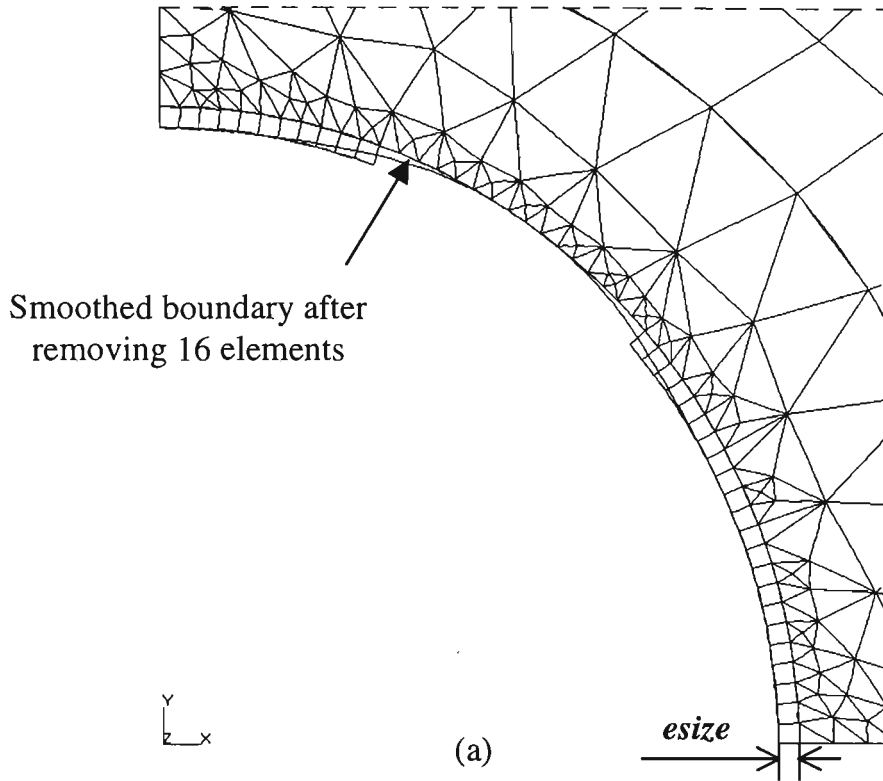


**Figure 3.3:** (a) Boundaries after removing 16 elements and after smoothing; (b) Boundaries after removing 1, 3 elements and after smoothing.

further mesh refinement. This refinement can take either the form of adding additional elements in the area to be refined or of increasing the order of the finite element, Haftka and Grandhi (1986) and Ding (1986). In this study, automated mesh generator and adaptive mesh refinement available in the ANSYS 5.3 software were employed. However, the adaptive mesh refinement requires considerably more computing effort and should be kept to a minimum. This is effected by proper design of the FEM model as shown in the next section.

### **3.2.3 Design of the FEM model**

One of the ways to achieve a finite element model that minimizes the mesh distortion problem is to use the ‘design element’ concept, firstly introduced by Imam (1982) and further adopted by many researchers, e.g. Braibant and Fleury (1984), Bennett and Botkin (1985).

In this approach, the structure is divided into a number of design elements. Each design element, which consists of several finite elements, is described by a set of master nodes that control the geometry. Associated with each design element is a set of design variables, which specify the location of the key nodes that are allowed to move. An illustration is shown in Figure 3.4, in which a FEM model is divided into four design elements.

In this study the ‘design element’ concept is employed. As shown in Figure 3.5, a quarter model of a plate with a hole can be divided into three areas. Area 1, which includes the section of the boundary to be optimized, is meshed with one layer of very fine elements of uniform size of  $esize$ . For plane problems there are two choices of

element shape: triangular or quadrilateral. It has been found that the use of the triangular shape does not result in a unique smooth curve as found in the case of quadrilateral shape. For instance, one removed triangular element with one side lying on the hole boundary results in a smooth curve different from the one with one vertex lying on the hole boundary as illustrated in Figures 3.6a and 3.6b.

Four subregions (design elements): 1, 2, 3, 4

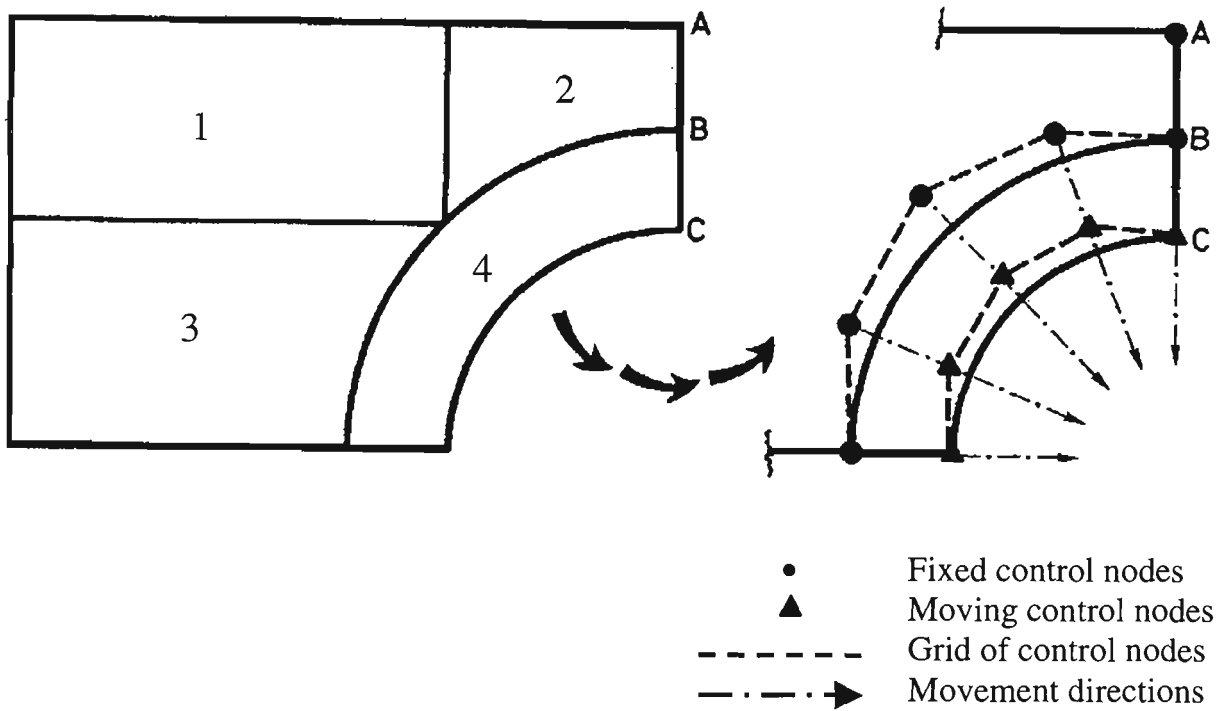


**Figure 3.4:** The design element concept (Braibant and Fleury 1985)

Area 3 can be meshed with coarse quadrilateral elements to reduce the number of elements in the model. Area 2 is meshed with transitional triangular elements to join very fine elements of area 1 to coarse elements of area 3 with the least error.

The boundary to be optimized is represented by a B-spline, which goes through the primary control points that are determined by Equations (3.1) and (3.2). The points  $Q_k$

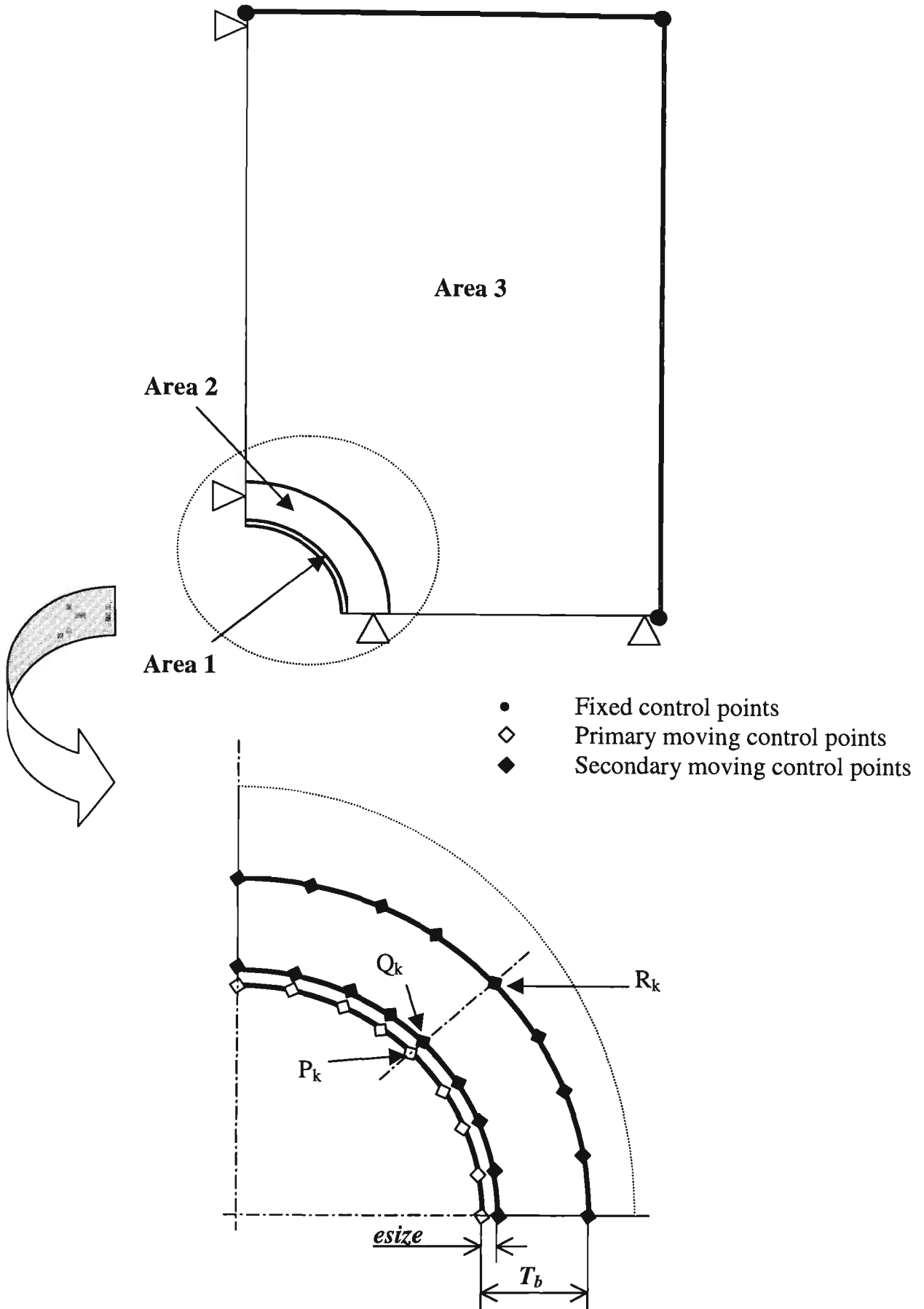
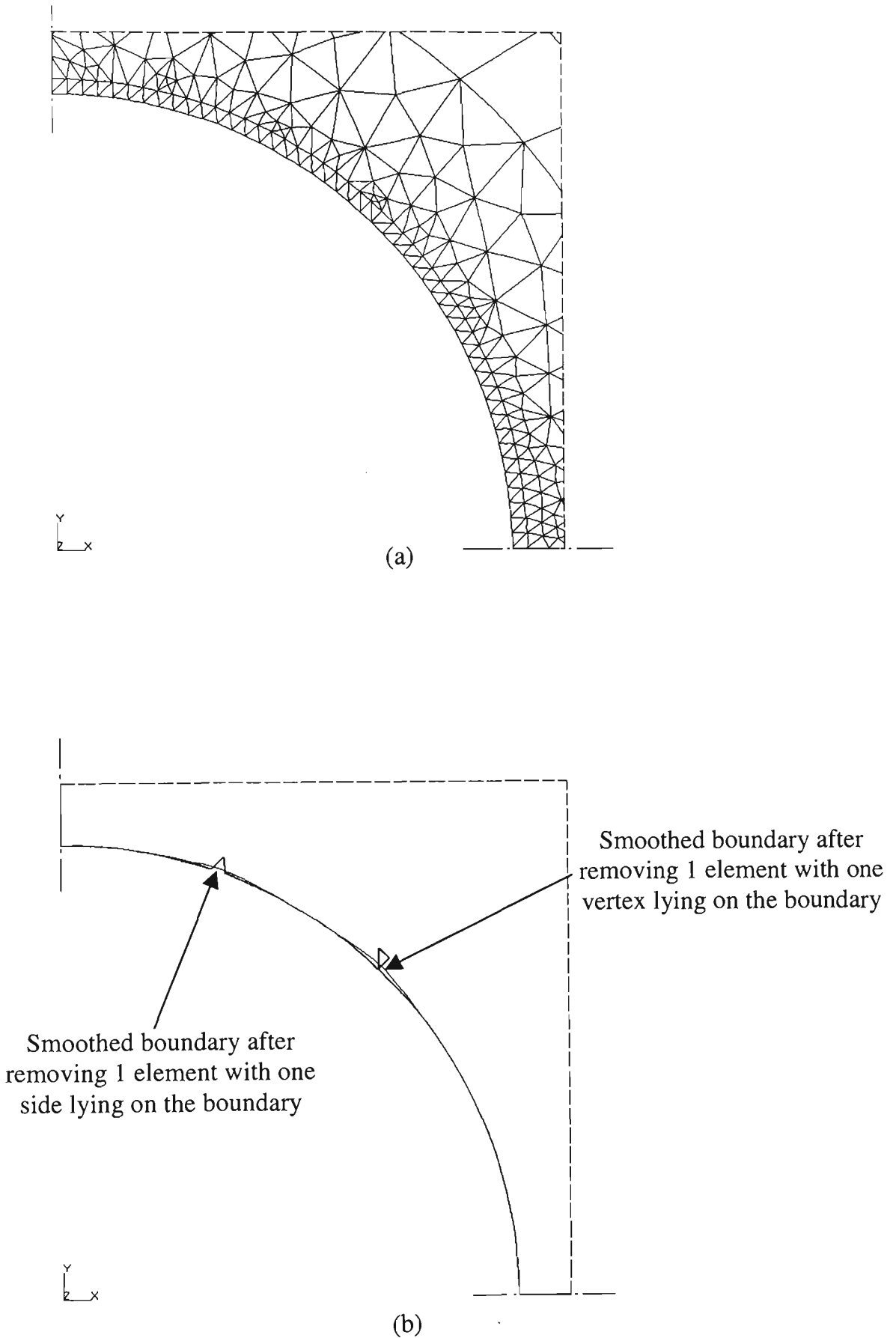
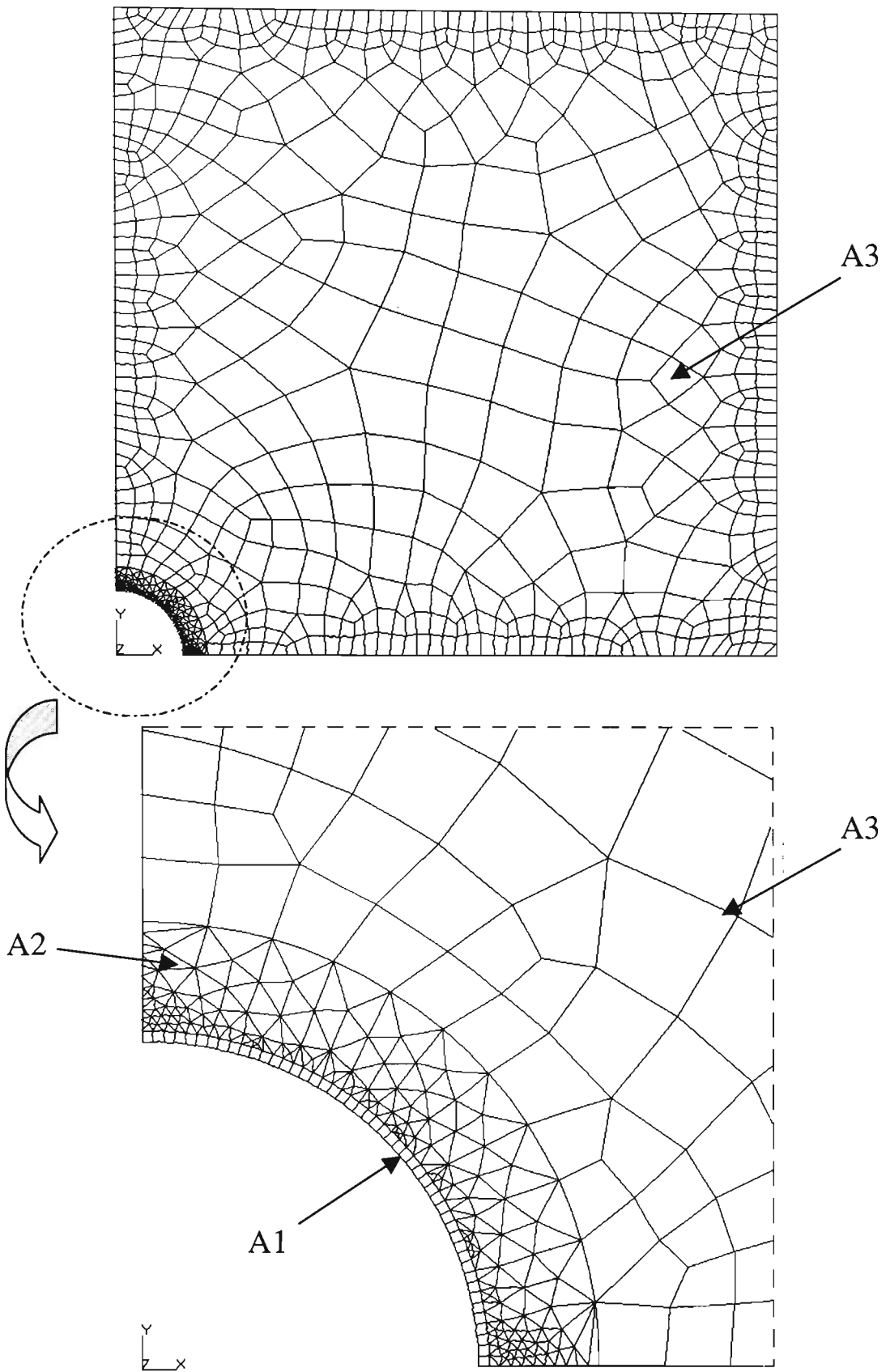


Figure 3.5: Design of the FEM model



**Figure 3.6:** (a) Meshing boundary with triangular shape elements  
(b) Boundaries after removing 1 element with different possibilities and after being smoothed.



**Figure 3.7:** A typical quarter FEM model of a square plate containing a circular hole

and  $R_k$ , corresponding to the primary control point  $P_k$  and lying on the normal direction to the B-spline at  $P_k$ , are called secondary control points, as illustrated in Figure 3.5. The distances from  $Q_k$  and  $R_k$  to  $P_k$  are *esize* and  $T_b$  respectively. Where *esize* and  $T_b$  are initially determined in an interactive fashion.

Figure 3.7 shows a typical quarter FEM model of a square plate containing a circular hole. The plate side is of 300mm, hole diameter is of 30mm, *esize* is 0.5mm and  $T_b$  is 5mm.

### **3.2.4 FEM simulation algorithm**

The proposed algorithm to simulate the PSM technique selects a number of elements out of the set of external elements lying on the current boundary of interest within the design domain having lower equivalent stress for removal, following by boundary smoothing and remeshing subroutines. The structure is reshaped iteratively and the maximum equivalent or Tresca stress on the boundary is monitored. The optimization process is considered to converge when the uniformity requirement of stress distribution along the optimized boundary is attained or the number of elements to be removed in each iteration reaches a preset minimum value, whichever comes first.

The algorithm is illustrated by a flowchart in Figure 3.8. Its main features are described as follows.

#### **3.2.4.1 Main features of the algorithm**

The optimization process proceeds through two stages:

(a) Initialization stage

The initialization task consists of steps 1 and 2. It involves preliminary modeling and carrying out stress analysis in an interactive fashion to help improving the FEM model and to provide information required in steps that follow. Constraints and the objective should be specified. The objective in this study is to minimize the stress concentration that occurs on the stress raiser boundary.

(b) Optimization stage

The optimization task is composed of three loops, named *I*, *J* and *K* loop, where:

- *I* loop consists of steps 10-13 and a number of *J* loops. It controls the process from the beginning of the optimization task until the process switches to the fine tuning stage that is controlled by the *K* loop. The *I* loop is designed to simulate the process of gradually removing material of PSM from rough to fine cuts.
- *J* loop is the basic loop (steps 3-9), within which the structure is modified while the maximum Tresca stress is monitored.
- *K* loop includes steps 10, 15-17 and a number of *J* loops. It is active at the fine tuning stage until the process converges. A few elements or even one element can be removed in each iteration at this stage to simulate the process of fine tuning stage of PSM using sharp files.

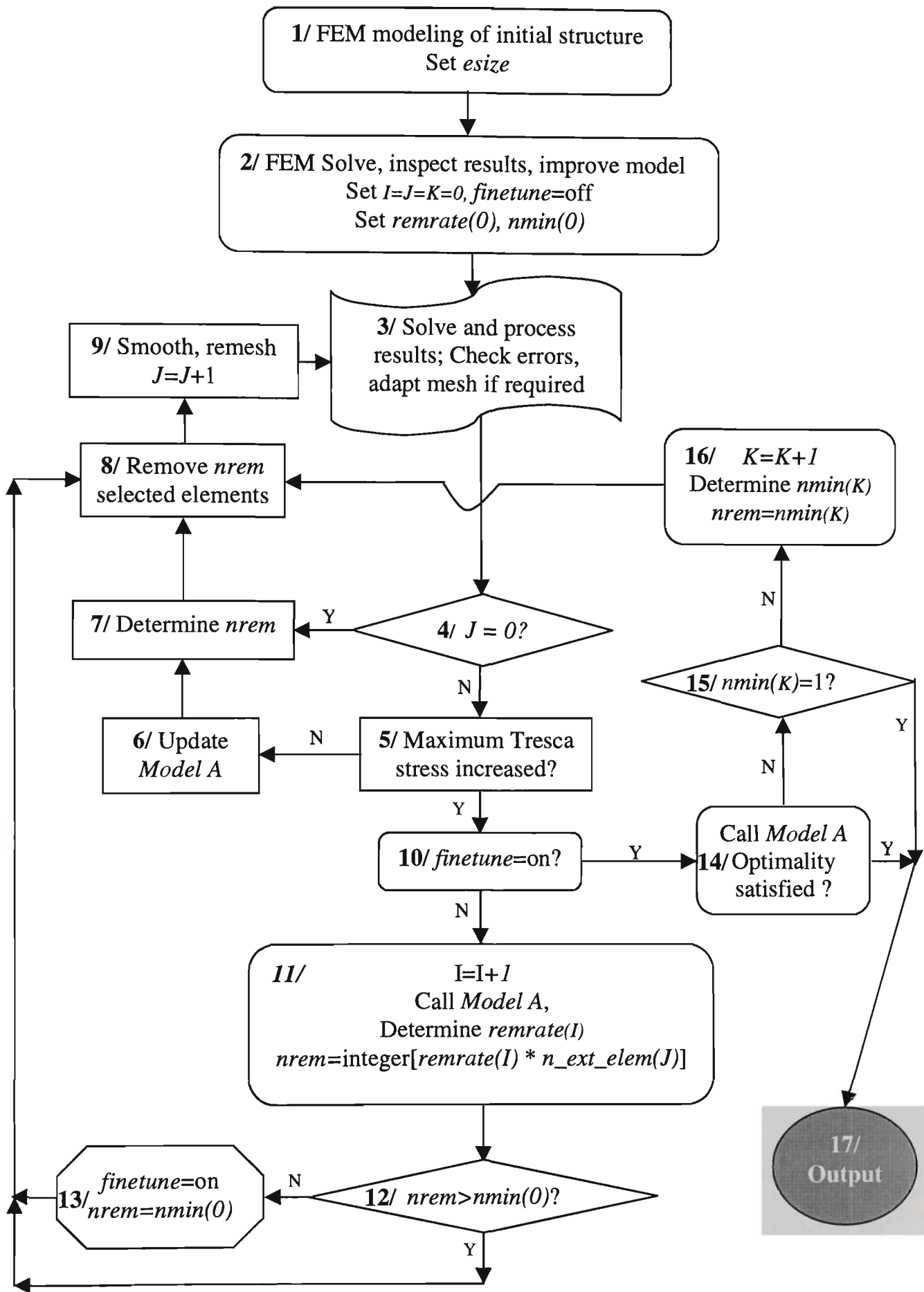


Figure 3.8: Flowchart of the FEM simulation

### 3.2.4.2 Definition of parameters used in the flowchart

- $I, J, K$  are loop indices.
- $Ext\_elem$  is the set of external elements currently lying on the stress raiser boundary within the design domain.
- $n\_ext\_elem$  is the total number of elements of the set  $Ext\_elem$ . It is counted at each iteration.
- $finetune$  is a flag indicating whether the cutting stage is fine or coarse. It is initially set as “off”. It is set to “on” when the process is switched to the fine tuning stage.
- $esize$  is the smallest element size used to mesh the area along the boundary of interest as illustrated in Figure 3.3. Uniform quadrilateral shape of small size elements should be used to mesh this area as discussed in Section 3.2.3.

It is found that a value of  $esize$  of one percent of the hole diameter would be appropriate to give acceptable results (Section 3.3.2). Being subject to the constraint of hardware and/or software, a setting of smaller  $esize$  would give better results but the computation cost would increase (Section 3.3.4).

- $remrate$  is the removal rate. This rate dictates how many elements out of all external elements on the current boundary of the discontinuity are selected for removal.  $remrate$  is active and continually reduced within the  $I$  loop as the optimization proceeds.

In this study, a linear reduction is applied to *remrate*; the value of removal rate in the  $I^{\text{th}}$  loop, *remrate (I)* is determined as (step 11 - Figure 3.8):

$$remrate (I) = remrate (0) - TF * I \quad remrate (I) > 0 \quad (3.3)$$

where,

- ◆ *remrate (0)* is the initial value of *remrate*, preset at step 2, Figure 3.8, *remrate (0)* is valid for any value between 0 and 1, a value between 0.4 and 0.7 is recommended (Section 3.3.5).
  - ◆ *I* is the loop index;
  - ◆ TF is the tuning factor; TF should be between 0 and 0.1. A typical value TF of 0.05 is used throughout the study unless otherwise stated.
- *nmin* is the number of elements which can be removed in each iteration of the fine tuning stage (*K* loop). It is continually decreased as the process proceeds. The smallest possible value of *nmin* could be one if the structure is asymmetrical. However, the value of *nmin* should be even when dealing with symmetrical structures.

In the flowchart, Figure 3.8, it is assumed that symmetrical properties are already utilized or the structure is asymmetrical so that the smallest value of *nmin* could be one. In this study, a linear reduction is applied to *nmin*. The value of *nmin* in the  $K^{\text{th}}$  loop, *nmin(K)* is determined as (step 16 - Figure 3.8):

$$nmin(K) = nmin(0) - NE * K \quad nmin(K) > 0 \quad (3.4)$$

where,

- ◆  $nmin(0)$  is the initial value of  $nmin$ , specified at step 2, Figure 3.8.  $nmin(0)$  can be preset as the nearest integer of 5% of initial  $n\_ext\_elem$ .
- ◆  $K$  is the loop index.
- ◆  $NE$  is the number of elements to be reduced in each step of the  $K$  loop,  $NE \leq nmin(0)$ , a typical value  $NE = 1$  is used throughout the study, except otherwise stated.
- $nrem$  is the number of selected elements that have lowest Tresca stress among elements of the set  $Ext\_elem$ , to be removed. It is determined in each iteration, step7 - Figure 3.8. Its determination depends on the cutting stage, which is identified by parameter  $finetune$ .

If  $finetune$  is set as off, at the  $J^{th}$  iteration in the  $I^{th}$  loop,  $nrem$  is determined as the nearest interger of the product of  $remrate(I)$  and  $n\_ext\_elem(J)$ , i.e.

$$nrem = \text{integer} [remrate(I) * n\_ext\_elem(J)] \quad (3.5)$$

Where,

- ◆  $remrate(I)$  is determined by Equation (3.3);
- ◆  $n\_ext\_elem(J)$  is the number of external elements lying on the stress raiser boundary, counted at the  $J^{th}$  iteration.

If  $finetune$  is set as on, at the  $J^{th}$  iteration in the  $K^{th}$  loop,  $nrem$  is determined as

$$nrem = nmin(K) \quad (3.6)$$

Where  $nmin(K)$  is determined by Equation (3.4).

### 3.2.4.3 Flow of the algorithm

The flow of the algorithm is as follows:

Step 1: Creating a FEM model of the structure with same loading and boundary conditions. The smallest element size used to mesh the area along the boundary of interest,  $esize$ , is set.

Step 2: Finite element analysis is carried out interactively. A criterion based on an equivalent stress is defined and evaluated for each element for the selection of elements to be removed. If the structure is made of homogeneous isotropic material, either Tresca or von Mises stress can be employed as a criterion to simulate PSM as both lead to the same equivalent stress, Tranxuan (1998) and Tran and Nguyen (1999).

Loop indices  $I, J, K$  are set to zero. Flag  $finetune$ , Parameters -  $remrate(0)$ ,  $nmin(0)$  - that control the optimization process are now initialized (Section 3.2.4.2).

A minor check at this point to ensure that the condition  $nrem > nmin(0)$  is satisfied so that the process can proceed to rough cutting stage.

Step 3: Finite element analysis is performed, utilizing solution and post processing phases. Errors are checked and mesh refinement is adapted if errors exceed the

limit. Element stress values are recorded for evaluation.

Step 4: Checking if the process is in the first iteration. In the first iteration when  $J = 0$ , the direction of the flow chart should be going straight to step 7, where external elements on the stress raiser boundary are selected to be removed. In other cycles, it goes to step 5.

Step 5: Monitoring the maximum Tresca stress. If the maximum Tresca stress increases or over-cutting occurs, the process goes to step 10. Otherwise, it goes to step 6.

Step 6: *Model A* is updated with new geometry and data.

Step 7: Determining external elements lying on the stress raiser boundary to be removed. The quantity of elements to be removed,  $nrem$  is determined by Equation (3.5) when *finetune* is 'off', or Equation (3.6) when *finetune* is 'on'. To ensure that the element removal starts from the current boundary, only *Ext\_elem*, the set of elements in the design domain and currently on the stress raiser boundary are selected. They are candidates for element removal.

Based on the element stress data recorded at step 3, elements of the set *Ext\_elem* are sorted in order.  $nrem$  elements that have lower Tresca stress values are now reselected, employing Equation (3.5) if *finetune* is set as "off" ( $J$  loop), or Equation (3.6) if *finetune* is set as "on" ( $K$  loop). The process goes to step 8.

Step 8: Removing  $nrem$  selected elements.

Step 9: The jagged boundary after element removal is then smoothed and the structure is

remeshed before being passed to the next iteration for the evaluation of the new maximum equivalent stress.

The model is iteratively reshaped and updated within the  $J$  loop (steps 3-9) until an over-cutting is reached that makes the maximum Tresca stress increase (checked at step 5), indicating that the cut is too rough or too many elements are removed. The process has to reduce the number of elements to be removed in the next iteration to simulate a finer cut of PSM by decreasing  $remrate(I)$  ( $I$  loop,  $finetune = off$ , Equation 3.3), or by reducing  $nmin(K)$  ( $K$  loop,  $finetune = on$ , Equation 3.4). In order to identify the status of the cutting stage, the process goes to step 10.

Step 10: Checking the status of the cutting stage by reading the flag  $finetune$ . If  $finetune$  is “on” or the process is in the fine tuning stage, indicating that the  $K$  loop is active, the flow goes to step 14. Otherwise the  $I$  loop is still active, the process goes to step 11.

Step 11: At this spot, *Model A* without over-cutting is recalled. The element removal rate,  $remrate(I)$  (Equation 3.3), and the number of elements to be removed,  $nrem$  (Equation 3.5) are redetermined.  $nrem$  elements in the set  $Ext\_elem$  that have lower Tresca stresses are then reselected for removal.

Step 12:  $nrem$  is now compared to  $nmin(0)$  which had been preset at step 2. If  $nrem$  is larger than  $nmin(0)$ , the process goes back to step 8 to start another cycle of the  $I$  loop again with a “finer cutting tool”, i.e. a smaller value of the element removal rate,  $remrate(I)$ .

After a number of  $I$  loops,  $remrate(I)$  is reduced to a value so small that  $nrem$ , determined by Equation (3.5), is not larger than  $nmin(0)$ , attesting that the stress raiser profile is very close to the optimal profile, the process goes to step 13 to activate the  $K$  loop.

Step 13: In order to deactivate the  $I$  loop and activate the  $K$  loop, the flag  $finetune$  is set to “on”. The optimizer now starts moving to the fine tuning stage with  $nrem$  takes the value of  $nmin(0)$ .  $nrem$  elements in the set  $Ext\_elem$  that have lower Tresca stress are then reselected for removal. The process then goes back to step 8 to enter the basic loop, i.e. the  $J$  loop.

After a number of  $J$  loops with  $nrem = nmin(0)$ , the over-cutting stage is reached, the process exits the  $J$  loop at step 5. Because the process is in the fine tuning stage, i.e.  $finetune$  is set to “on”, from step 10 the process proceeds to step 14, signaling a possible convergence to the optimum profile.

Step 14: *Model A* is recalled for checking optimality, i.e. checking the uniformity of stress distribution along the stress raiser profile by calculating the standard deviation. If the optimality requirement is satisfied, the process goes to step 17 and results are output.

Otherwise, it indicates that the process requires a finer cut compared to the previous fine cut that could not make the boundary meet the stress uniformity requirement. This can be simulated by reducing  $nmin$  (Section 3.2.1, Figure 3.3).

Step 15: If the smallest value of  $nmin$  is not reached i.e.  $nmin(K) > 1$ , the process goes to step 16, where  $nmin(K)$  is reduced to simulate a finer cut of PSM.

If the smallest possible value of  $nmin$  is reached i.e.  $nmin(K) = 1$ , indicating the optimizer has used the “finest tool” to modify the structure. The process should go to step 17 where results are output.

Step 16: The number of elements to be removed,  $nmin(K)$  are redetermined by Equation (3.4),  $nrem$  elements [ $nrem = nmin(K)$ ] in the set  $Ext\_elem$  that have lower Tresca stresses are then reselected for removal. The process goes back to step 8 to start another cycle of the  $K$  loop.

Step 17: Output results. Results are checked in an interactive fashion at this step.

If the uniformity of stress distribution along the optimized profile is not satisfied, the optimizer needs a finer “cutting tool”, which can be simulated by reducing  $esize$  (Section 3.2.1, Figure 3.3). The structure can then be subjected to the optimization cycles again.

If the specified standard deviation at step 14 is set to zero, or the required uniformity of stress distribution is absolute, then the obtained result is the best possible outcome of the process. A number of minor checks and on-line output of results in the form of stress plots, element plots, maximum stress values, accumulative material removal, etc. are also included but not shown in the flowchart.

### **3.3. Case study—a plate with a hole under biaxial tensions**

A plate with a hole has been a classical example of a stress concentration problem. It has served as an example to demonstrate and validate shape optimization techniques by many researchers, see Haftka and Grandhi (1986).

In the case of an infinite plate with a circular or an elliptical hole under biaxial tensile stress, the analytical solution for the stress distribution was found by Inglis (1913) and confirmed by Durelli and Murray (1943). It has been shown experimentally, Durelli and Murray (1943) and analytically, Banichuk (1989), that for an infinite plate under biaxial tension, the optimal hole profile is an ellipse, the ratio of major axis to the minor axis is equal to the ratio of the stresses in the two respective directions. The availability of the analytical solution of this problem has served as an excellent benchmark to study the sensitivity and stability of the solution process under perturbations.

### 3.3.1 Description of the structure

The structure investigated is a thin square plate of side  $L = W = 300$  mm, of constant thickness  $T$  of 1 mm, with an initial circular hole of diameter  $D$  of 30 mm. The material is assumed to be homogeneous isotropic, with Young's modulus of 205 GPa. and Poisson ratio of 0.3.

The plate is under uniform biaxial tensile stresses as shown in Figure 3.9. The greater stress,  $\sigma_y$  along Y-axis is kept constant for all cases at 10 MPa. The smaller stress  $\sigma_x$ , is determined from  $\sigma_y$  and the stress ratio  $S_r$ , where:

$$S_r = \sigma_y / \sigma_x \quad (3.7)$$

The stress concentration factor  $k_{\text{biax}}$ , is determined (Durelli and Murray 1943) as:

$$k_{\text{biax}} = \sigma_{\text{max}} / \max\{\sigma_y, \sigma_x\} \quad (3.8)$$

Where,  $\sigma_{max}$  is the maximum Tresca stress occurring on the hole boundary. As  $\sigma_y > \sigma_x$  and  $\sigma_y = 10\text{MPa}$  for all cases, equation (3.8) can be written as:

$$k_{biax} = \sigma_{max}/\sigma_y \tag{3.9}$$

It can be seen that  $k_{biax}$  is proportional to  $\sigma_{max}$ . Thus the reduction in  $\sigma_{max}$ , which also means the reduction in stress concentration factor  $k_{biax}$ , can be used to present results obtained by the FEM simulation in this section.

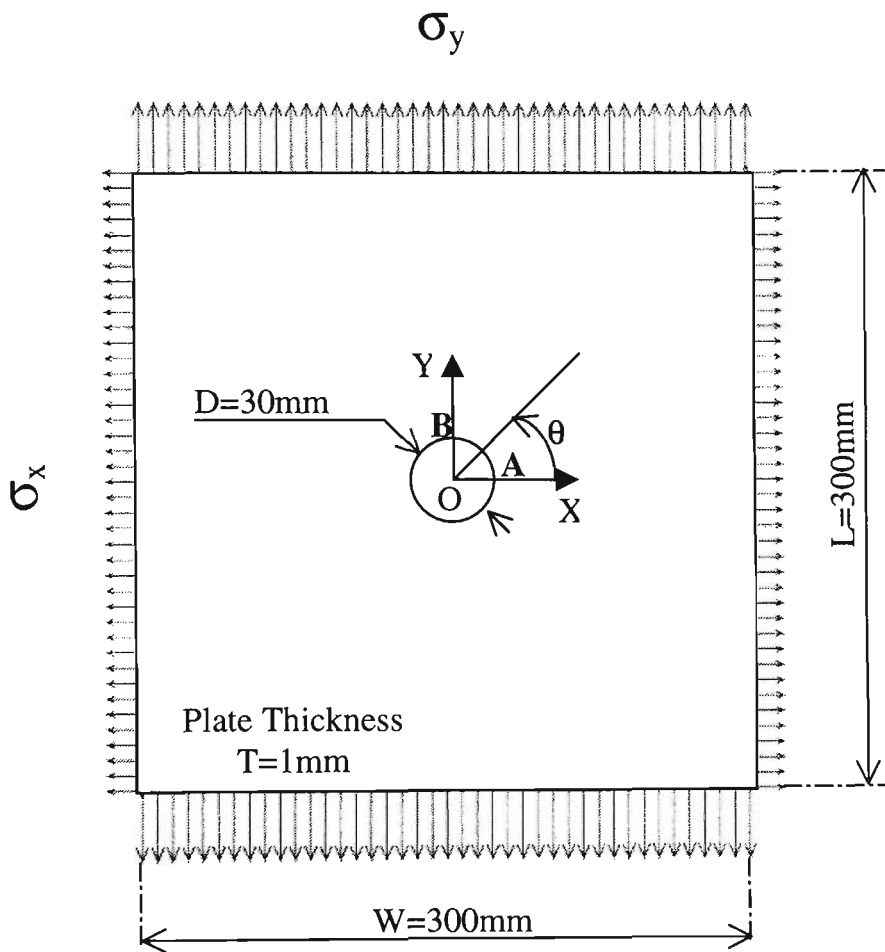


Figure 3.9: Description of the problem

A typical case study when  $S_r$  takes the value of 1.5 is presented, followed by the study of the effects of parameters that control the optimization process and of the applied stress ratios. As the hole boundary is free, Tresca criterion or von Mises criterion leads to

the same equivalent stress. In order to produce the best possible outcome, the specified standard deviation of the equivalent stress distribution along the stress raiser profile is set to zero for all cases. The number of primary control points used is twenty-one and the minimum value of  $nmin(K)$  is set to 1 throughout this section, except otherwise stated.

### 3.3.2 Optimal hole profile when $S_r=1.5$

Due to symmetry, a quarter of plate was modelled as illustrated in Figure 3.10. The initial mesh consists of 1094 eight node plate elements. Area 1 was meshed with 81 uniform quadrilateral elements (thus  $n_{ext\_elem}(0) = 81$ ), of which element size was 0.3 mm, Area 3 was meshed with 593 elements, of which element sizes vary from 3 mm to 8mm, and Area 2 was meshed with 420 triangular elements. For displaying the Tresca stress distribution along the hole boundary, a polar co-ordinate system was used for which the zero angle position ( $\theta = 0^\circ$ ) was at point A and the  $90^\circ$  angle position ( $\theta = 90^\circ$ ) was at point B of the hole.

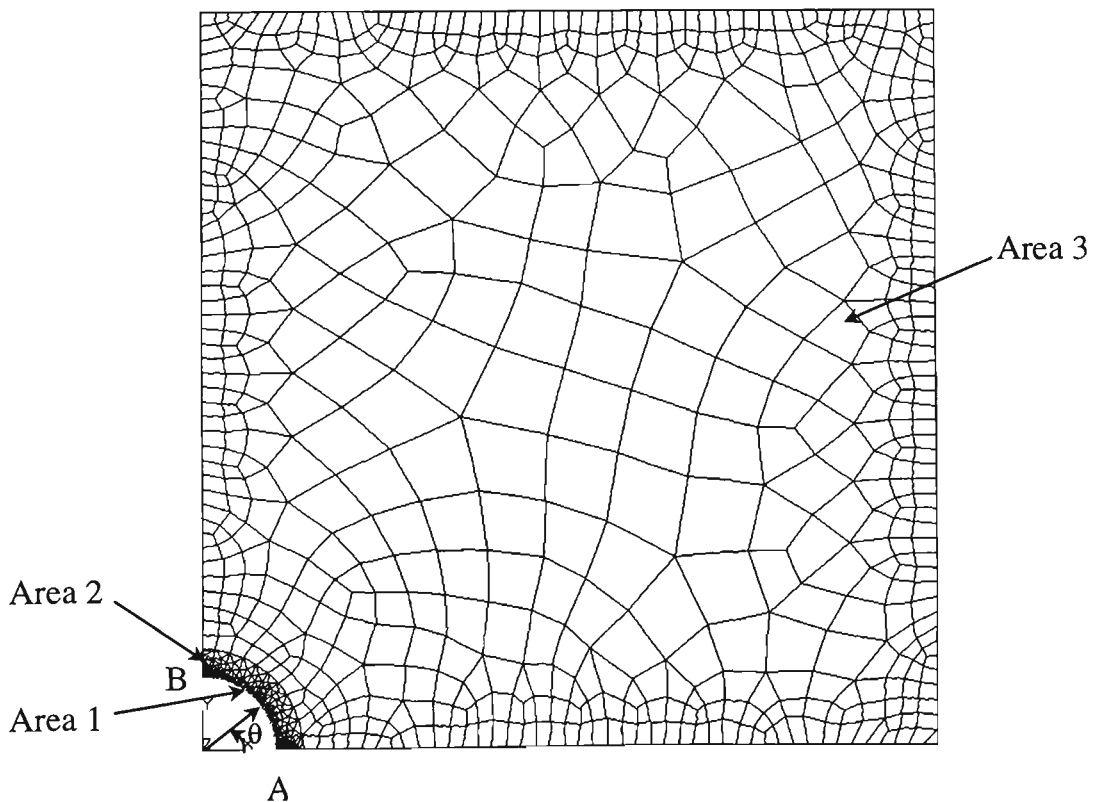


**Figure 3.10:** The FEM model

Parameters were initially set as follows:

$$esize = 1\% * D = 0.3 \text{ mm} \tag{3.10}$$

$$nmin(0) = \text{Integer} [5\% * n\_ext\_elem(0)] = \text{Integer} [5\% * 81] = 4 \tag{3.11}$$

$$remrate(0) = 0.5 \tag{3.12}$$

The initial stress distribution in the plate generated by the FEM is shown in Figure 3.11. Stress concentration occurs at point A ( $\theta = 0^\circ$ ), the maximum Tresca stress is 23.37 MPa. The minimum Tresca stress is 9.93 MPa occurring at point B ( $\theta = 90^\circ$ ). For an infinite plate, the theoretical solution by Durelli and Murray (1943) gives the maximum stress as 23.33 MPa, and the minimum stress on the hole boundary as 10 MPa. The agreement between numerical and the theoretical results indicates that at the ratio of W/D of 10, the width of the square was sufficiently large to ensure a uniform stress distribution at a distance from the hole, and that the edge boundary conditions do not affect greatly the stress distribution in the region around the hole.

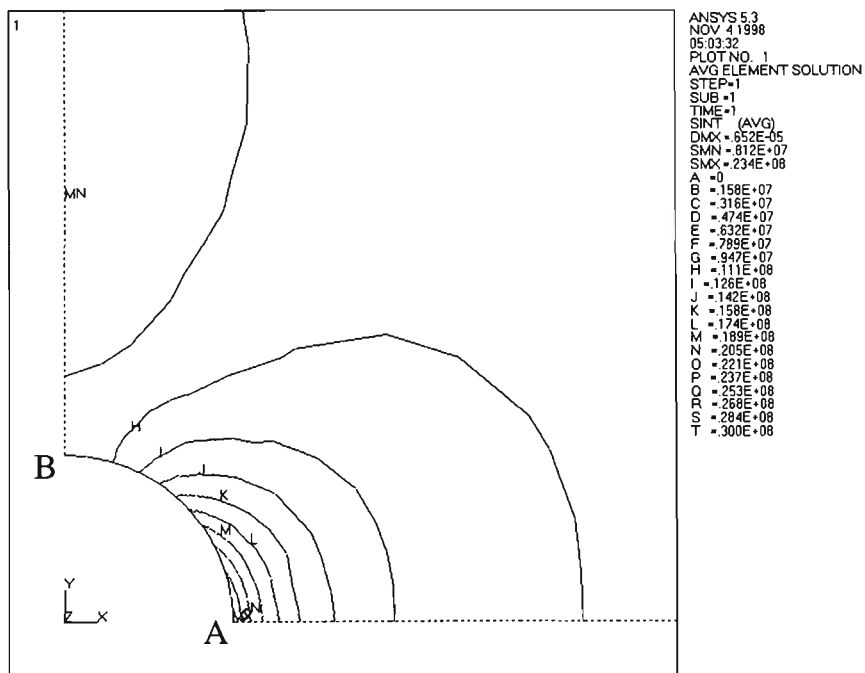
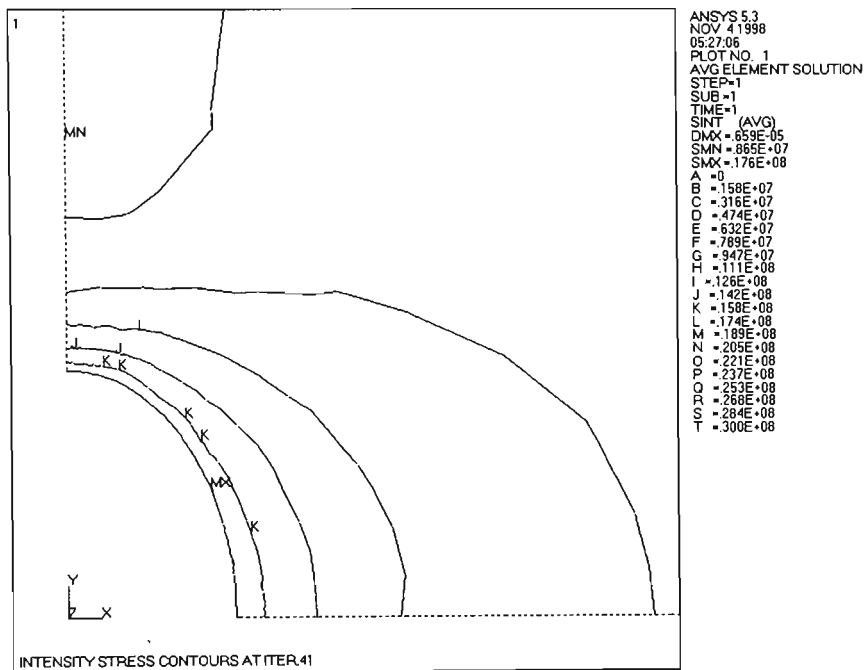


Figure 3.11: Initial Tresca stress distribution in the plate,  $S_r = 1.5$

The optimal profile was reached after 41 iterations. A drop of 24.82 percent in maximum Tresca stress was found. The standard deviation of the distribution of Tresca stress along the profile was reduced from 4.75 MPa (initial) to 0.41 MPa (optimal). The optimal profile of the hole was almost an ellipse, of which the major axis per minor axis ratio was of 1.5. Figure 3.12 shows the maximum Tresca stress distribution in the plate at iteration 41 (optimal).



**Figure 3.12:** Tresca stress distribution in the plate at iteration 41(optimal),  $S_r = 1.5$

Figure 3.13 shows the shape variation of the hole profile at a number of iterations during the optimization process: iterations 0 (initial), 10, 20 and 41 (optimal). The hole shape changed rapidly from iteration 0 (initial) to iteration 20, but then slowly to the optimal shape (iteration 41), reflecting respectively the rough cutting and fine tuning characteristics of PSM.

Figure 3.14 shows the variation of the Tresca stress with respect to the angular position at iteration 0 (initial), iteration 41 (optimal) and the optimal stress distribution

obtained by the analytical solution. The waviness of the curve corresponding to the hole boundary at iteration 41 indicates the degree of non-uniformity of the Tresca stress distribution.

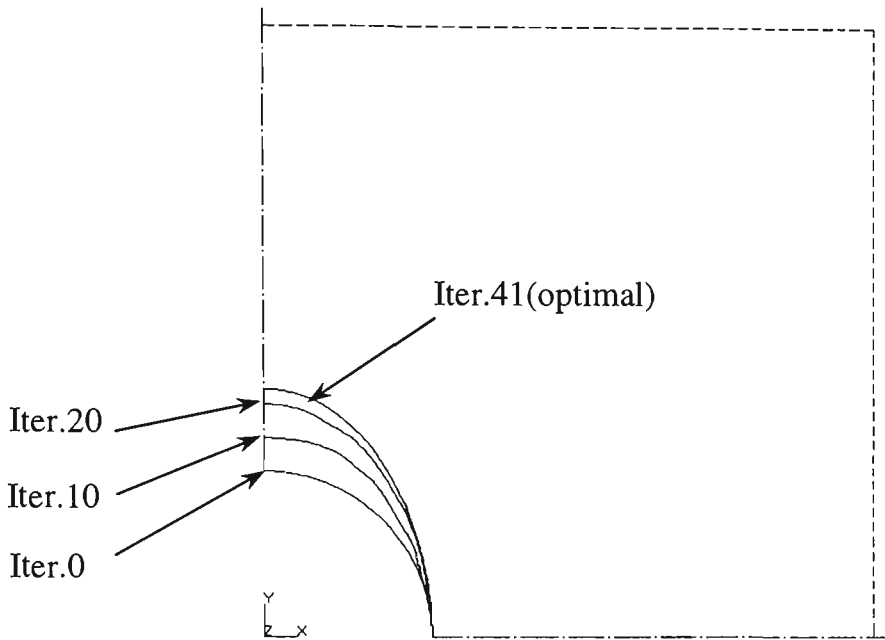


Figure 3.13: Hole shapes at iteration 0 (initial), 10, 20, and 41 (optimal),  $S_r = 1.5$

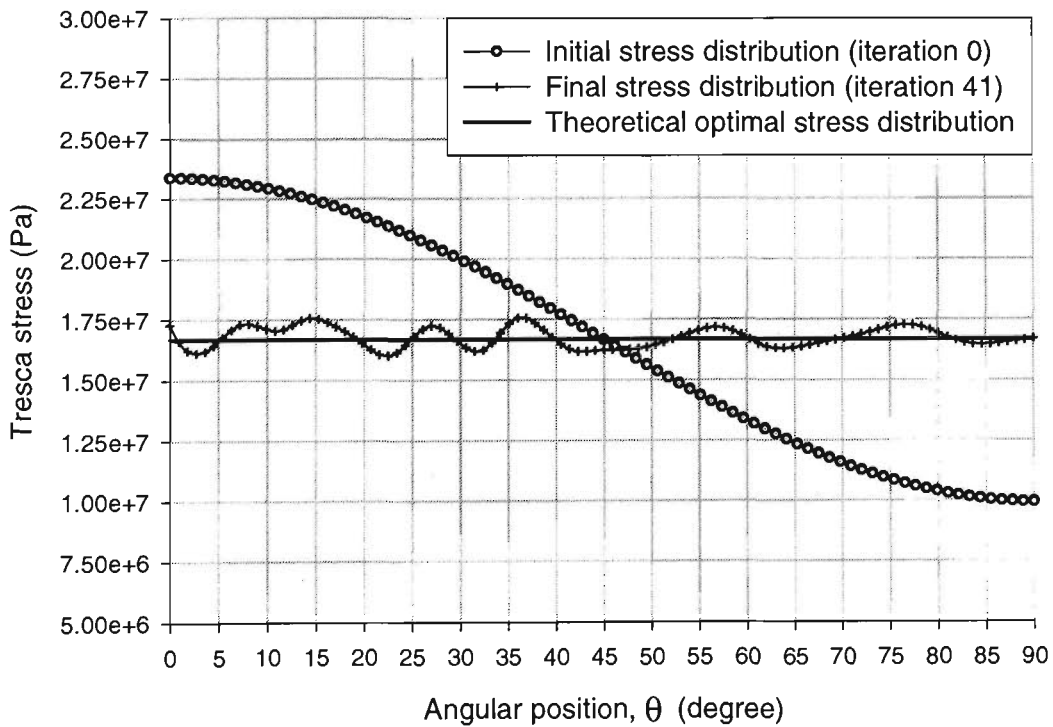


Figure 3.14: Tresca stress distribution along the hole boundary at iteration 0 (initial), 41 (optimal) and theoretical optimal stress distribution,  $S_r = 1.5$ .

Figure 3.15 shows the optimization history including the variation of the maximum-minimum Tresca stresses and material removal ratio  $m_r$  versus iteration number, where  $m_r$  is defined as the ratio of the accumulative removed area to the original hole area, it measures the saving in weight due to optimization. The graph of  $m_r$  indicates that there was a large rate of material removed at first but from iteration 20, it was gradually switched to smaller rates corresponding to the fine tuning stage of the optimization process.

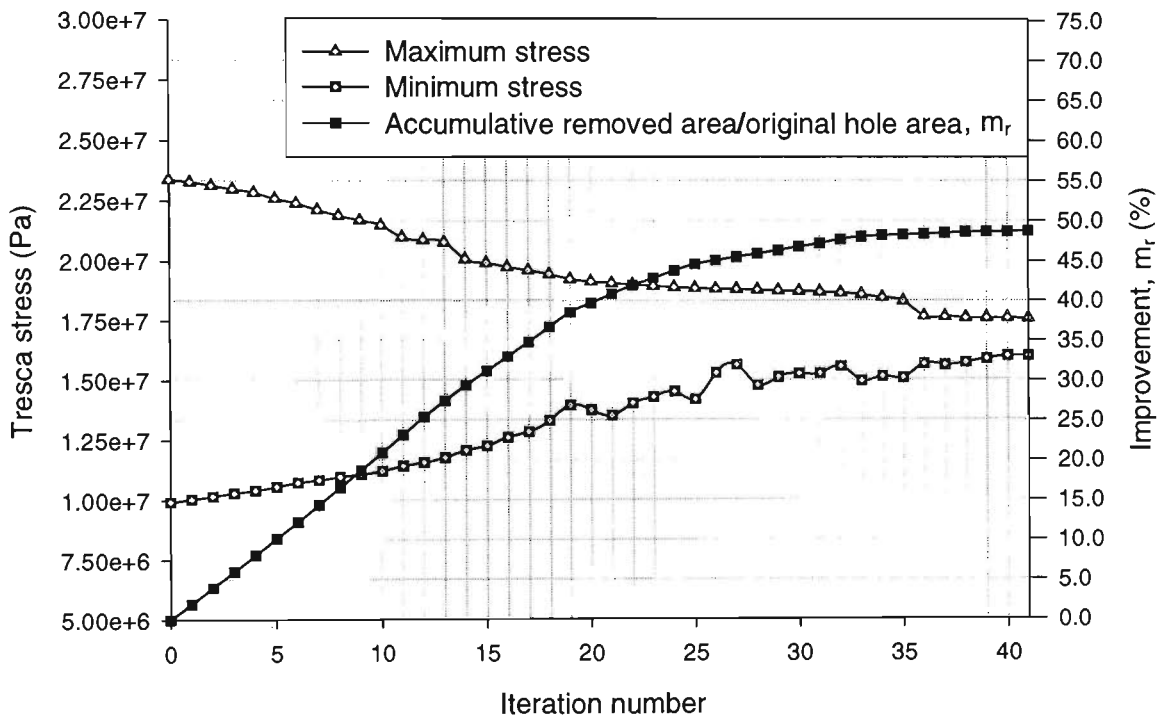


Figure 3.15: Optimization history,  $S_r = 1.5$ .

Table 3.1 shows optimal results obtained by the FEM simulation and by the analytical solution for an infinite plate.  $\sigma_{\max}$ ,  $\sigma_{\min}$ ,  $\sigma_{\text{mean}}$  are the maximum, minimum and mean values of Tresca stress distribution along the hole boundary, respectively. It can be seen that the standard deviation (STDV) of Tresca stress distribution along the hole boundary obtained by the FEM simulation is 2.5 percent in comparison to the theoretical

$\sigma_{\text{mean}}$ , indicating the proposed algorithm is capable of reaching the acceptable limits. The structural percentage error in energy norm (SEPC) (ANSYS Theory Reference, 1996) was of 0.083 % for the whole structure, ensuring the reliability of results obtained by the FEM simulation.

**Table 3.1:** Results obtained by the analytical solution and by the FEM simulation

Stress ratio, $S_r=1.5$	SEPC (%)	$\sigma_{\text{max}}$ (MPa)	$\sigma_{\text{min}}$ (MPa)	$\sigma_{\text{mean}}$ (MPa)	STDV (MPa)	STDV/ $\sigma_{\text{mean}}$ (%)
Analytical solution for an infinite plate	nil	16.67	16.67	16.67	0	0
FEM simulation	0.83E-1	17.57	16.01	16.75	0.41	2.5

### 3.3.3 Effects of the minimum number of elements removed at the fine tuning stage - $\min \{nmin(K)\}$ :

$nmin(K)$  sets the number of elements removed in each iteration in the fine tuning stage and signifies possible convergence to the optimum profile (Section 3.2.4). For the case  $S_r$  of 1.5,  $esize$  of 0.3 mm, initial  $remrate(0)$  of 0.5, the effect of minimum values of  $nmin(K)$  is shown in Table 3.2. The results in Table 3.2 were obtained by initially setting  $nmin(0)$  as 4, then reducing  $nmin(K)$  gradually from 4 to 1 by 1 after each K loop (see the FEM flowchart in Figure 3.8) within one run of the program. The structural percentage errors in energy norm (SEPC) in all cases were less than 0.1 %.

As expected, the smaller  $nmin(K)$ , the finer the cut that can be simulated i.e. the larger reduction of the maximum Tresca stress is gained but the number of iterations is increased. The STDV values are also decreased as  $nmin(K)$  is reduced.

**Table 3.2:** Effects of minimum values of  $nmin(K)$ 

Case	Min. of $nmin(K)$	Initial $\sigma_{max}$ (MPa)	Final $\sigma_{max}$ (MPa)	$\sigma_{max}$ reduction (%)	Initial STDV (MPa)	Final STDV (MPa)	SEPC (%)	Number of iteration	CPU time (min.)
1	1	23.37	17.57	24.82	4.75	0.41	0.83E-1	41	20
2	2	23.37	17.60	24.71	4.75	0.48	0.82E-1	38	18
3	3	23.37	17.67	24.40	4.75	0.57	0.69E-1	36	17
4	4	23.37	18.58	20.50	4.75	0.78	0.82E-1	33	15

### 3.3.4 Effects of element size ( $esize$ ) on the optimal solutions:

As mentioned previously, Area 1 shown Figure 3.10 was uniformly meshed with fine elements having dimension  $esize$ . For the case  $S_r$  of 1.5,  $nmin(0)$  of 4, initial  $remrate(0)$  of 0.5, the effect of  $esize$  on the optimum solutions were investigated for values of 0.20, 0.30, 0.40, 0.50 and 0.60mm. The results are tabulated in Table 3.3. The structural percentage errors in energy norm (SEPC) for all cases were less than 0.103 %.

**Table 3.3:** Effects of  $esize$ 

Case	$esize$ (mm)	Initial $\sigma_{max}$ (MPa)	Final $\sigma_{max}$ (MPa)	$\sigma_{max}$ reduction (%)	Initial STDV (MPa)	Final STDV (MPa)	SEPC (%)	Number of iteration	CPU time (min.)
1	0.2	23.49	17.48	25.59	4.80	0.29	0.85E-1	56	35
2	0.3	23.37	17.57	24.82	4.75	0.41	0.83E-1	41	20
3	0.4	23.25	17.67	24.00	4.71	0.50	0.74E-1	25	11
4	0.5	23.13	17.75	23.25	4.66	0.46	1.02E-1	20	8
5	0.6	23.02	17.69	23.15	4.62	0.49	0.92E-1	17	7

It can be seen that finer element size would result in greater reduction of stress, less fluctuation of Tresca stress distribution along the hole boundary i.e. smaller standard

deviation (STDV) obtained, but as expected it requires more iteration steps to converge and the computation cost is increased substantially. The increase of computation cost was mainly due to larger numbers of elements as smaller *esize* is used.

### 3.3.5 Effects of the initially set element removal rate - $remrate(0)$

$remrate$  dictates how many elements out of all external elements on the current boundary of the discontinuity are selected for removal.  $remrate(0)$  initially can be set at a value between 0 and 1. It is controlled and is continually reduced during the course of optimization every time an over-cutting occurs (Section 3.2.4).

For the case  $S_r$  of 1.5,  $nmin(0)$  of 4, minimum value of  $nmin(K) = 1$ , *esize* of 0.30 mm, effects of initial  $remrate(0)$  values were investigated by running the program for seven sets of  $remrate(0)$  at: 0.1, 0.2, 0.3, 0.4, 0.5, 0.6 and 0.7 respectively. The results are shown in Table 3.4.

**Table 3.4:** Effects of  $remrate(0)$

Case	1	2	3	4	5	6	7
$remrate(0)$	0.1	0.2	0.3	0.4	0.5	0.6	0.7
Number of iteration	107	61	42	38	33	32	34
CPU time (min.)	46	24	17	16	15	16	20
Final $\sigma_{max}$ (MPa)	18.74	18.62	18.98	18.67	18.58	18.56	18.83

It can be seen that for the cases 1, 2, 3, 4, 5, the number of iterations and running time decreased with larger setting of  $remrate(0)$  as expected. However, when  $remrate(0)$  was set at a value larger than or equal 0.5, the running time starts to increase while the

number of iterations slightly varies.

It should be noted that for the same *esize* and shape, a larger value of *remrate(0)* results in a coarser cut (see Figure 3.3). For this structure a value of *remrate(0)*, which is larger than or equal 0.6, results in cuts so coarse that they cause over-cutting. The process has to reduce element removal rate to smaller values, which increases processing time. Thus, a too small or too large initial setting of *remrate(0)* can result in a longer process. A too small value of *remrate(0)* can however substantially increase time and should be avoided.

### 3.3.6 Effects of stress ratio ( $S_r$ )

Effects of the applied stress ratios to the optimization process are studied in this section. Three cases of stress ratios,  $S_r$  of 1.5, 2, 2.5, were investigated. Parameters were set as follows: *nmin(0)* of 4, *remrate(0)* of 0.5, *esize* of 0.4mm. Different optimum profiles for stress ratio values of 1.5, 2 and 2.5 are illustrated in Figures 3.16, 3.17 and 3.18 respectively. The results are tabulated in Table 3.5, including analytical solutions for an infinite plate.

**Table 3.5:** Effects of stress ratio ( $S_r$ )

Case	$S_r$	Initial $\sigma_{\max}$ (MPa)	Final $\sigma_{\max}$ (MPa)	$\sigma_{\max}$ reduction (%)	Initial STDV (MPa)	Final STDV (MPa)	SEPC (%)	No. of iter.	CPU time (min.)	Analytical Solution	
										Initial $\sigma_{\max}$ (MPa)	Final $\sigma_{\max}$ (MPa)
1	1.5	23.25	17.67	24.00	4.71	0.50	0.74E-1	25	11	23.33	16.67
2	2.0	24.92	16.17	35.09	7.06	0.39	1.03E-1	47	22	25.00	15.00
3	2.5	25.92	15.35	39.59	8.47	0.54	0.98E-1	70	28	26.00	14.00

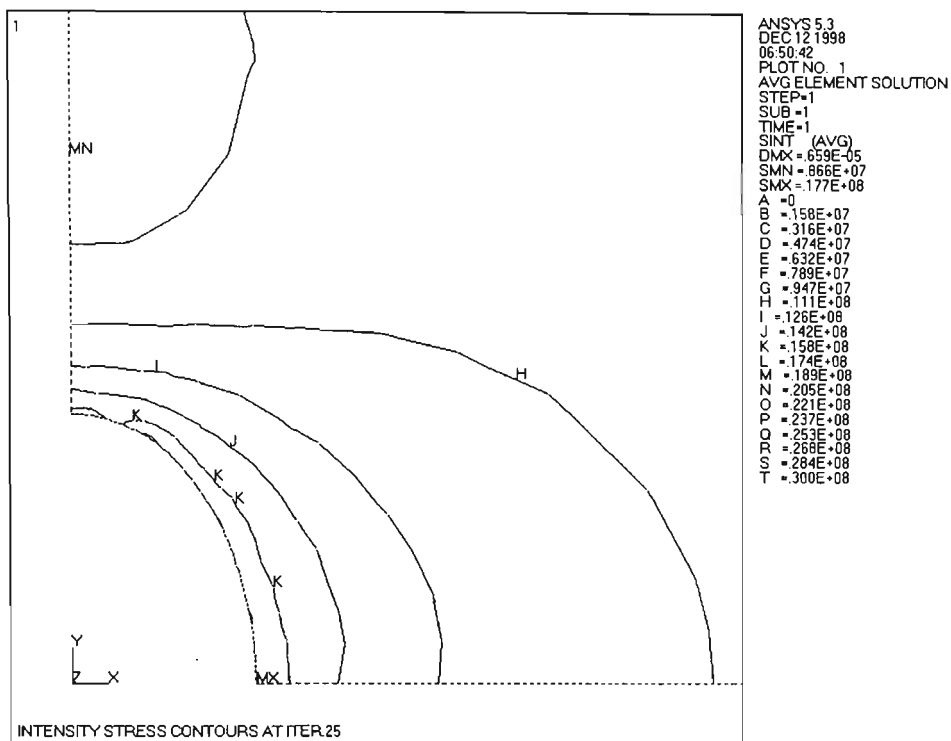


Figure 3.16: Effects of stress ratio,  $S_r = 1.5$

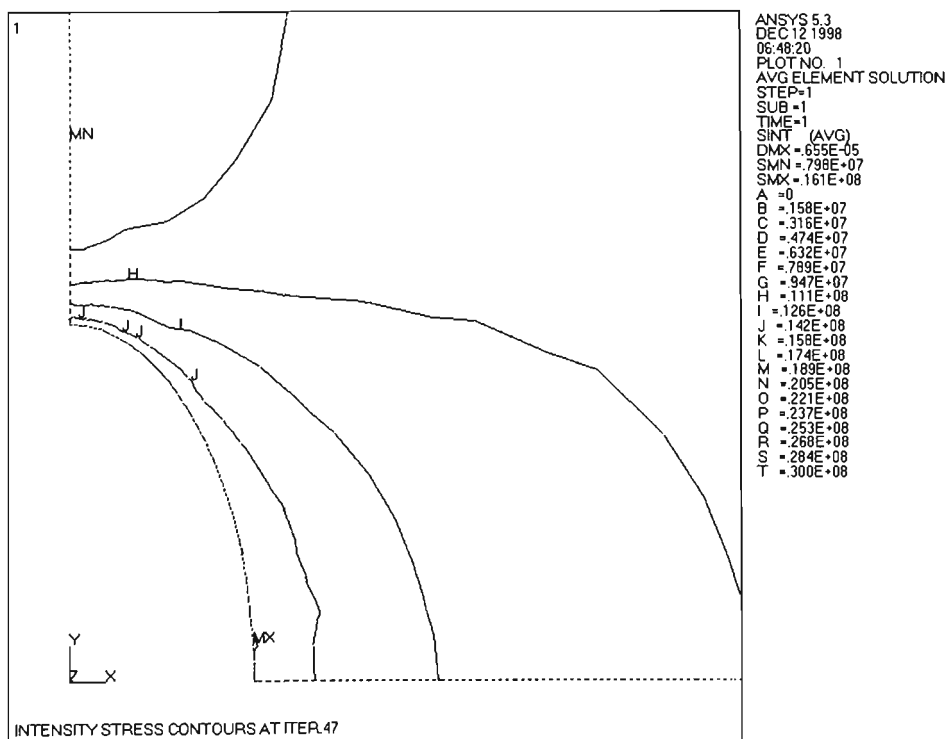
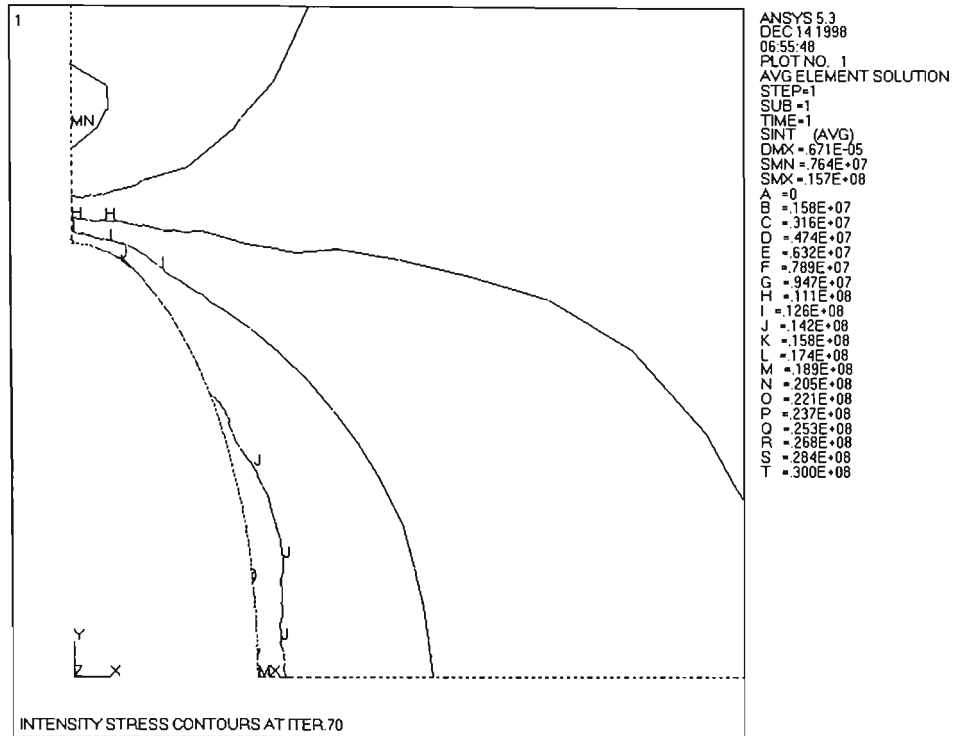


Figure 3.17: Effects of stress ratio,  $S_r = 2.0$



**Figure 3.18:** Effects of stress ratio,  $S_r = 2.5$

The optimal hole shapes obtained are almost ellipses as predicted by the analytical solution. It can be seen that larger stress ratios result in greater rewards, i.e. larger reduction in stress concentration and larger savings in material can be obtained by shape optimization. As  $S_r$  is increased, the major axis of the hole is increased or the hole becomes elongated. However the FEM simulation requires more iteration steps.

### 3.4. Concluding remarks

It can be seen that a practical algorithm, incorporating boundary smoothing and remeshing subroutines as proposed can simulate the PSM procedure.

The boundary smoothing subroutine adopting cubic B-spline curves can produce smooth boundaries with least oscillatory shapes. The use of B-spline boundary

representation and primary moving control points based on the simple approximation, Equations (3.1) and (3.2), simulates successfully material removal mechanism of the PSM procedure.

By employing the design element concept with automatic mesh generators and adaptive mesh refinement, the mesh distortion problems can be avoided. It also reduces the computation efforts required in adaptive mesh refinement.

The proposed algorithm has been applied to find optimal hole profiles in homogeneous isotropic plates under biaxial tensions. The excellent agreement between results found by the FEM simulation and the closed-form theoretical solutions validates the feasibility of the proposed algorithm to simulate the PSM by FEM. The study of the effects of parameters given in Section 3.3 highlights the influence of the initial values of parameters on the convergence of the optimization process.

In practice, a completely constant maximum shear stress distribution along a profile cannot always be obtained due to the existence of zero stress points on the boundaries of the optimized profile. There are usually sections of the discontinuities under tension and compression stresses; these sections are joined together by zero stress points which exist during the course of optimization. Such problems require more attention as presented in the next chapter.

## Chapter 4

# OPTIMAL STRESS RAISER PROFILES CONTAINING ISOTROPIC POINTS

### 4.1. Introduction

The optimal solution, which can result in a completely constant shear stress distribution along a discontinuity profile, as in the case of a large plate with a hole under biaxial tensions, exists only in rare cases (Schnack 1979).

Optimal solutions that result in profiles, sections of which are under compression and tension, are more generally found in technically interesting problems. Those sections are joined together by *isotropic points* of zero stress, separating a tensile stress section from a compressive stress one. They are always present in the course of optimizing the structures given below. The existence of such points prevents the optimization process not only from obtaining a completely constant stress distribution over the stress raiser boundary, but from eventually converging toward the optimal profile. The proposed FEM simulation algorithm (Section 3.2) therefore requires additional characteristics to solve

these optimization problems properly.

Two typical examples of such problems are:

- (i) A large plate with a hole under biaxial stress with negative stress ratios;
- (ii) A finite width plate with a hole under uniaxial tension.

While the second case has been studied by various researchers e.g. Durelli and Rajaiiah (1979), Snack (1979), and Tran and Nguyen (1999), to the author's knowledge the first optimization problem has not been investigated so far.

#### **4.2 A large plate with a hole under biaxial stress with negative stress ratios**

Let us consider a large plate with a hole under biaxial stress. If the applied stress ratio is negative there will be sections of the boundary of stress raisers under tension and compression. A typical case when the applied stress ratio takes the value of minus one ( $S_r = -1$ ) is studied first.

Using the same notation as presented in Section 3.3.1, the applied stress  $\sigma_y$  along Y-axis is kept constant for all cases at 10 MPa. The other applied stress  $\sigma_x$  along X-axis is determined from  $\sigma_y$  and the stress ratio  $S_r$  (Equation 3.7). For cases that  $S_r \leq -1$ , the absolute value of  $\sigma_x$  is always kept equal or smaller than  $\sigma_y$ . Consequently the stress concentration factor  $k_{biax}$  determined by Equation (3.8) is still valid. Due to the relationship between the maximum Tresca stress and the stress concentration factor (Equation 3.9), the reduction of the maximum Tresca stress also reflects the decrease in the stress concentration factor and can be used to present results obtained by the FEM simulation in this section.

### 4.2.1 Optimal hole profile when $S_r = -1$

The initial stress pattern in the plate is illustrated in Figure 4.1 using a quarter FEM model since this is a symmetrical structure. It can be seen that:

- The maximum stress occurs at points such as point A and B with a very steep stress gradient around them.
- Points such as point C are positions of zero stress with a very steep stress gradient around them. It should be noted that isotropic points of zero stress are confirmed by theoretical solutions and the photoelasticity technique. However due to the finite size of elements, exact zero stress is not found by FEM at points like point C. For example, in this case the maximum stress at point A and B is found to be 40.9 MPa and the minimum stress found at point C ( $\theta = 45^\circ$ ) is 0.81 MPa.

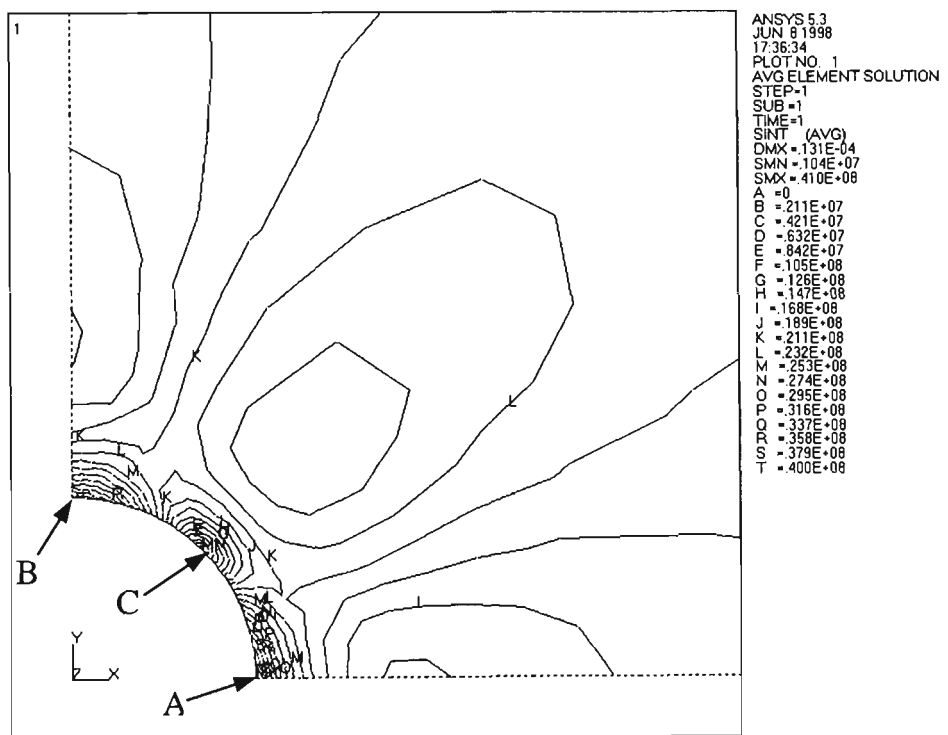


**Figure 4.1:** Initial Tresca stress distribution,  $S_r = -1$

- Instability (buckling) could be a factor in the response of the plate, but it is not considered here in finding the optimal profiles.

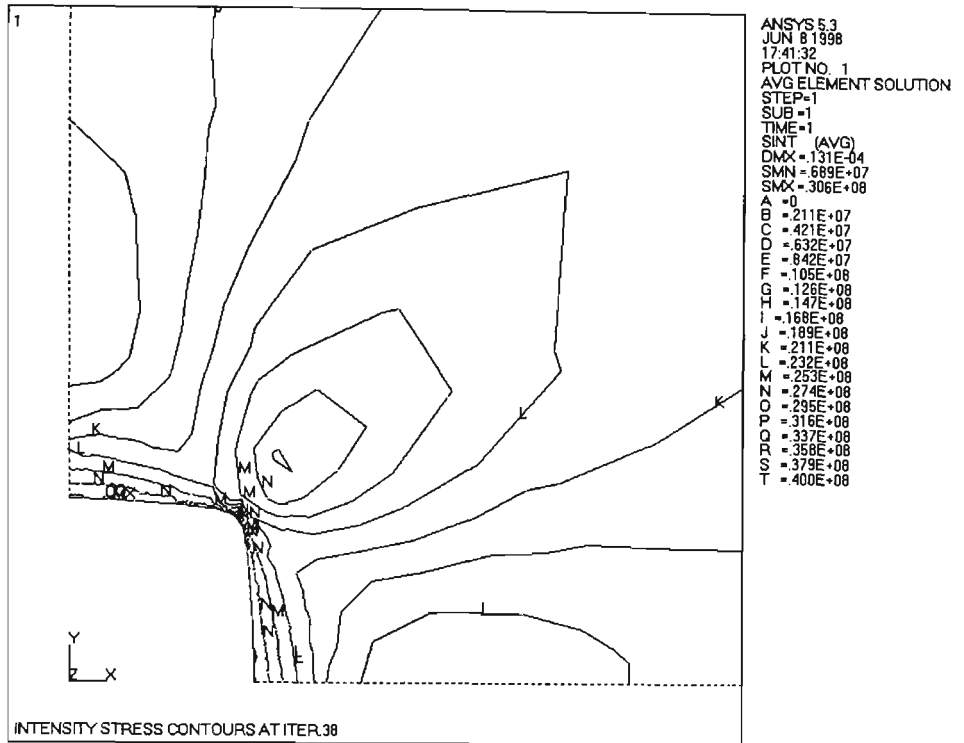
The structure is now optimized, employing the FEM simulation algorithm proposed in Section 3.2.4. Parameters are initially set as follows:  $esize = 0.3\text{mm}$ ,  $nmin(0) = 4$ ,  $remrate(0) = 0.7$ .

The required standard deviation is set to zero so that the process can produce the best possible outcome. The optimization process converged after 38 iterations and a decrease of 24.9 percent in the maximum Tresca stress was found. The stress pattern in the plate and Tresca stress distribution along the stress raiser profile against angular positions at iteration 38 are shown in Figures 4.2a, b respectively. It can be seen that:

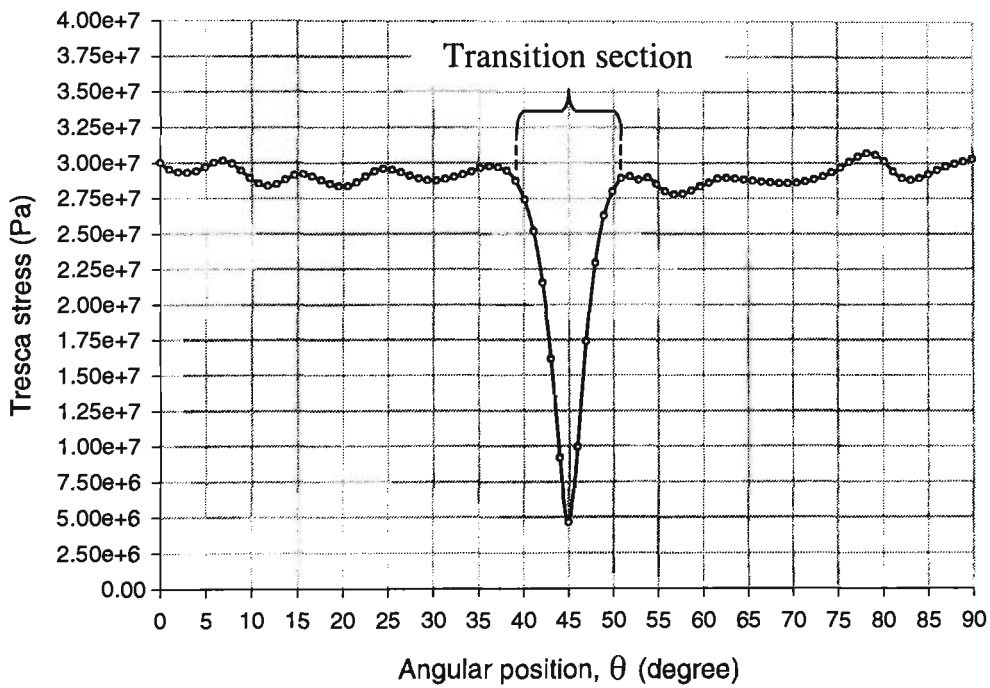
- The vertical and horizontal edges are under almost uniform Tresca stresses.
- There is a very steep stress gradient around the isotropic point (point C), of which the angular position  $\theta$  is about  $45^\circ$ . The isotropic point lies on the transition section of the hole boundary ( $38^\circ < \theta < 52^\circ$ ), where the stress reverses from tension (vertical edge) to compression (horizontal edge).

#### **4.2.2 FEM algorithm improvement in the fine tuning stage**

Inspecting the log file of the optimization process, however, reveals that there was no further improvement obtained when the process was switched to the fine tuning stage. This is influenced by the existence of the transition section mentioned above. It should be noted that the process starts the very fine tuning stage with a few elements having lower stress values in the set *Ext\_elem* to be removed in each iteration. Thus the elements



(a)



(b)

**Figure 4.2:** a- Tresca stress distribution in the plate at iteration 38,  $S_r = -1$ ;  
 b- Stress distribution along the hole boundary versus angular position at iteration 38,  $S_r = -1$ .

selected for removal would be neighbors of the isotropic points, lying on the transition sections (Figure 4.2b). However, any attempt to remove elements at these corners will make the maximum Tresca stress increase as recorded. The process therefore keeps on reducing continually the number of elements to be removed until the process converges without further improvements. As shown in Table 4.1, the process began the very fine tuning stage with four elements, and ended with one element to be removed in each iteration without the reduction of the maximum Tresca stress as compared to that obtained at iteration 38.

**Table 4.1:** effects of removing elements lying on the transition section

Number of elements to be removed	Observed $\sigma_{\max}$ (MPa)	$\sigma_{\max}$ (MPa) at iteration 38
4	30.7117	30.6924
3	30.7300	
2	30.7259	
1	30.6981	

In a PSM procedure, at the fine tuning stage the operator can easily detect those transition sections by observing directly the isochromatic fringe orders. He then only files away lower stressed materials by moving back and forth from one section to the other of the boundary, but not the transition sections, until the uniformity of stress distribution is satisfied. Thus at this stage, the material to be removed is no longer at the location of the minimum Tresca stress occurring on the stress raiser boundary. This can be implemented in the FEM simulation by defining elements lying on the transition sections as non-design elements or excluding them from the set *Ext\_elem* that contains candidates for the element removal at the fine tuning stage.

In order to incorporate the above characteristic into the FEM simulation algorithm proposed in Section 3.2, a protection scheme for transition sections should be added to steps 13 and 16 of the flowchart shown in Figure 3.8. The modified flowchart is shown in Figure 4.3. The protection scheme includes:

- Determining isotropic points of zero stress lying on the boundary.
- Identifying small sections with very steep stress gradient locating next to the isotropic points, i.e. transition sections (Figure 4.2b).
- Excluding elements lying on the transition sections from the set *Ext\_elem*.

At steps 13 and 16 of the modified algorithm, if there are no isotropic points detected, the process then bypasses the protection scheme. Thus the new algorithm is also applicable to the case which results in a completely constant stress distribution along a discontinuity.

The structure in the example given above ( $S_r = -1$ ) is now re-optimized employing the modified algorithm with new added features. All optimization parameters were set at the same values as those in the previous run. The new process converged after 42 iterations and a decrease of 25.2 percent in the maximum Tresca stress was found.

Compared to the result obtained by the original algorithm in Section 4.2.1, the new optimization process took a further 4 iterations and a further decrease of 0.3 percent in the maximum Tresca stress was obtained. Figure 4.4 illustrates the maximum Tresca stress distribution in the plate at iteration 42 (optimal) produced by the improved algorithm.

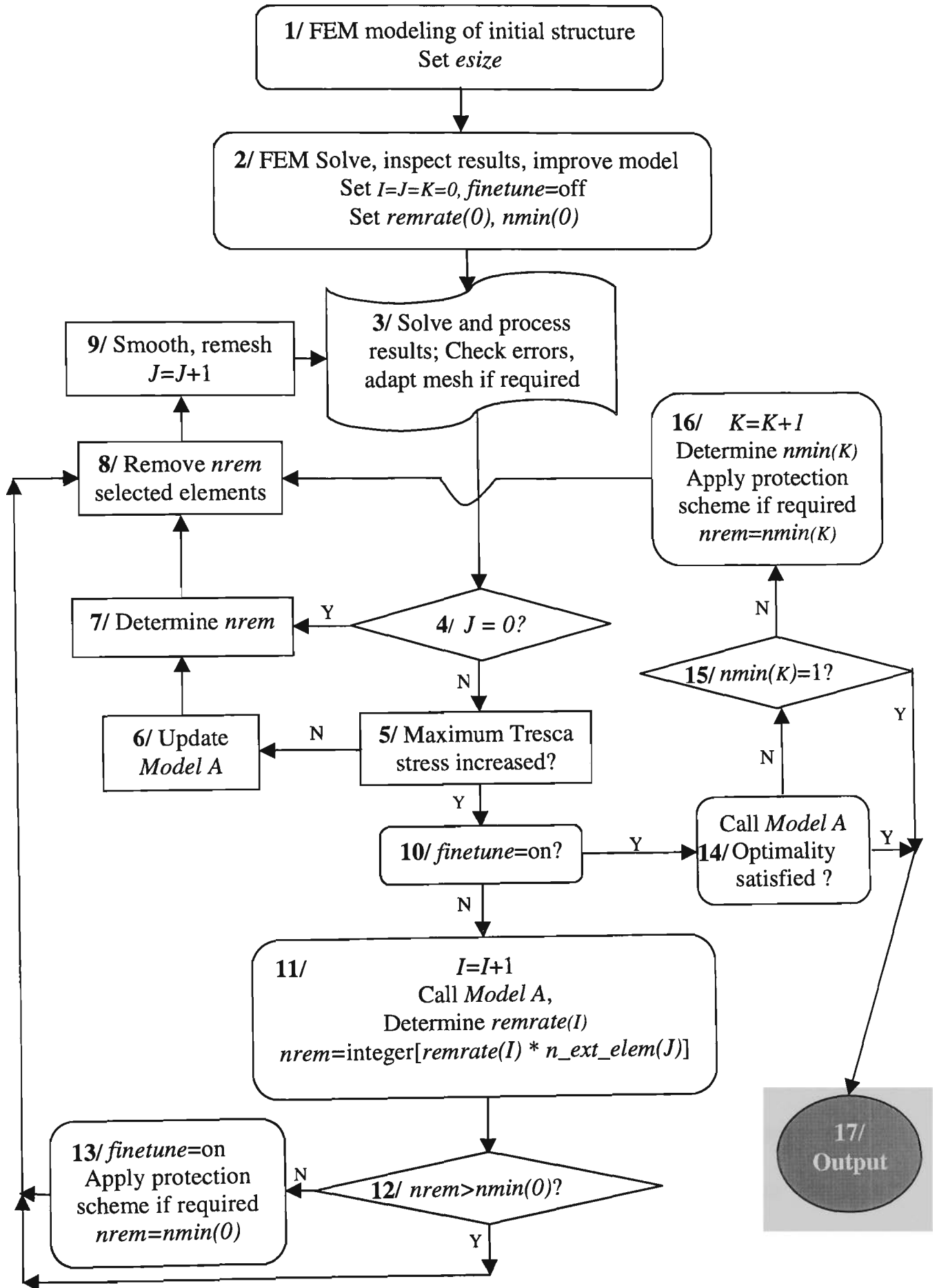


Figure 4.3: Flowchart of the improved FEM simulation algorithm

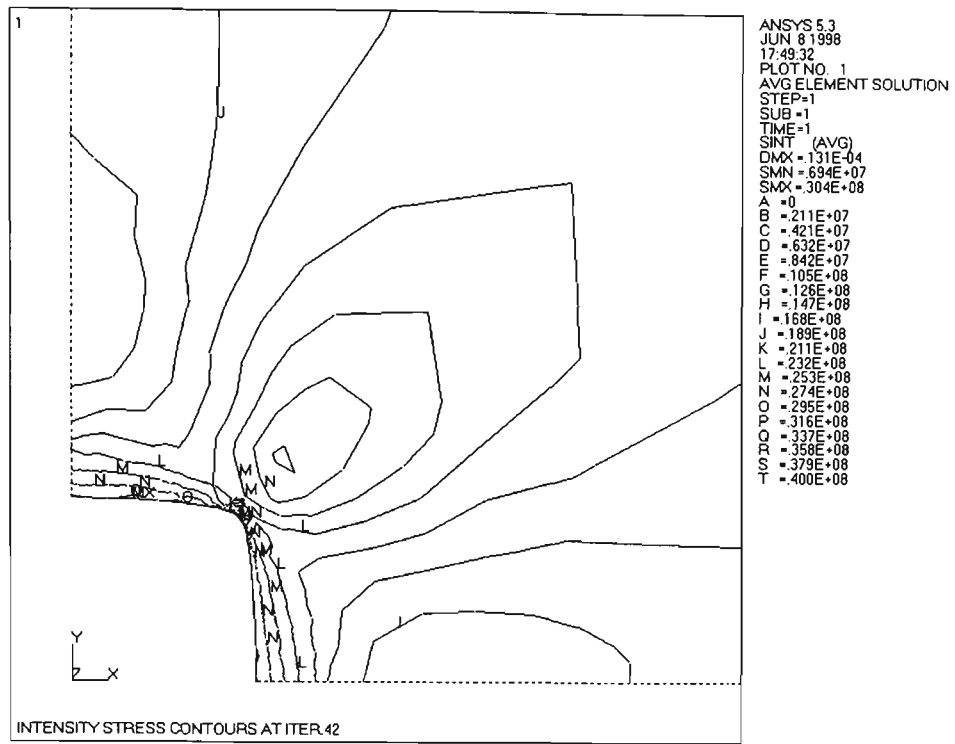


Figure 4.4: Tresca stress distribution at iteration 42 (optimal), case  $S_r = -1$ .

Figure 4.5 shows the hole shape variation at a number of iterations during the optimization process: iterations 0 (initial), 10, 20, 42 (optimal). The hole shape was changed very fast from iteration 0 (initial) to iteration 10, slower from iteration 10 to iteration 20, then slowly to the optimal shape (iteration 42), reflecting rough cutting and fine tuning characteristics of the PSM.

Figure 4.6 shows the optimization history including the variation of the maximum Tresca stresses and the material removal ratio  $m_r$  versus iteration number. The graph of  $m_r$  indicates that there is a large rate of material removed at first, then it is gradually reduced to smaller rates until the process converges. The maximum Tresca stress is decreased quickly in the first five iterations, slower until iteration 27, then very slowly until the process converges. The minimum Tresca stress occurring on the boundary is not plotted since its values are always near zero during the optimization process.

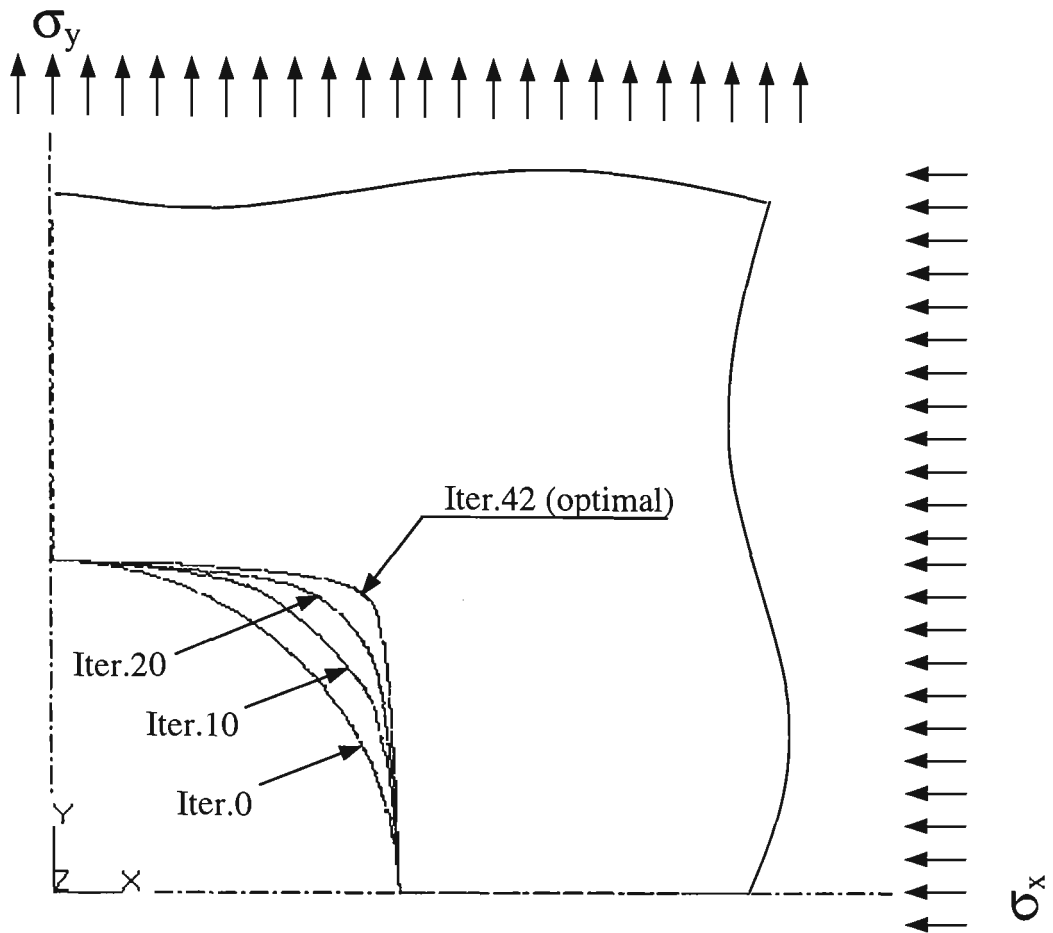


Figure 4.5: Hole shapes at iterations 0(initial), 10, 20 and 42 (optimal), case  $S_r = -1$ .

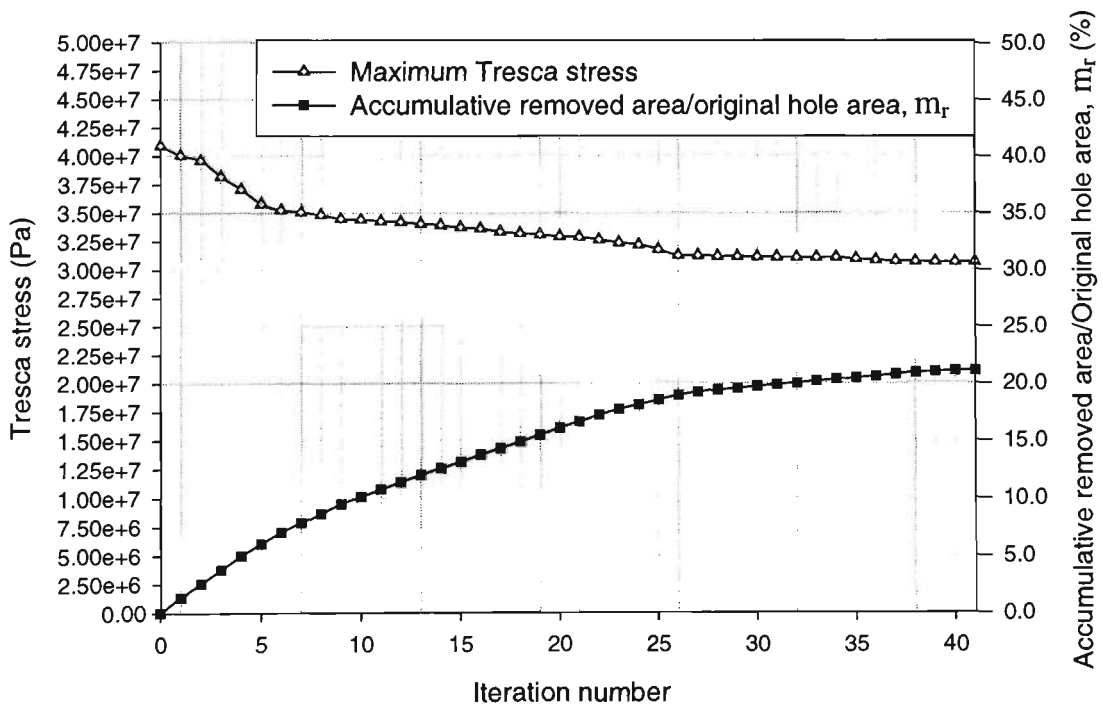


Figure 4.6: Optimization history,  $S_r = -1$

### 4.2.3 Results and discussion

Two additional cases of stress ratios  $S_r$  of -1.5 and -2.0 were investigated, employing the improved algorithm. Parameters were set at the same values as in the case  $S_r$  of -1 (Section 4.2.1). Different optimal profiles for stress ratio values of -1.5 and -2.0 are illustrated in Figures 4.7 and 4.8 respectively.

The results for three cases  $S_r$  of -1, -1.5 and -2.0 are tabulated in Table 4.2. It can be seen that larger absolute values of stress ratios result in greater rewards, i.e. larger reduction in stress concentration, larger savings in material can be obtained, and more iterations are required.

**Table 4.2:** Effects of negative stress ratios ( $S_r < 0$ )

Case	$S_r$	$esize$ (mm)	Initial $\sigma_{max}$ (MPa)	Final $\sigma_{max}$ (MPa)	$\sigma_{max}$ reduction (%)	Initial STDV (MPa)	Final STDV (MPa)	Hole area increase (%)	SEPC (%)	Number of iteration	CPU time (min.)
1	-1.0	0.3	40.92	30.61	25.20	12.56	4.31	21.17	0.48	42	18
2	-1.5	0.3	37.42	26.39	29.48	10.77	2.96	58.69	0.21	56	29
3	-2.0	0.3	35.56	24.37	31.47	10.12	2.41	103.46	0.37	82	44

The optimal hole shapes obtained were no longer ellipses but more like quadrangle holes with rounded corners as illustrated in Figure 4.9. As the absolute value of the stress ratio was increased, the major axes of the holes were increased or the holes become elongated. It is interesting to note that starting from the case  $S_r$  of -1, while the absolute values of stress ratios were increased at intervals of 1/2, the optimal holes' lengths were increased approximately with intervals of 1/3.

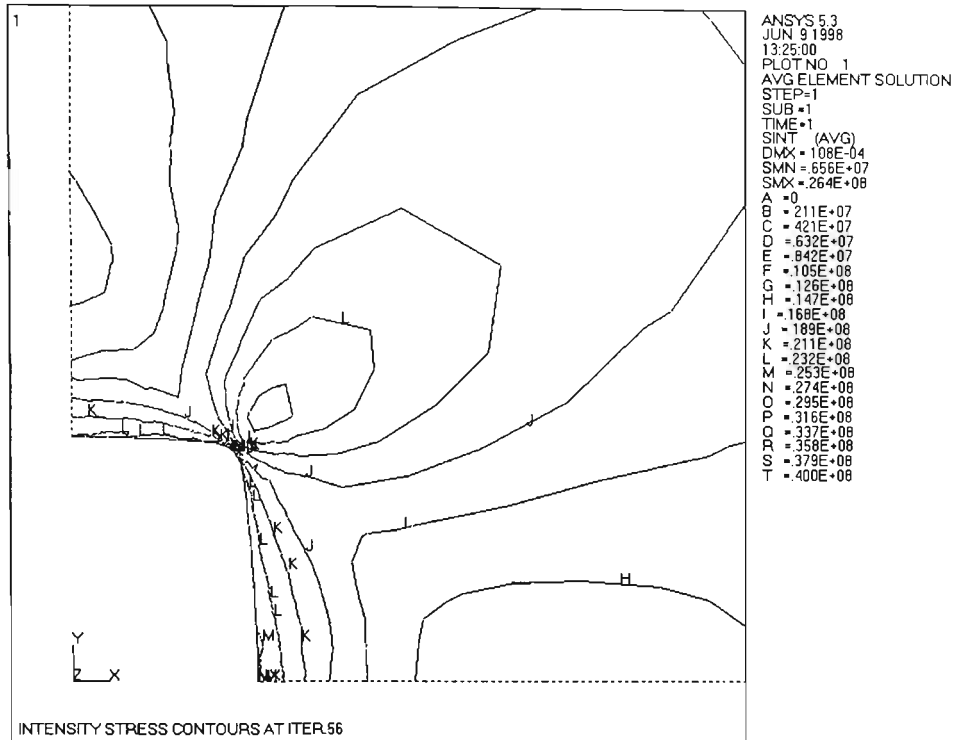


Figure 4.7: Optimal hole profile, case  $S_r = -1.5$

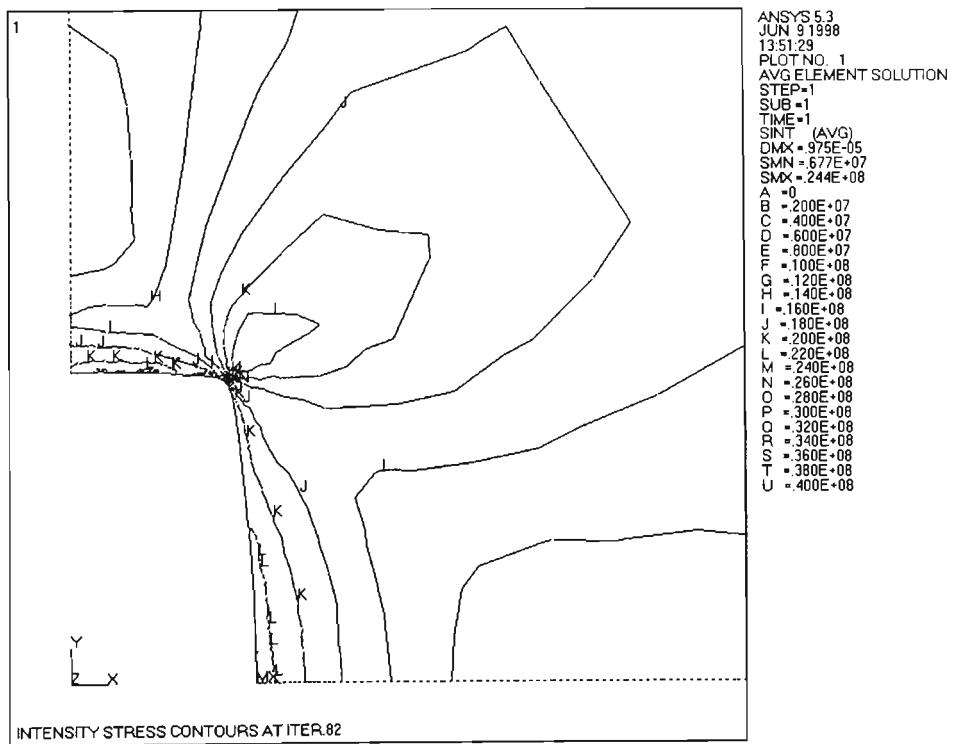
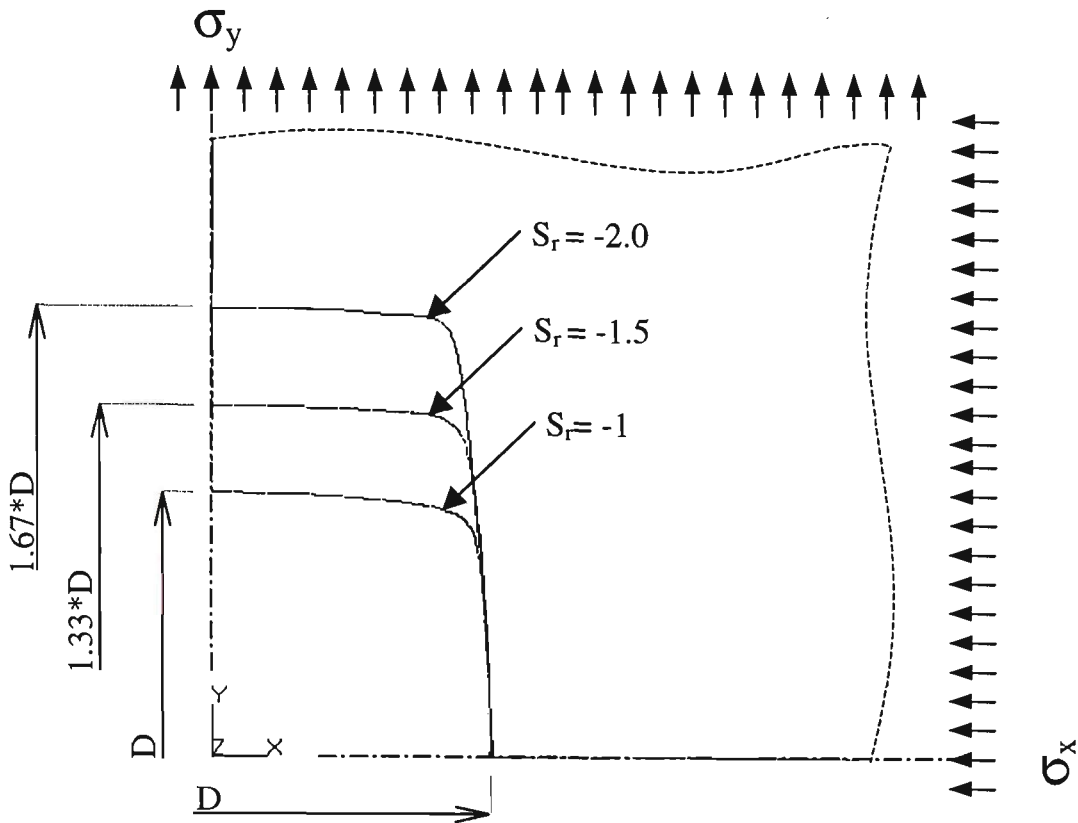


Figure 4.8: Optimal hole profile, case  $S_r = -2.0$



**Figure 4.9:** Various optimal hole profiles with different negative stress ratios, where  $D$  is the diameter of the initial circular hole

### 4.3 Finite width plates with holes under uniaxial tensions

Plates of finite width with holes are common structural elements in many engineering applications. The analytical solution for the stress distribution of an infinite plate with a circular hole under uniaxial stress was given by Howland (1929-30). This solution can be used for a plate of finite width and with the ratio of hole diameter to width  $D/W$  up to 0.55, Peterson (1953). For finite plates of higher  $D/W$ , the determination of the stress concentration factor must rely on experimental techniques such as photoelasticity or on computational methods, mainly FEM.

Durelli and his associates have used PSM to study this problem extensively and it has served as a benchmark for various shape optimization techniques.

### 4.3.1 Problem description

The structure investigated is a thin plate of constant thickness  $T$ , of finite width  $W$  with a central circular hole of diameter  $D$ , under uniform axial stress as shown in Figure 4.10. Its length  $L$  is supposed to be sufficiently long with respect to  $D$  so that the upper and lower edge boundary conditions do not affect the stress distribution around the hole and hence the optimal profile. The stress concentration effect can be expressed in terms of  $K_{tg}$  or  $K_{tn}$ . These notations are adopted from Pilkey (1997) where  $K_{tg}$  is the stress concentration factor based on the gross cross section and  $K_{tn}$  is the stress concentration factor based on the minimum net cross section. A graph of  $K_{tg}$  and  $K_{tn}$  (based on FEM results) versus  $D/W$  is shown in Figure 4.11, where it can be seen that the highest value of  $K_{tn}$ , is 3 for an infinite plate, the limiting value of  $K_{tn}$ , when  $D/W$  tends to 1 has been confirmed as 2 by Parks (1975).

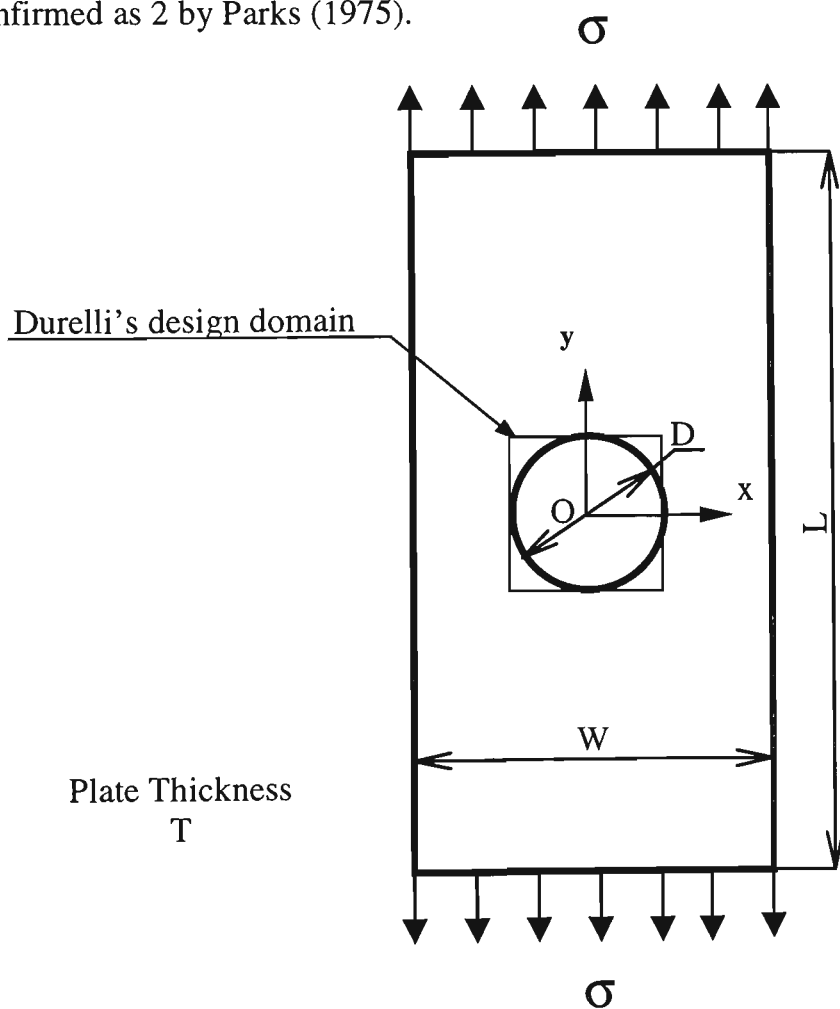


**Figure 4.10:** Problem description

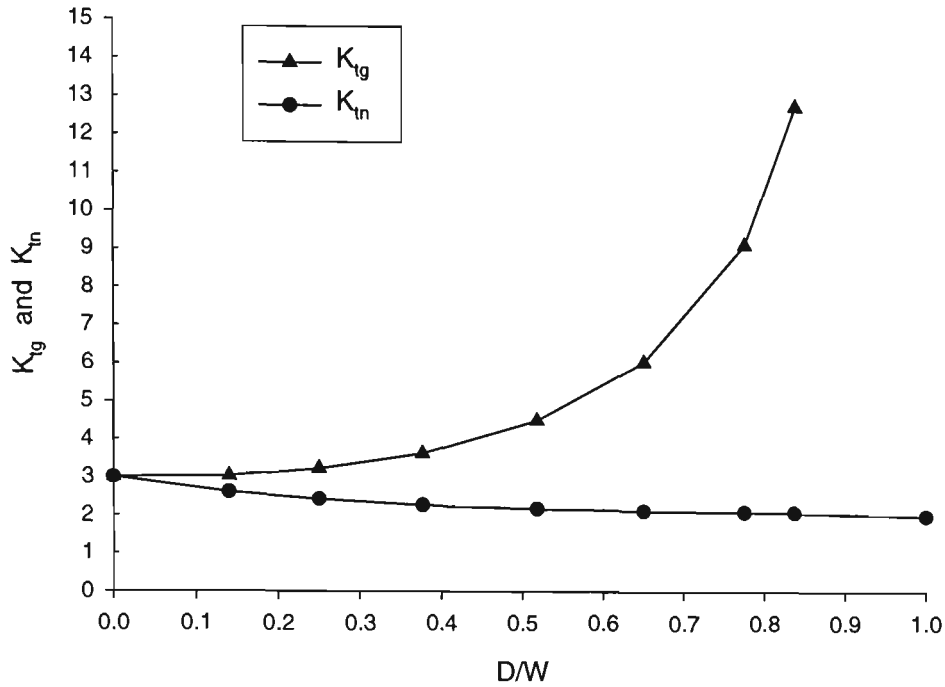


**Figure 4.11:**  $K_{tg}$  and  $K_{tm}$  versus  $D/W$

The task is to find the optimal hole profile to reduce  $K_m$  for an initial circular hole of various  $D/W$  ratios, from 0.140 to 0.837 such that the maximum stress occurring at points on the hole boundary is minimized. The design domain of the problem is the region around the hole boundary limited to within a square of side  $D$ . The problem has been investigated experimentally by Durelli and Rajaiah (1979) and numerically by Tran and Nguyen (1999).

It should be noted that the choice of the design domain by Durelli and Rajaiah (1979) was probably due to practical requirements since the optimum profiles do depend on the length of the design domain along the plate axis. As the hole profile is a free boundary, the Tresca or von Mises criterion leads to the same equivalent stress. To facilitate the comparison of results of different cases of  $D/W$ , the width  $W$  was fixed and the applied tensile stresses were also of fixed value  $\sigma$  as illustrated in Figure 4.10.

The optimization was carried out on a plate of dimensions  $W = 100\text{mm}$ ,  $L = 300\text{mm}$ ,  $T = 1\text{mm}$ , for the  $D/W$  ratios of 0.140, 0.250, 0.377, 0.518, 0.650, 0.775, and 0.837. The Young's modulus was assumed to be of 205 GPa, Poisson ratio was assumed to be of 0.3 and the applied loads were assumed to be uniform tensions of 10 MPa.

Due to symmetry, a quarter of the plate was modelled as illustrated in Figure 4.12. The initial Tresca stress pattern of a typical case when  $D/W = 0.837$  is shown in Figure 4.13. It can be seen that:

- The maximum stress occurs at points such as point 1 in Figure 4.13 with a very steep stress gradient around it.
- Points such as point 2 in Figure 4.13 are positions of isotropic points of zero stress.

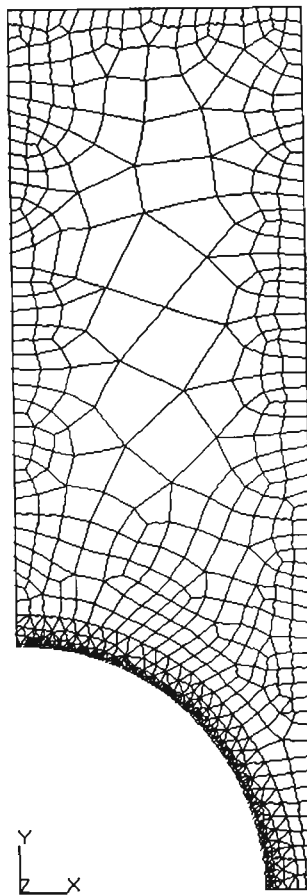


**Figure 4.12:** FEM model ( $D/W=0.837$ )

- Besides these isotropic points, there are nearby regions of relative low stress values (region 3, Figure 4.13). This implies that if Durelli's design domain is not imposed and elements are not removed in layers, there is a possibility of encroaching on regions like region 3, resulting in an unstable sudden "avalanche" of removed elements as reported by Tran and Nguyen (1998a).

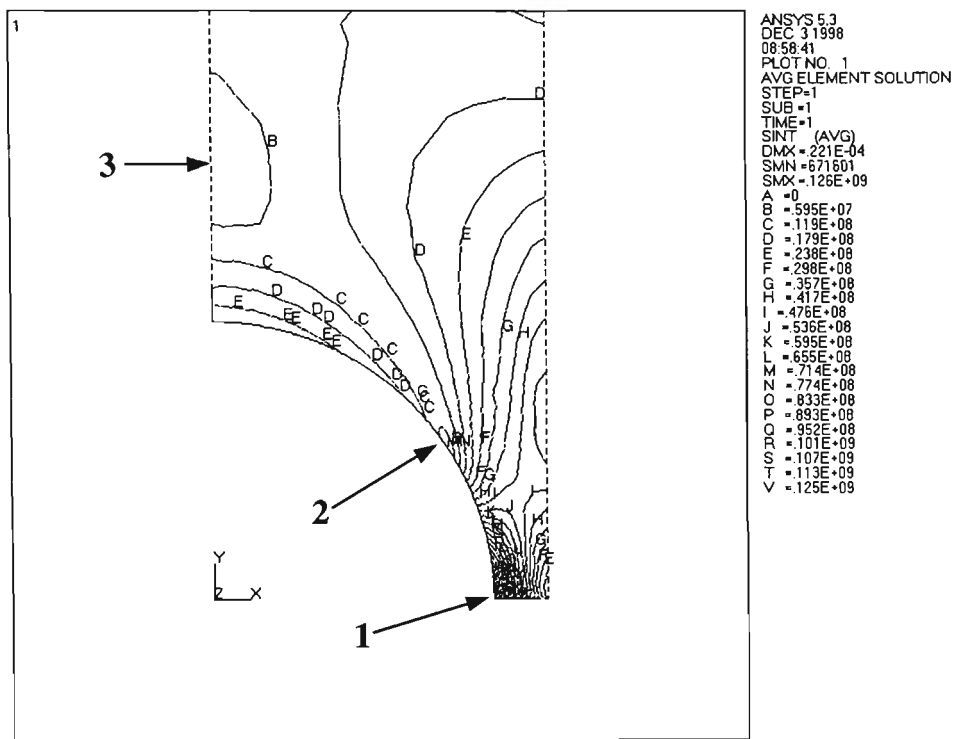


**Figure 4.13:** Initial Tresca stress distribution in the plate ( $D/W = 0.837$ )

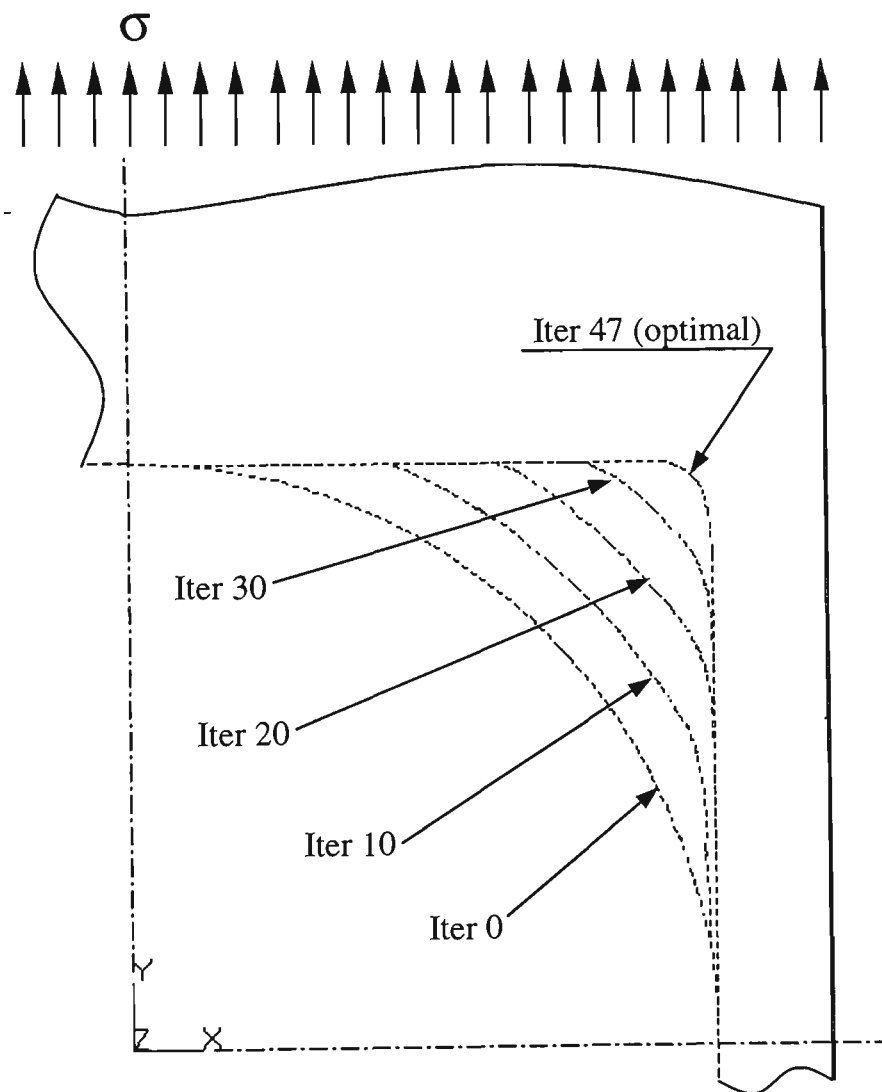
### 4.3.2 Results and discussion

The structure is now optimized, employing the modified FEM simulation algorithm (Section 4.2.2). For all cases studied in this section, parameters were initially set as follows:  $remrate(0) = 0.7$ ,  $nmin(0) = 4$ .

Settings of  $esize$  are given in Table 4.3. The required standard deviation was set to zero to produce the best outcome. The number of primary control points used to represent

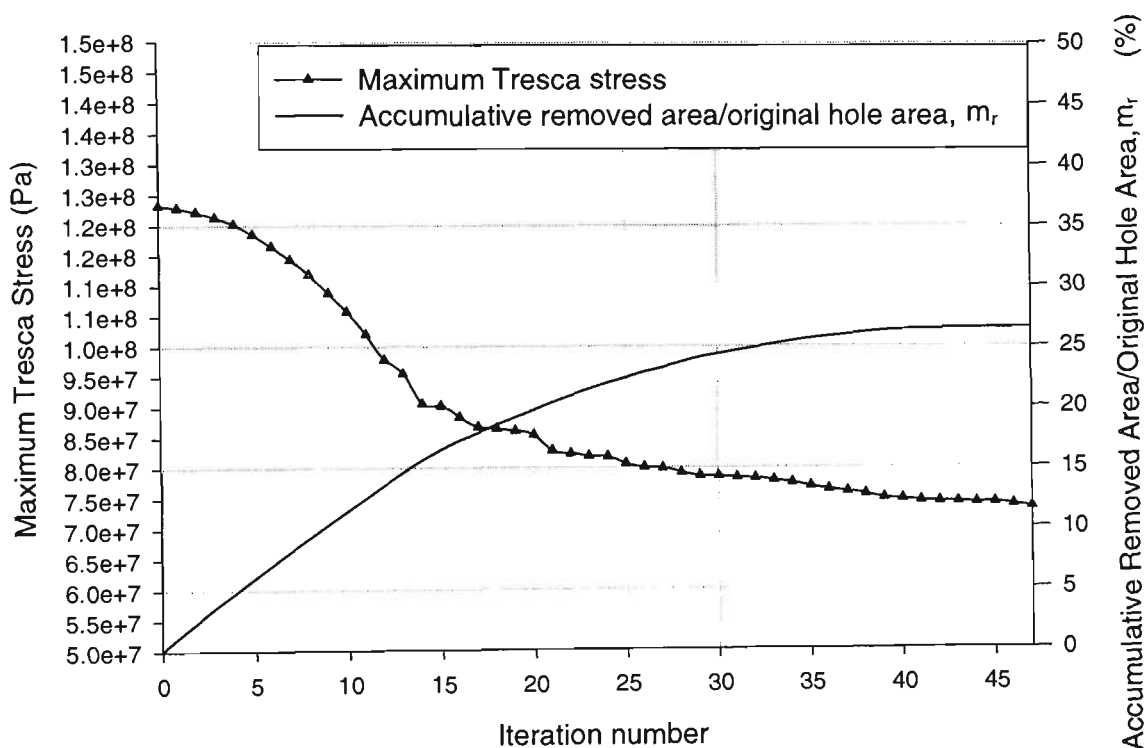
the boundary was 31 for all cases. Results are tabulated in Table 4.3 and illustrated in Figures 4.14 – 4.24.

Figure 4.14 shows the changing hole profiles in the course of optimization (quarter model) at iterations 0 (initial), 10, 20, 30, 47 (optimal) for the case  $D/W = 0.837$ . It can be seen that materials were removed quickly from iteration 0 (initial) to iteration 20, slower from iteration 20 to iteration 30, then very slowly from iteration 30 to iteration 47 (optimal), reflecting the characteristics of PSM.



**Figure 4.14:** Hole shapes at iterations 0(initial), 10, 20, 30, 47 (optimal) ( $D/W = 0.837$ )

Figure 4.15 shows the optimization history for the case  $D/W = 0.837$  including the variation of the maximum Tresca stress and material removal ratio  $m_r$  versus the iteration number. It can be seen that the maximum Tresca stress decreases quickly from initial iteration to iteration 15, then slowly from iteration 15 to iteration 40, and finally it reduces very slowly until the process converges. The minimum Tresca stress occurring on the boundary was not plotted since its values were always near zero during the optimization process.



**Figure 4.15:** Optimization history ( $D/W = 0.837$ )

It can be seen that the reduction in STDV for these cases (Table 4.3) was not much since all horizontal edges of the optimal profiles were still under low Tresca stresses. Figures 4.16 - 4.22 show the full optimum profiles for various  $D/W$  studied, 0.140, 0.250, 0.377, 0.518, 0.650, 0.775 and 0.837 respectively, which include all cases studied by Durelli and Rajaiah (1979) plus two intermediate cases of 0.250 and 0.650. It can be seen that the optimal profiles obtained in this example as compared to those

obtained by PSM, have sharper corners, especially at  $D/W = 0.140$ .

**Table 4.3:** Results obtained by the FEM simulation for various  $D/W$  ratios

$D/W$	$esize$ (mm)	Initial $\sigma_{max}$ (MPa)	Final $\sigma_{max}$ (MPa)	$K_{in}$ reduction (%)	Initial STDV (MPa)	Final STDV (MPa)	Hole area increase (%)	SEPC (%)	Number of iteration	CPU Time (min.)
0.140	0.10	30.49	22.70	25.56	9.79	7.13	19.42	0.39	50	17
0.250	0.15	32.24	23.64	26.69	10.22	7.29	19.79	0.41	52	19
0.377	0.15	36.19	25.90	28.45	11.26	7.81	21.42	0.78	58	22
0.518	0.20	44.61	31.03	30.44	13.48	8.96	23.41	0.64	52	19
0.650	0.25	59.99	38.67	35.53	17.55	11.51	25.98	0.72	52	17
0.775	0.35	91.03	55.80	38.70	25.33	16.87	27.01	0.79	47	18
0.837	0.40	125.95	72.90	42.12	32.86	23.75	27.13	0.65	47	17

At the larger values of 0.775 and 0.837, the profiles found by FEM simulation, which can be described as square holes with rounded corners, do not show the dimpled horizontal curves as given by PSM. It should be noted that the profiles are to be bounded by the design domain and that the optimization objective is to minimize the maximum stress occurring on the boundaries of holes. For the case  $D/W = 0.837$ , it can be seen that FEM simulation removes more material, i.e. FEM goes further than PSM in optimization, with the percentage hole area increase of about 27 percents, compared to 20 percents given by Durelli and Rajaiyah (1979). The reduction in the stress concentration factor was similar to or better than those obtained by the PSM. This was confirmed by the optimality criteria proposed by Schnack (1979) i.e. the profiles obtained by the FEM simulation have less stress concentration than those given by PSM, as they were of longer lengths under the constant maximum Tresca stress.

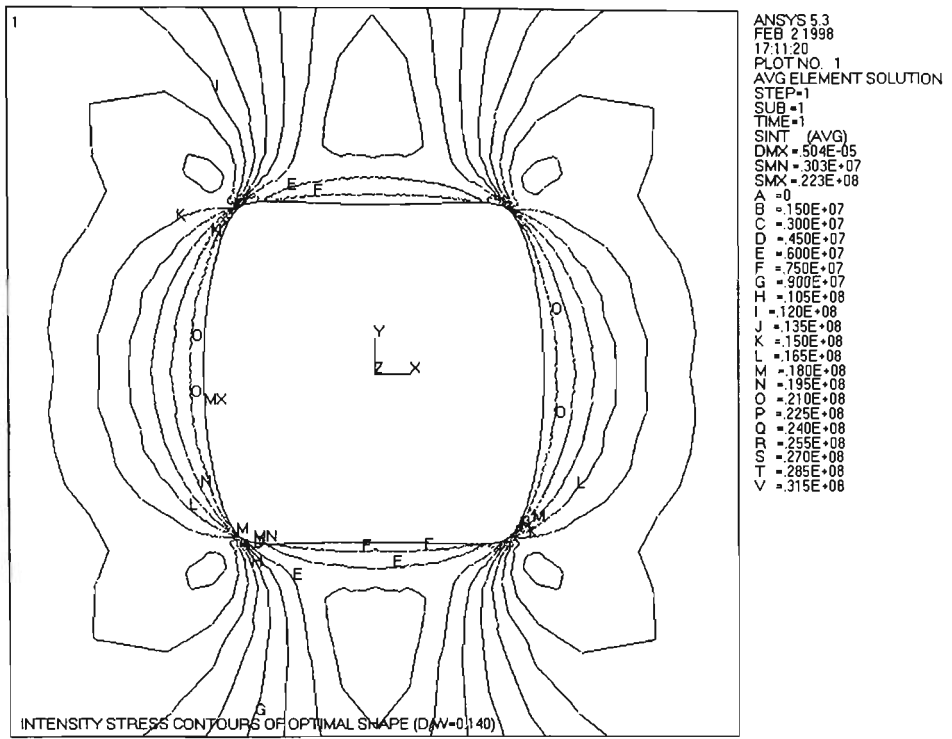


Figure 4.16: Optimal hole profile, case D/W = 0.140

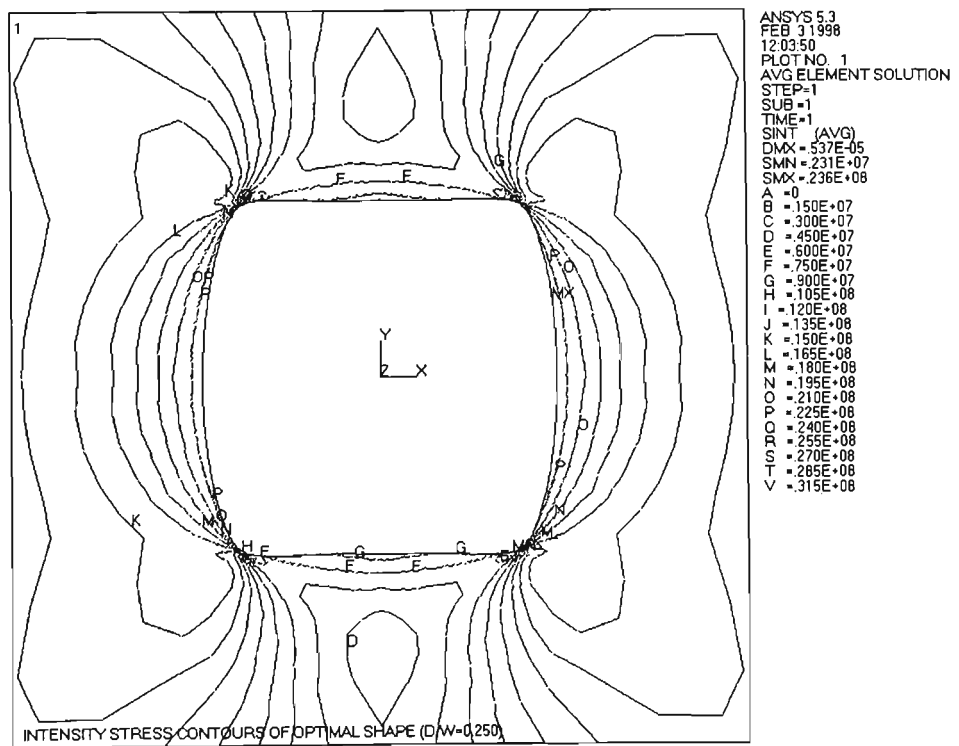


Figure 4.17: Optimal hole profile, case D/W = 0.250

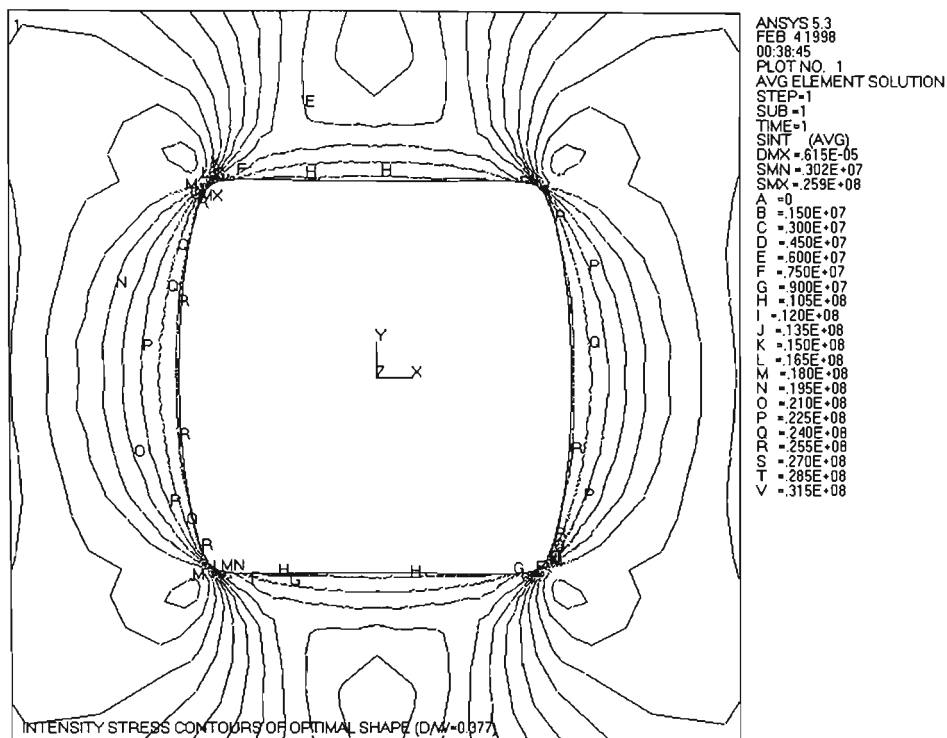


Figure 4.18: Optimal hole profile, case  $D/W = 0.377$

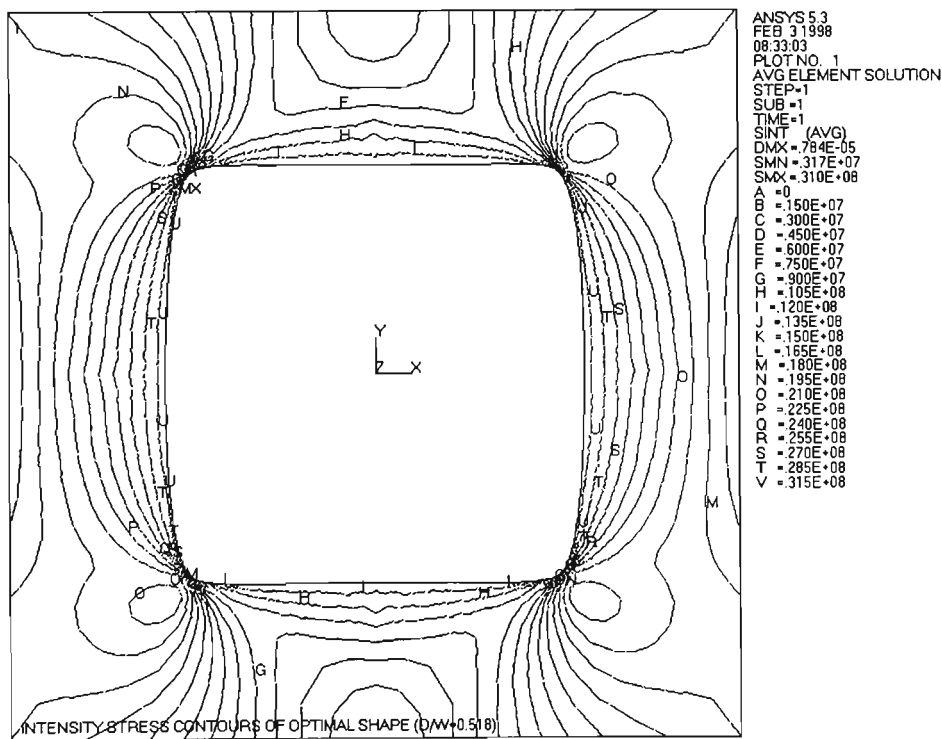


Figure 4.19: Optimal hole profile, case  $D/W = 0.518$

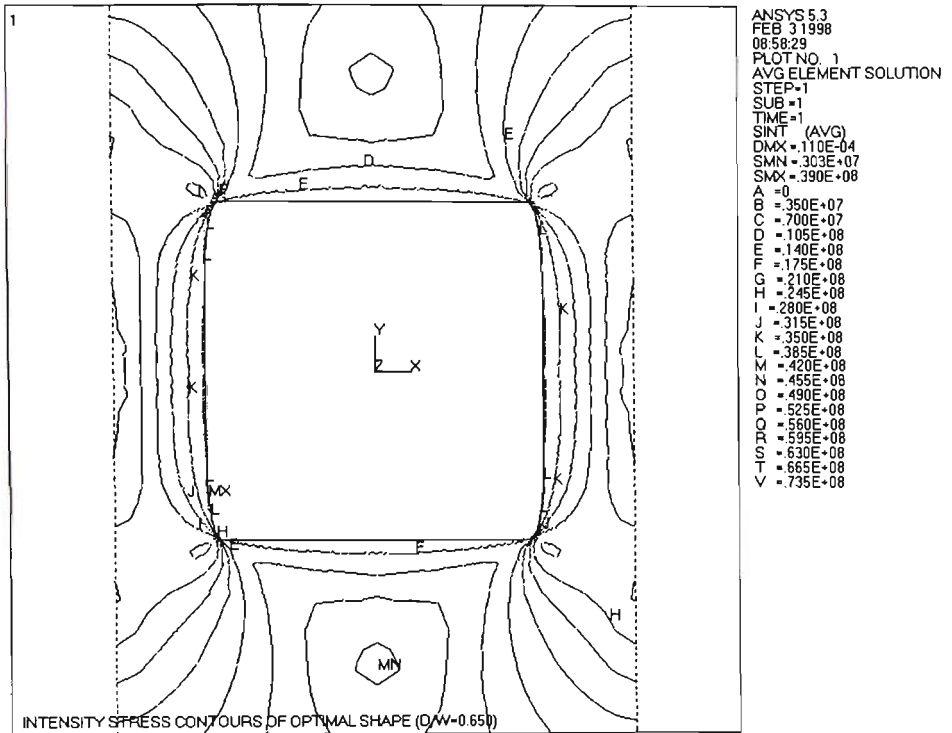


Figure 4.20: Optimal hole profile, case  $D/W = 0.650$

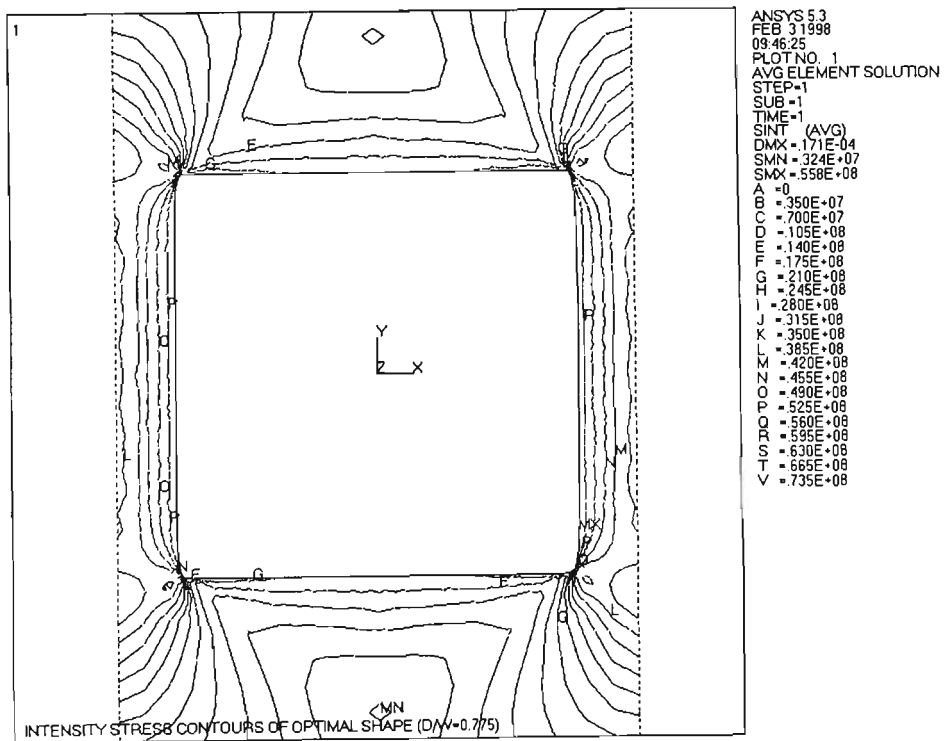


Figure 4.21: Optimal hole profile, case  $D/W = 0.775$

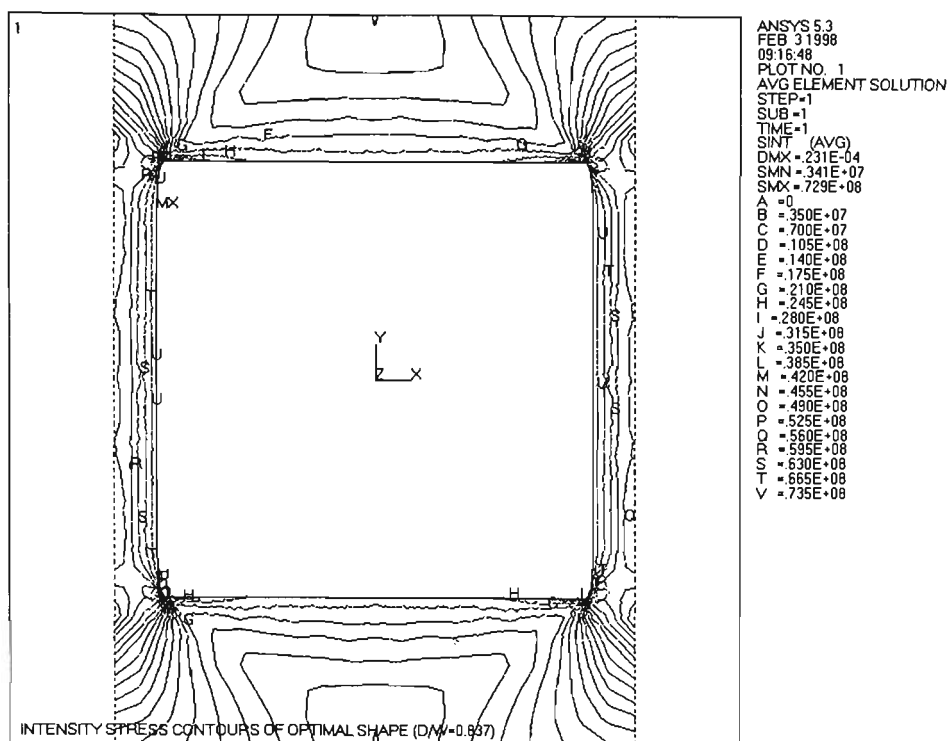


Figure 4.22: Optimal hole profile, case  $D/W = 0.837$

Figure 4.23 shows the variation of  $K_{tn}$  for the original circular holes and for the optimum profiles obtained by FEM simulation. It can be seen that the reduction in the net stress concentration factor is quite remarkable, about 42 % for the case  $D/W = 0.837$ .

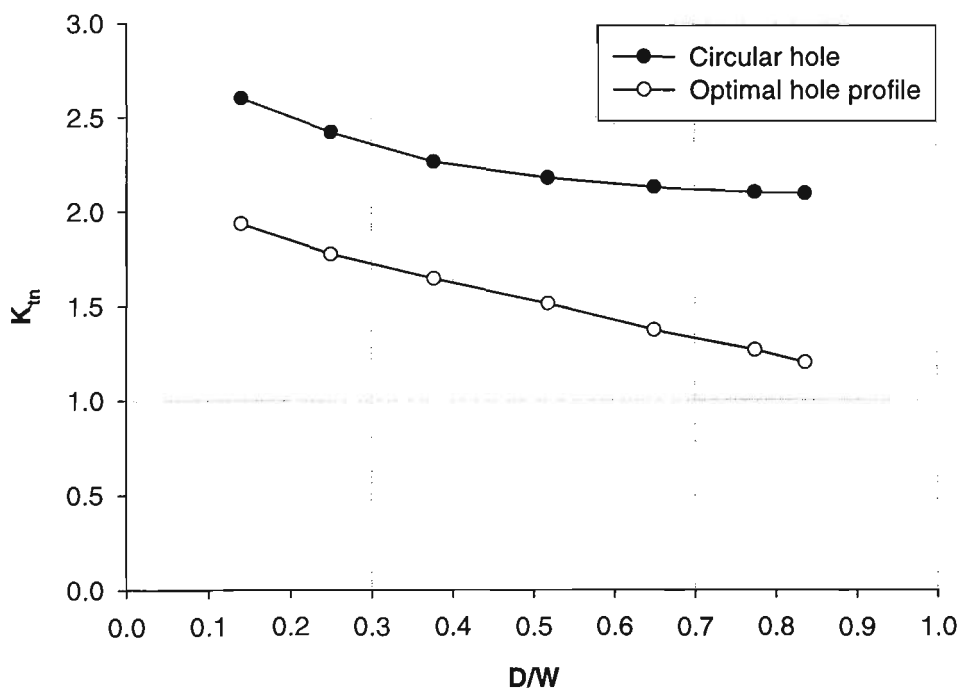
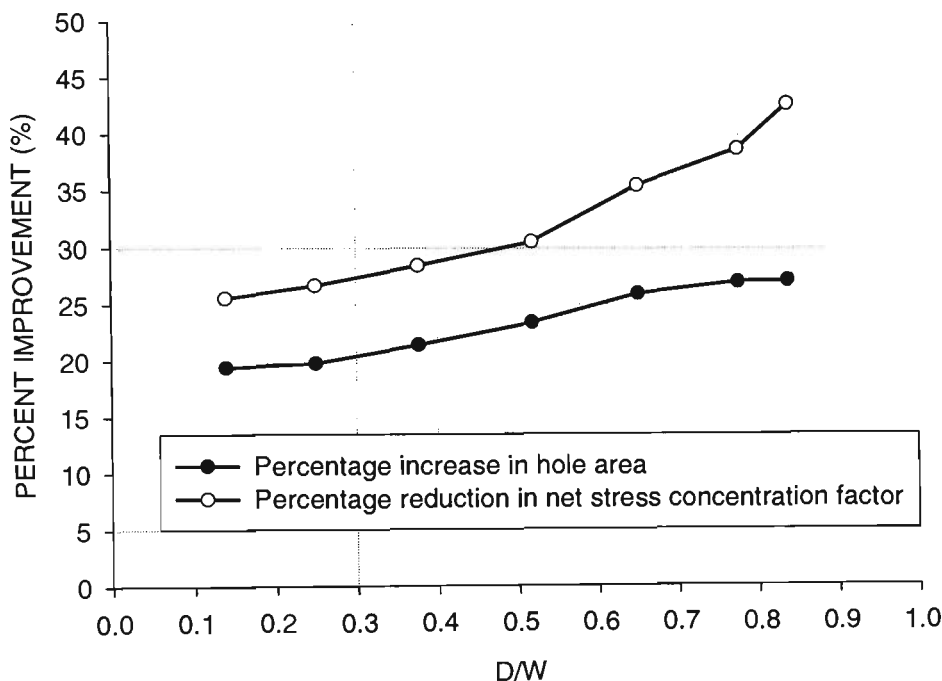


Figure 4.23: Variation of  $K_{tn}$  versus  $D/W$  for circular hole and optimal hole profile

Figure 4.24 shows the percent improvement due to the optimum profiles in reducing  $K_{tn}$  and increasing in the holes' areas. The PSM's results indicate that the percentage increase in the holes' areas reached a maximum at  $D/W$  of about 0.60 and then decreased afterwards as reported by Durelli and Rajaiah (1979) whereas the results by FEM showed a continual increase.



**Figure 4.24:** Variation of  $K_{tn}$  versus  $D/W$  for circular hole and optimal hole profile

#### 4.4 Concluding remarks

It is evident that the modified algorithm with the added feature of protection scheme, which takes into account the existence of isotropic points and transition sections, has improved results obtained by FEM simulation and can handle more general classes of stress minimization problems.

The modified algorithm has been applied to find optimal stress raiser profiles in

homogeneous isotropic plates under biaxial tension-compression stresses, which have not been considered in the literature.

In finding optimal hole profiles of finite width plates under uniaxial tension, the results found by the FEM simulation demonstrated some improvement over PSM solutions. This is due to the fact that PSM faces difficulties in optimizing a plate with a very small hole. This is reflected in the comparatively more rounded shapes obtained by Durelli and Rajaiah (1979). Furthermore, it is not possible to experiment freely at will and to venture too far with cuts in the photoelastic model, as models cannot be 'recut' as in cases of FEM simulation.

Another point of interest in all the cases studied in this chapter concerns the small radius corner of the optimal profile. It is well accepted that in structural discontinuities any re-entrant corner with a very small radius is a potential source of stress concentration and should be avoided. However, in the profiles optimized, the corner regions or transition sections happen to be lowly stressed areas with isotropic points of zero stress. Hence, there may be stress raiser profiles with sharp re-entrant corners, which do not introduce stress concentration.

With the development of FEM applications in analyzing advanced composite structures, the proposed FEM simulation of the PSM now can be extended to find optimal stress raiser profiles in advanced fibrous composite panels as studied and presented in the next chapter.

## *Chapter 5*

# **OPTIMAL STRESS RAISER PROFILES IN A LAMINATED COMPOSITE PLATE**

### **5.1. Introduction**

The behavior of composite laminates with stress concentration is of great interest in design because of the resulting reduction of strength and life due to damage growth around the points of stress concentration, as discussed by Daniel and Ishai (1994). Minimizing stress concentrations occurring on discontinuities in a composite laminate consequently increases the strength and life of that laminate under comparable boundary conditions.

The FEM simulation technique has proved to be very efficient in optimizing stress raiser profiles in plates made of isotropic materials as shown in Chapters 3 and 4. In this chapter the FEM simulation is further extended to solve the optimization problems involving advanced composite materials. Finding optimal stress raiser profiles in composite structures presents a more challenging task due to both the complex behavior

of these structures, as well as the variations possible in a wide range of parameters e.g. the choice of number of plies, ply orientation, stacking sequence. For these reasons, the study presented in this chapter is confined within a pre-configured composite laminate, i.e. parameters that configure composite laminates are kept unchanged during the course of the optimization process. The objective is to find the optimal stress raiser profiles such that a certain index representing the maximum failure criterion occurring on the discontinuity boundaries of the composite laminate is minimized.

A large quasi-isotropic laminated composite plate with a hole under various biaxial stress states is used as an example to validate the capability of the FEM simulation in optimizing composite structures. The initial results of this study were reported by Tran and Nguyen (1998b).

## **5.2 Composite laminate**

A laminated composite material plate is a stack of bonded plies, where a ply or a lamina is a single sheet of the resin pre-impregnated tape with the fibres aligned in a particular direction. A ply may be of the form where all the fibres are aligned in one direction and the ply is then said to be a unidirectional ply. Figure 5.1 illustrates a laminate formed by four unidirectional plies with different orientations, where axes 1 and 2 denote the fibre and transverse directions of each ply.

In Chapters 3 and 4, the Tresca or von Mises criterion can be used for analyzing structures made of isotropic materials. Such criteria are not appropriate for composite materials since these materials are anisotropic. Consequently, macro-mechanical failure theories for composites are employed.

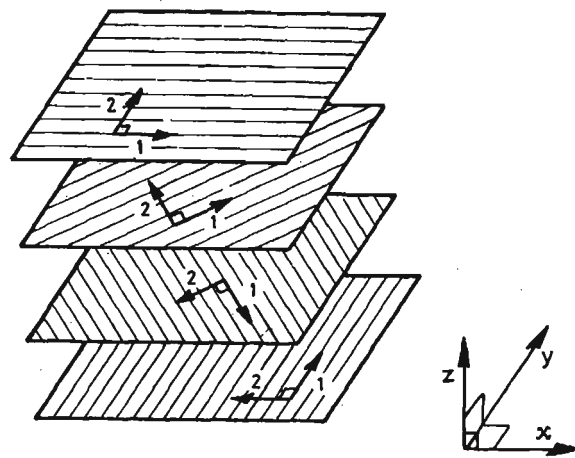


**Figure 5.1:** A laminate formed by four unidirectional plies

### 5.2.1 Failure criterion for element selection and removal

Among failure theories available, the following four are most widely used:

- (i) Maximum stress theory;
- (ii) Maximum strain theory;
- (iii) Deviatoric strain energy theory for anisotropic materials (Tsai-Hill criterion);
- (iv) Interactive tensor polynomial theory (Tsai-Wu criterion).

Brief discussions about the validity and applicability of the above theories can be found in Dato (1991), Daniel and Ishai (1994) and Kaw (1997). Although any of the above failure criteria can be adopted, the Tsai-Wu theory with the plane stress assumption is employed in this study, since the Tsai-Wu criterion is mathematically consistent and operationally simple. It also allows for the distinction between tensile and compressive strengths, Daniel and Ishai (1994).

In a plane stress condition, Tsai and Wu (1971) considered a lamina to fail if the condition

$$H_1\sigma_1 + H_2\sigma_2 + H_6\tau_{12} + H_{11}\sigma_1^2 + H_{22}\sigma_2^2 + H_{66}\tau_{12}^2 + 2H_{12}\sigma_1\sigma_2 < 1 \quad (5.1)$$

is violated. Where,  $\sigma_1$  and  $\sigma_2$  are stress components in the 1-2 reference axes, and  $\tau_{12}$  is the shear component in plane 1-2. The components  $H_1$ ,  $H_2$ ,  $H_6$ ,  $H_{11}$ ,  $H_{22}$ ,  $H_{66}$  of the theory are found using the five strength parameters of a unidirectional lamina (Kaw 1997).

$$H_1 = \frac{1}{(\sigma_1^T)_{ult}} - \frac{1}{(\sigma_1^C)_{ult}} \quad (5.2)$$

$$H_2 = \frac{1}{(\sigma_2^T)_{ult}} - \frac{1}{(\sigma_2^C)_{ult}} \quad (5.3)$$

$$H_6 = 0 \quad (5.4)$$

$$H_{11} = \frac{1}{(\sigma_1^T)_{ult} (\sigma_1^C)_{ult}} \quad (5.5)$$

$$H_{22} = \frac{1}{(\sigma_2^T)_{ult} (\sigma_2^C)_{ult}} \quad (5.6)$$

$$H_{66} = \frac{1}{(\tau_{12})_{ult}^2} \quad (5.7)$$

Where,

$(\sigma_1^T)_{ult}$  : the ultimate longitudinal tensile strength (direction 1)

$(\sigma_1^C)_{ult}$  : the ultimate longitudinal compressive strength (direction 1)

$(\sigma_2^T)_{ult}$  : the ultimate transverse tensile strength (direction 2)

$(\sigma_2^C)_{ult}$  : the ultimate transverse compressive strength (direction 2)

$(\tau_{12})_{ult}$  : the ultimate in-plane shear strength (in plane 1-2)

The component  $H_{12}$  cannot be found directly from the five strength parameters of the unidirectional lamina. It can be found by a biaxial test or by some empirical rules (Kaw 1997). Instead of carrying out a biaxial test, Tsai and Hahn (1980) employed von-Mises criterion and derived:

$$H_{12} = -\frac{1}{2} \sqrt{\frac{1}{(\sigma_1^T)_{ult} (\sigma_1^C)_{ult} (\sigma_2^T)_{ult} (\sigma_2^C)_{ult}}} \quad (5.8)$$

In this chapter, the component  $H_{12}$  determined by equation (5.8) is employed throughout. As the material property is very complex and damage may occur when the operator files away materials from the stress raiser boundary, it is not practical to apply Durelli's PSM. The FEM simulation of Durelli's PSM consequently is used to find the optimal profiles for laminated composite plates.

### 5.2.2 FEM simulation algorithm

The flowchart of the FEM simulation algorithm for laminated composite materials is shown in Figure 5.2. It inherits all characteristics of the modified FEM simulation algorithm in Section 4.2.2; the difference is the criterion assigned to each element for

element selection and removal, i.e. a failure criterion for composite materials is used instead of a yield criterion for isotropic materials.

The composite structure under a pre-defined boundary condition is analyzed by FEM. It should be noted that failure criteria for composite materials are applied at the ply level rather than the laminate level. An index based on a failure criterion (e.g. Tsai-Wu criterion) is assigned to each ply or layer within each finite element. By adopting the first ply failure philosophy, Daniel and Ishai (1994) and Kaw (1997), the ply with the maximum failure index within an element is chosen as the limiting ply for that element. Based on the failure indices of the limiting plies, elements with lower limiting ply failure indices lying on the boundary of interest are selected as candidates for removal.

While the optimality criteria for minimizing stress concentrations involving isotropic materials have been confirmed theoretically, for example by Schnack (1979) and Banichuk (1989), an optimality criterion for minimizing the stress concentration occurring on the hole boundary in composite laminates has not been derived mathematically.

In this study, the uniformity of the elements' limiting ply failure indices distributed along the stress raiser profile is assumed to be the optimality criterion, which minimizes the maximum failure index occurring on the boundary of interest. The uniformity of the failure index distribution can be measured by calculating the standard deviation of the failure indices along the boundary.

### **5.3. Case study - a large composite plate with a hole under biaxial stress**

Stress distributions and stress concentrations around notches can be determined

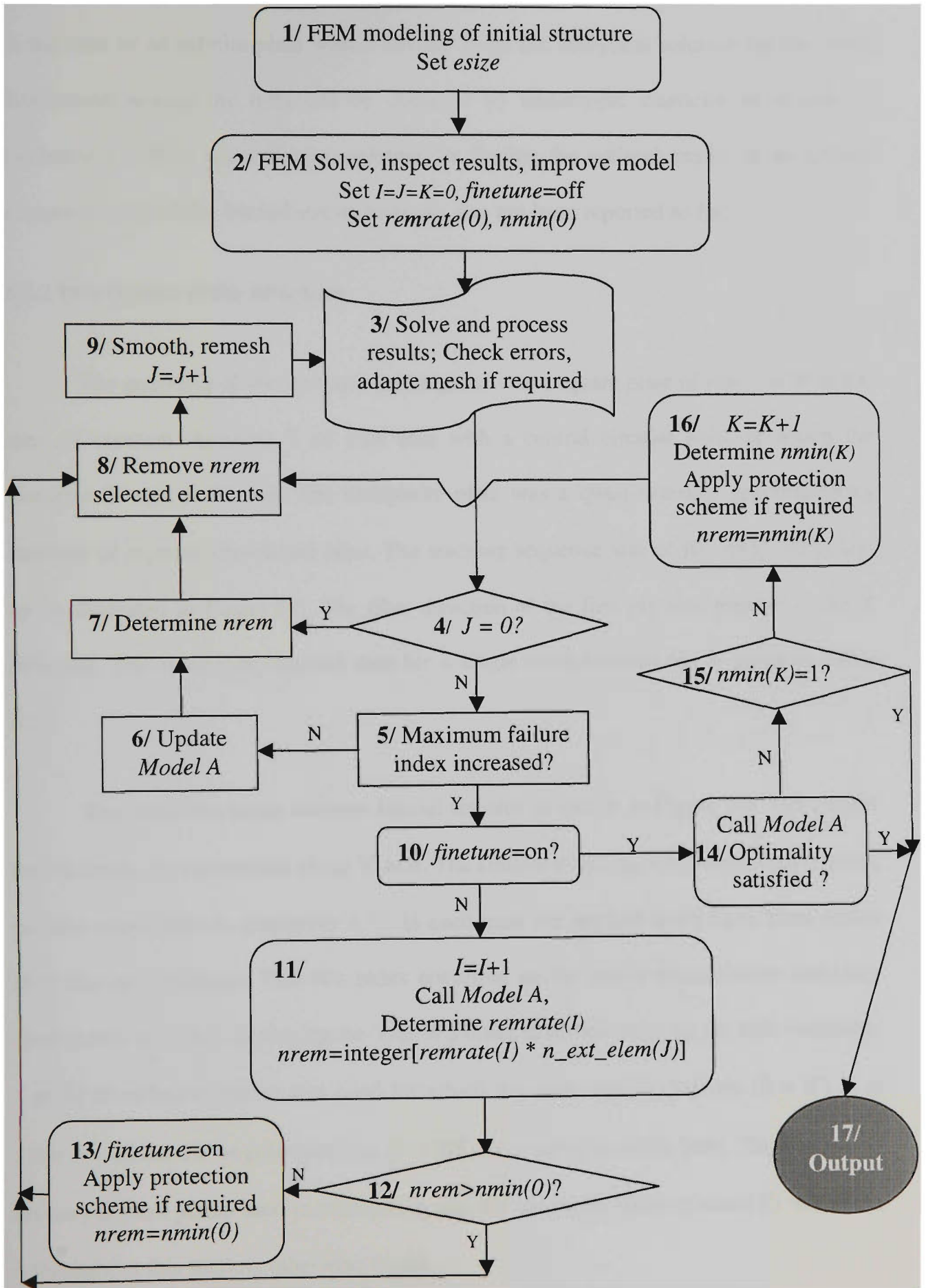


Figure 5.2: Flowchart of the FEM simulation algorithm for laminated composite plates

by linear elastic analysis, FEM and experimental techniques, Daniel and Ishai (1994). In the case of an infinite plate with a circular hole, the analytical solution for the stress distribution around the hole can be obtained by anisotropic elasticity as shown by Lekhnitskii (1963). An analytical solution for finding the optimal profile in an infinite composite plate under biaxial stress, however, has not been reported so far.

### 5.3.1 Description of the structure

The geometry of the structure investigated was a square plate of side  $L = W = 300$  mm, of constant thickness  $T$  of 1.04 mm with a central circular hole, of which the diameter  $D$  was of 30 mm. The composite plate was a quasi-isotropic graphite/epoxy laminate of eight unidirectional plies. The stacking sequence was of  $[0^0, \pm 45^0, 90^0]_S$  lay-up as illustrated in Figure 5.3. The fiber direction of the first ply was parallel to the X direction. The composite material data for a single unidirectional ply is given in Table 5.1.

The plate was under uniform biaxial stresses as shown in Figure 5.4. The greater tensile stress,  $\sigma_y$  was applied along Y-axis. The smaller stress  $\sigma_x$ , was determined from  $\sigma_y$  and the stress ratio  $S_r$  (Equation 3.7). In each case the applied loads have been scaled such that the maximum Tsai-Wu index occurring on the initial discontinuity boundary corresponds to 1. For displaying the Tsai-Wu index distribution along the hole boundary, a polar co-ordinate system was used for which the zero angular position ( $\theta = 0^0$ ) is at point A and the  $90^0$  angular position ( $\theta = 90^0$ ) is at point B of the hole. The number of primary control points used is twenty-one, and the minimum value of  $nmin(K)$  was set to 1 throughout this section, otherwise stated.

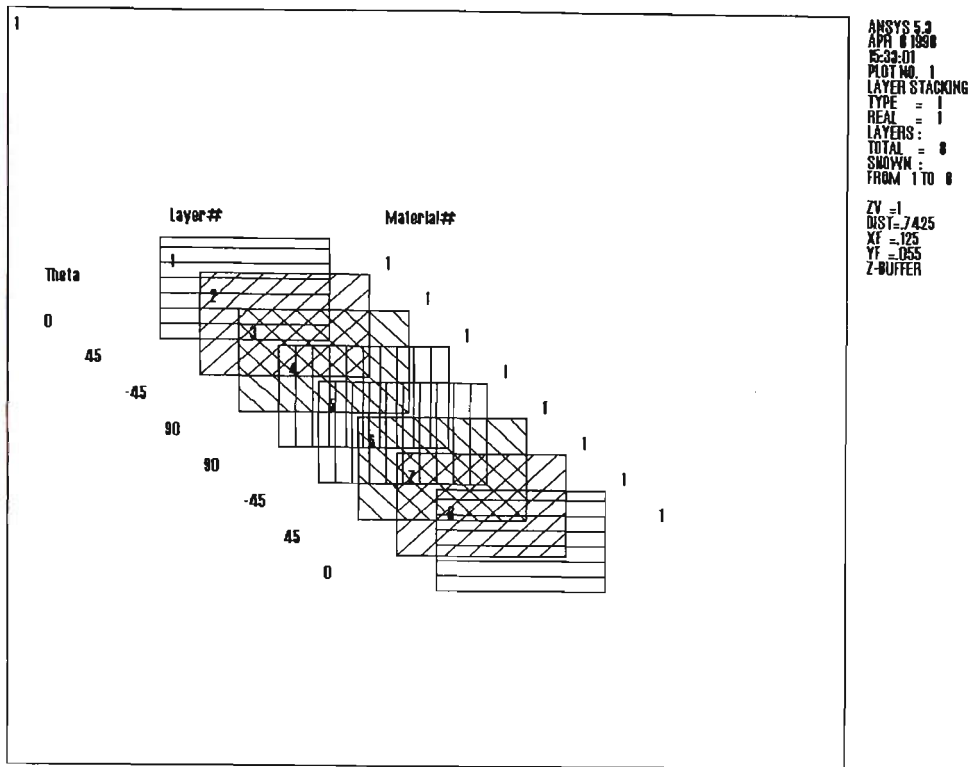


Figure 5.3: Stacking sequence of the laminate  $[0^0, \pm 45^0, 90^0]_s$

Table 5.1: Material data

Nominal material data for Carbon fiber/Epoxy unidirectional preimpregnated tape		
Longitudinal Young's modulus, $E_1$	151 GPa	
Transverse Young's modulus, $E_2$	10.6 GPa	
Shear modulus, $G_{12}$	6.6 GPa	
Poisson ratio, $\nu_{12}$	0.31	
Ply thickness	0.13 mm	
Ultimate strength	Tensile	Compressive
Longitudinal	1.401 GPa	1.132 GPa
Transverse	54 MPa	211 MPa
Shear	72 MPa	

Due to symmetry, a quarter of the plate was modelled as illustrated in Figure 5.5.

The element used for modeling is SHELL99-100 layer structural shell element (ANSYS Theory Reference, 1996).

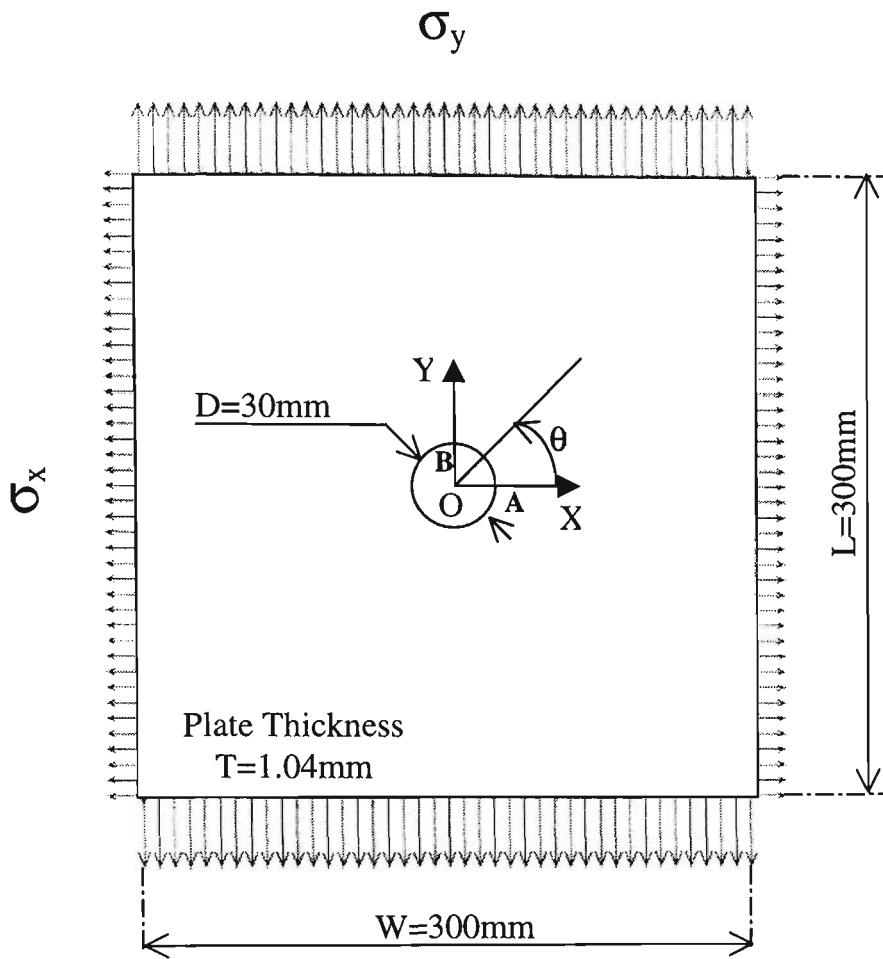


Figure 5.4: Description of the problem

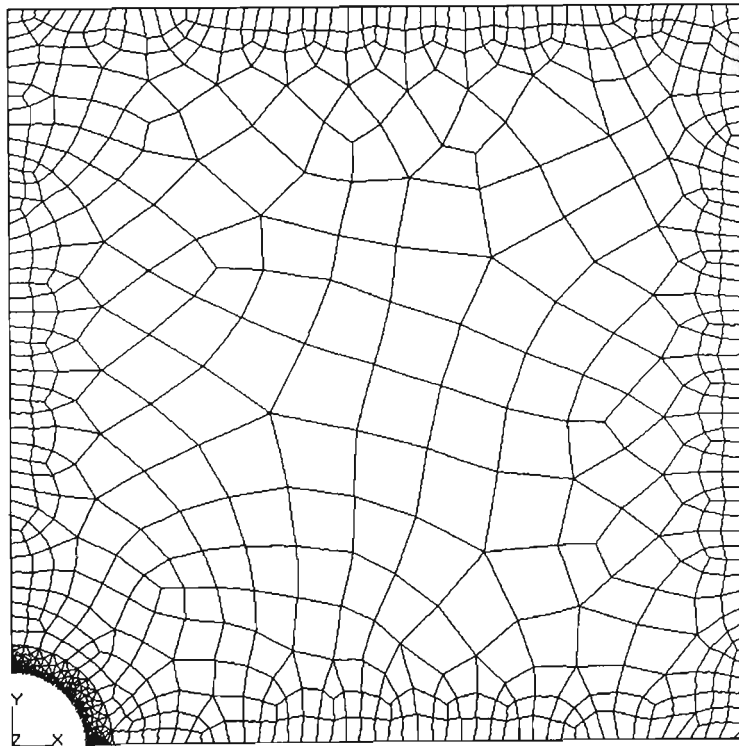


Figure 5.5: The FEM model

### 5.3.2 Results and discussion

The case when the plate was under biaxial tension ( $S_r > 0$ ) is presented first, followed by the case when the plate was under biaxial tension-compression ( $S_r < 0$ ). All the contour plots in the following sections of this chapter are based on the average element solution (ANSYS Theory Reference, 1996).

#### 5.3.2.1 Optimal stress raiser profiles in a composite plate under biaxial tension

( $S_r > 0$ )

The structure was optimized employing the FEM simulation algorithm for composite laminates as presented in Section 5.2. For three cases with stress ratios  $S_r$  of 1.5, 2 and 2.5 studied in this section, parameters were initially set as follows:  $esize = 0.3$  mm,  $remrate(0) = 0.5$ ,  $nmin(0) = 4$ . The objective standard deviation was set to zero to produce the best outcome. The results are tabulated in Table 5.2 and illustrated in Figures 5.6 – 5.12.

**Table 5.2:** Results for stress ratios  $S_r = 1.5, 2$  and  $2.5$

Case	$S_r$	Initial Max. Tsai-Wu index	Final Max. Tsai-Wu index	Reduction in Max. Tsai-Wu index (%)	Initial STDV	Final STDV	Number of iteration	CPU time (min.)
1	1.5	1	0.786	21.4	0.21	0.020	45	90
2	2	1	0.664	33.6	0.29	0.019	74	131
3	2.5	1	0.622	37.8	0.33	0.018	97	194

Figures 5.6 and 5.7 show respectively the initial and optimal Tsai-Wu index distributions in the plate of a typical case when  $S_r$  is of 1.5. It is seen that the maximum

Tsai-Wu index initially occurs at point A corresponding to 0 degree angular position ( $\theta = 0^\circ$ ). The optimal profile was reached after 45 iterations. A drop of 21.4 percent in the maximum Tsai-Wu index was found. The standard deviation of the distribution of Tsai-Wu indices along the profile was reduced from 0.21 (initial) to 0.02 (optimal). The optimal profile of the hole was almost an ellipse, of which the major axis per minor axis ratio was about 1.5.

Figure 5.8 shows the plot of the initial (iteration 0) and final (iteration 45) Tsai-Wu index distribution along the profile versus angular positions ( $0^\circ \leq \theta \leq 90^\circ$ ) for the case  $S_r = 1.5$ . It can be seen that the Tsai-Wu index distribution at iteration 45 was much more uniform than the initial one, resulting in the reduction in the maximum Tsai-Wu index. This confirms that the assumed optimality criterion (Section 5.2.2) is applicable.

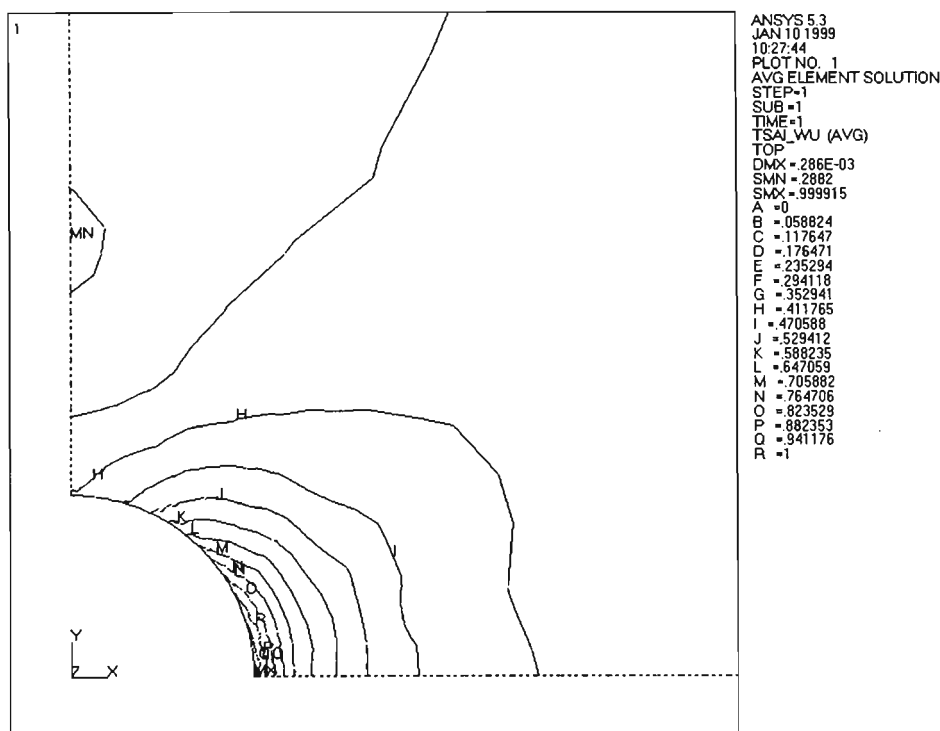


**Figure 5.6:** Tsai-Wu index distribution at iteration 0 (initial), case  $S_r = 1.5$

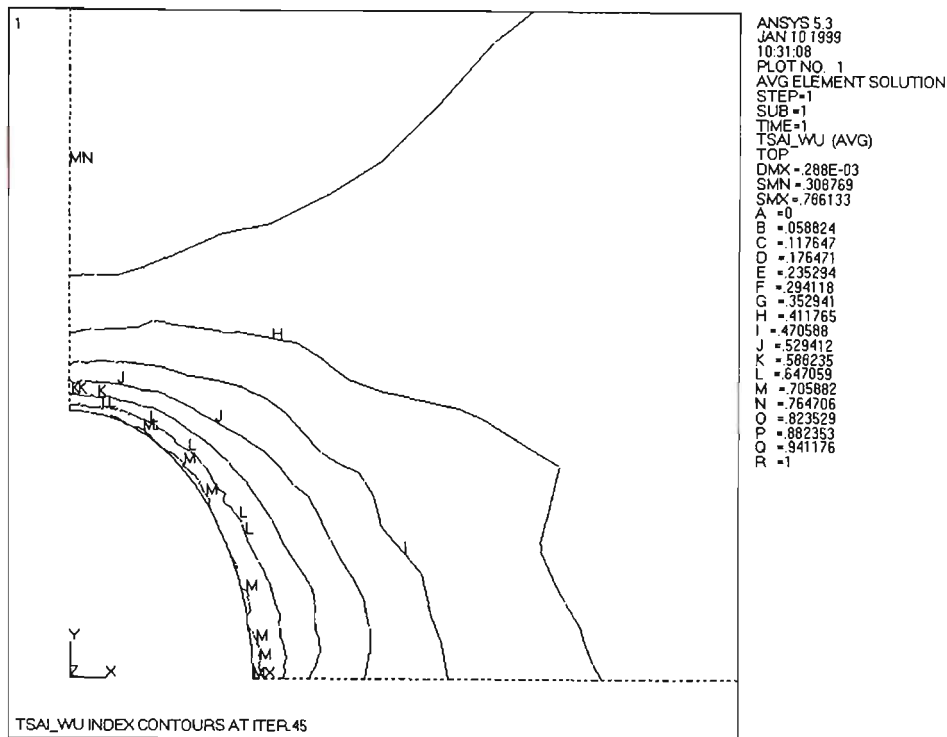


Figure 5.7: Tsai-Wu index distribution at iteration 45 (optimal), case  $S_r = 1.5$

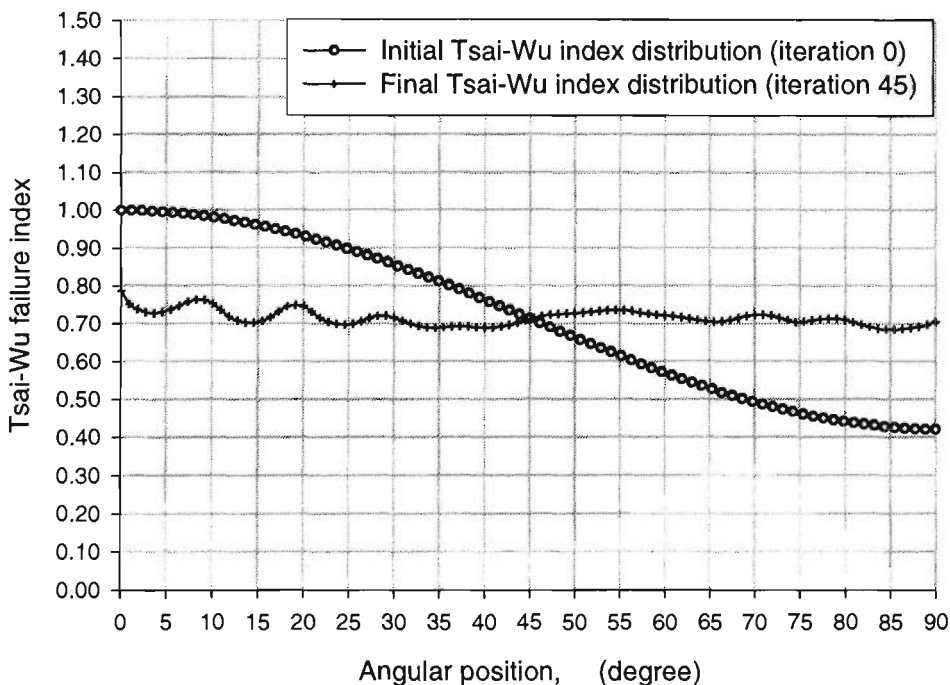
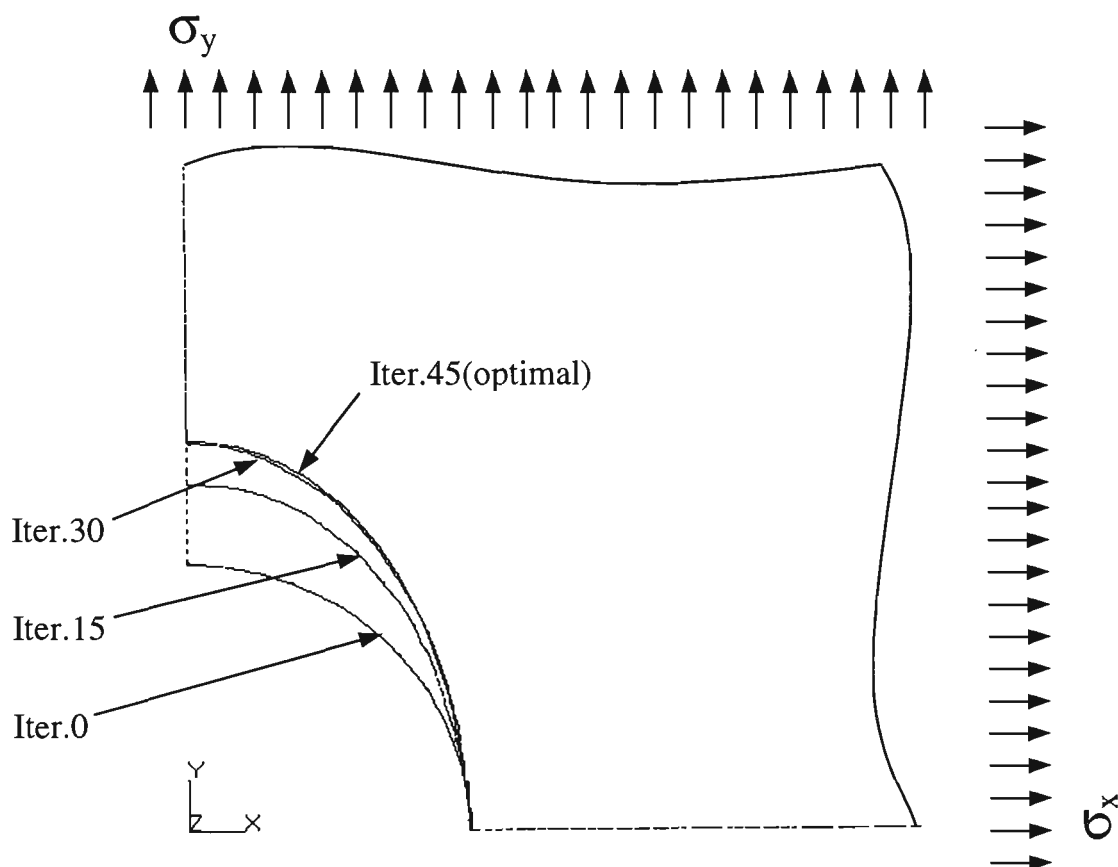


Figure 5.8: Tsai-Wu index distribution along the profile versus angular positions at iteration 0 (initial) and iteration 45 (optimal) for the case  $S_r = 1.5$

Figure 5.9 shows the changing hole profiles in the course of optimization (quarter model) at iterations 0 (initial), 15, 30, 45 (optimal) for the case  $S_r$  of 1.5. It is seen that materials were removed quickly from iteration 0 (initial) to iteration 15, slower from iteration 15 to iteration 30, then very slowly from iteration 30 to iteration 45 (optimal), reflecting the characteristics of PSM.



**Figure 5.9:** Hole shapes at iterations 0(initial), 15, 30 and 45 (optimal), case  $S_r = 1.5$

Figure 5.10 shows the optimization history for the case  $S_r$  of 1.5, including the variation of the maximum, minimum Tsai-Wu indices and material removal ratio  $m_r$  versus the iteration number. It is seen that while the maximum Tsai-Wu index keeps decreasing as the optimization proceeds, the minimum is increasing continually, resulting in a more uniformity of the Tsai-Wu index distribution along the profile. The graph of  $m_r$  indicates that a large amount of materials has been removed from iterations 0 to 15,

slower from iterations 15 to 30, and very slowly from iteration 30 to 45, reflecting PSM's characteristics.

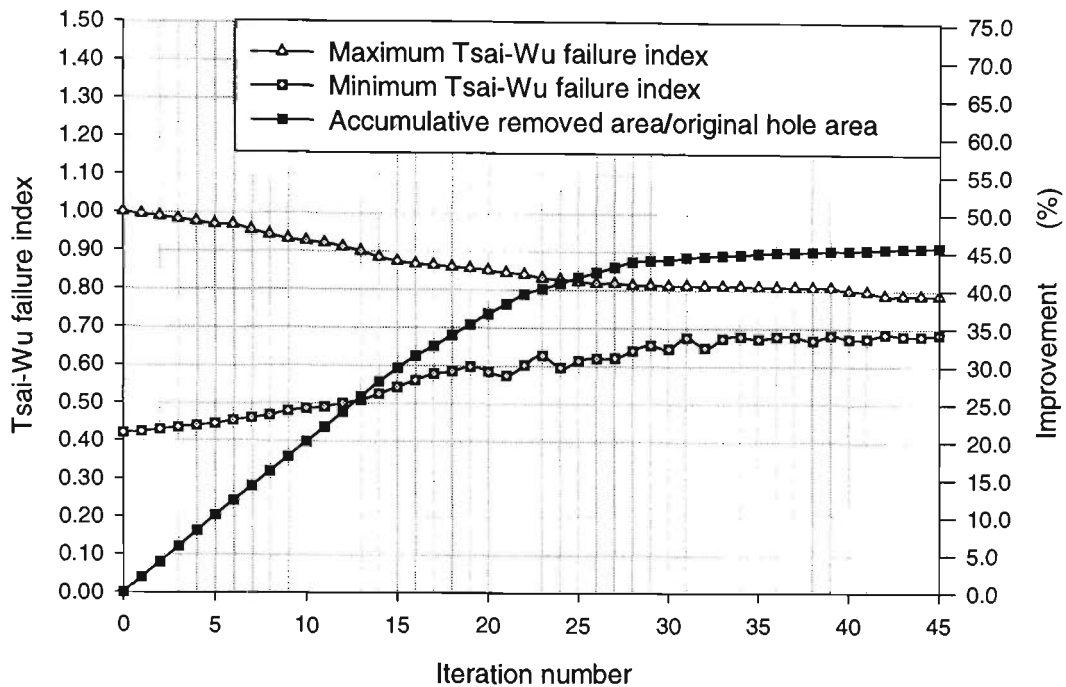


**Figure 5.10:** Optimization history for the case  $S_r = 1.5$

Figures 5.11 and 5.12 show the optimum profiles for the cases when stress ratios  $S_r$  takes values of 2 and 2.5 respectively. The optimal hole shapes obtained were almost ellipses with the major axis to minor axis ratio proportional to the applied stress ratio. It can be seen that larger stress ratios result in greater rewards, i.e. larger reduction in the maximum Tsai-Wu index and larger savings in material can be obtained by shape optimization. As  $S_r$  was increased, the major axis of the hole was increased or the hole became more elongated, and the FEM simulation required more iterations.

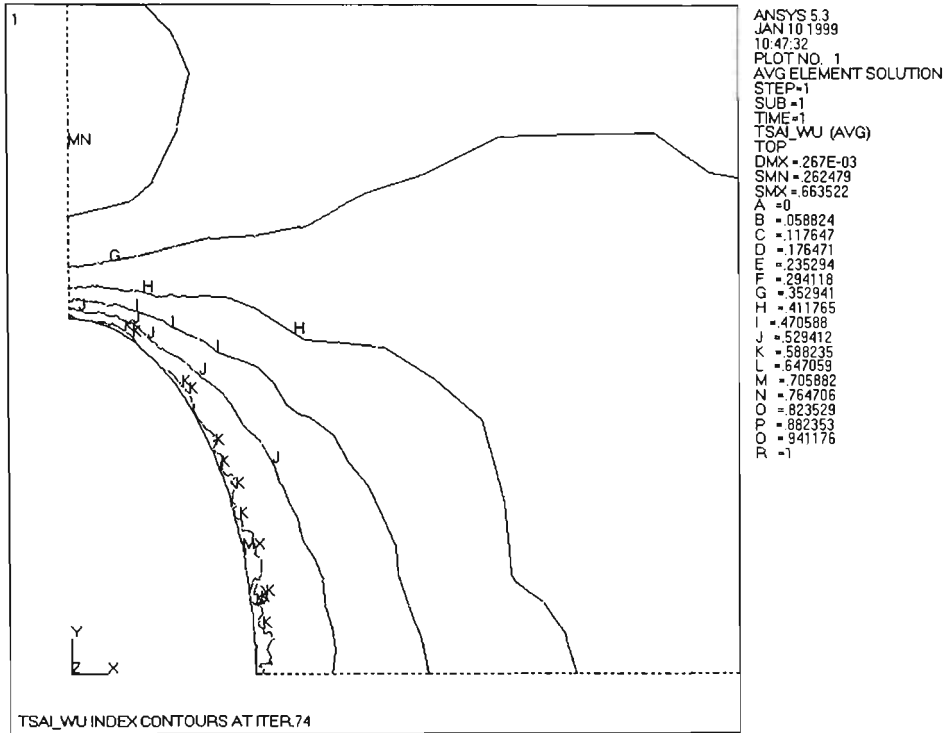


Figure 5.11: Tsai-Wu index distribution at iteration 74 (optimal), case  $S_r = 2.0$

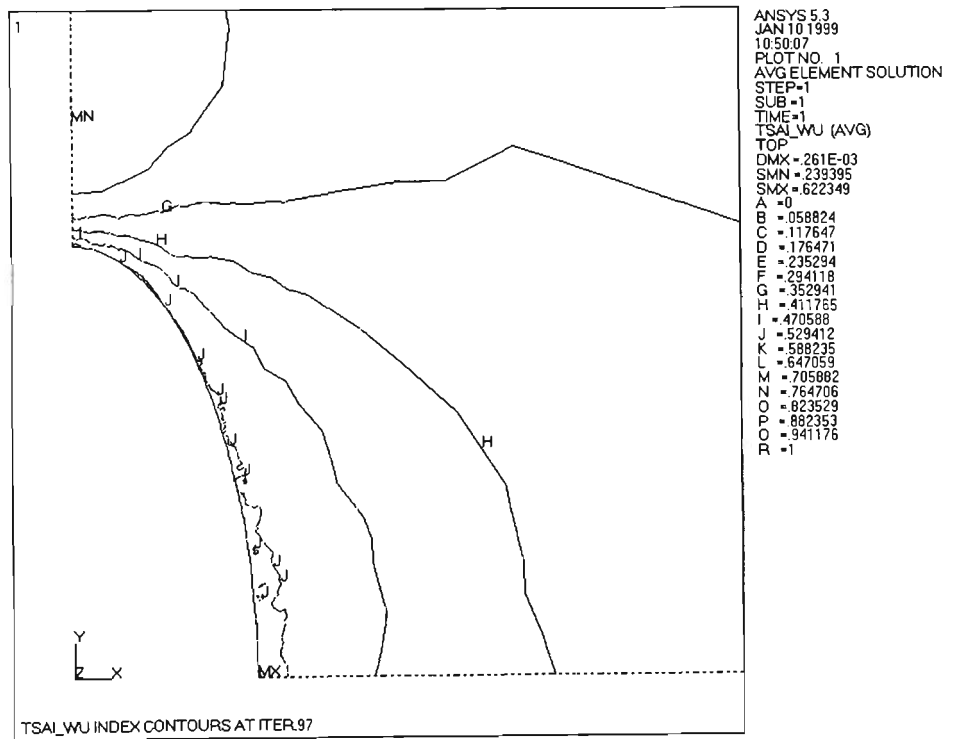


Figure 5.12: Tsai-Wu index distribution at iteration 97 (optimal), case  $S_r = 2.5$

### 5.3.2.2 Optimal stress raiser profiles in a composite plate under biaxial tension-compression ( $S_r < 0$ )

Employing the FEM simulation algorithm for composite laminates (Section 5.2). For three cases with stress ratios  $S_r$  of -1, -1.5 and -2 studied in this section, parameters were initially set as follows:  $esize = 0.3 \text{ mm}$ ,  $remrate(0) = 0.7$ ,  $nmin(0) = 4$ . The objective standard deviation was set to zero to produce the best outcome. The results are tabulated in Table 5.3 and illustrated in Figures 5.13 – 5.19.

Figure 5.13 shows the initial Tsai-Wu index distributions in the plate of a typical case when  $S_r$  is of -1. It can be seen that:

- The maximum Tsai-Wu occurs at points such as point A ( $\theta = 0^\circ$ ) with a very steep Tsai-Wu index gradient around them.
- Points such as point C ( $\theta = 45^\circ$ ) were positions of ‘near zero’ Tsai-Wu index with a very steep stress gradient around them as well. These points always exist during the course of the optimization process as observed.
- The pattern of the index contours however was not symmetrical with respect to the direction of  $45^\circ$  as in the case of isotropic materials (Figure 4.1).
- Instability (buckling) could be a factor in the response of the plate, but it is not considered here in finding the optimal profiles.

**Table 5.3:** Results for stress ratios  $S_r = -1, -1.5, -2$

Case	$S_r$	Initial Max. Tsai-Wu index	Final Max. Tsai-Wu index	Reduction in Max. Tsai-Wu index (%)	Initial STDV	Final STDV	Number of iteration	CPU time (min.)
1	-1	1	0.700	30.0	0.281	0.108	71	126
2	-1.5	1	0.698	30.1	0.287	0.129	119	223
3	-2	1	0.651	34.9	0.295	0.142	140	265

For the case  $S_r = -1$ , the optimal profile was reached after 71 iterations as shown in Figure 5.14. A reduction of 30 percent in the maximum Tsai-Wu index was found. The standard deviation of the distribution of Tresca stress along the profile was reduced from 0.281 (initial) to 0.108 (optimal), indicating that the uniformity of the Tsai-Wu index distribution along the profile was not high. This is due to the existence of the transition sections and ‘isotropic points’ as shown in Figure 5.15.

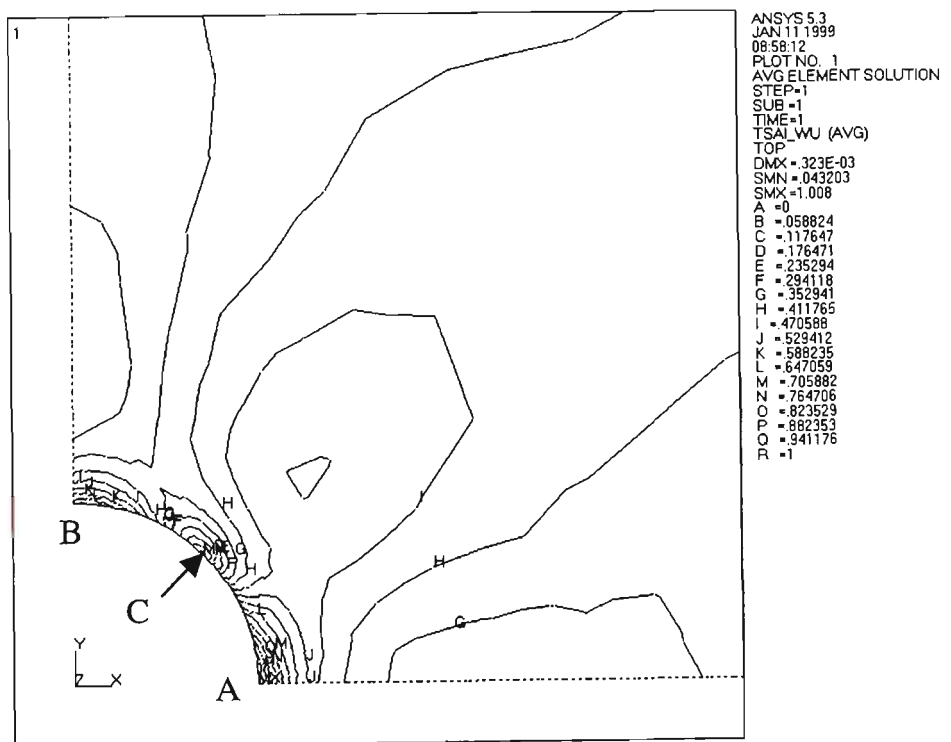


**Figure 5.13:** Tsai-Wu index distribution at iteration 0 (initial), case  $S_r = -1$

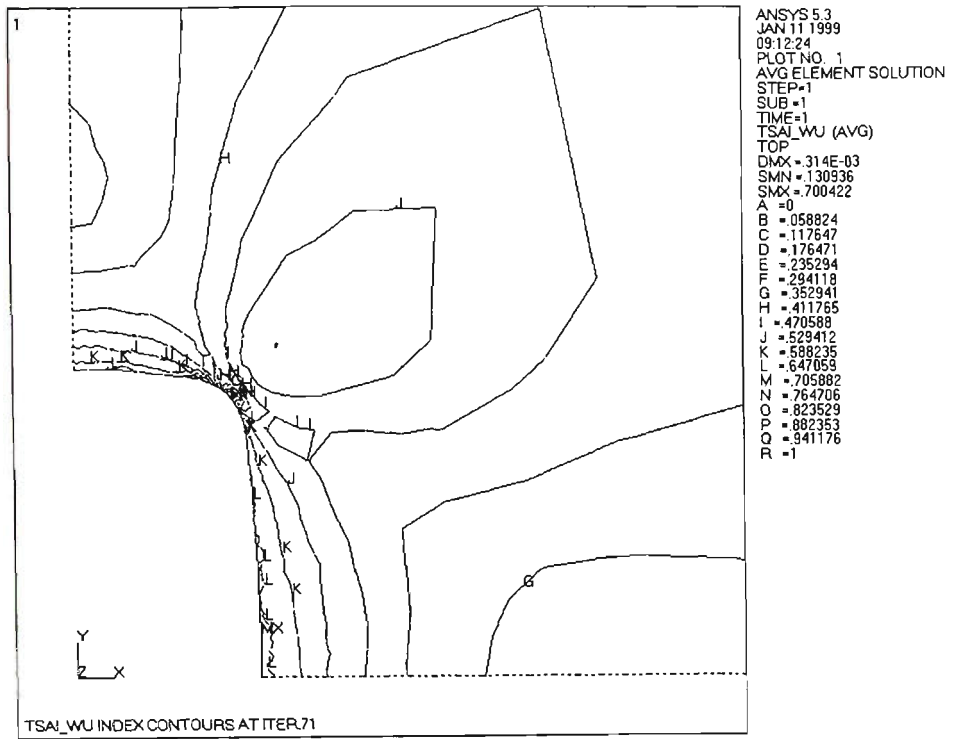


Figure 5.14: Tsai-Wu index distribution at iteration 71 (optimal), case  $S_r = -1$

Figure 5.15 shows the plot of the initial (iteration 0) and final (iteration 71) Tsai-Wu index distribution along the profile versus angular positions ( $0^\circ \leq \theta \leq 90^\circ$ ) for a quarter model (case  $S_r = -1$ ).

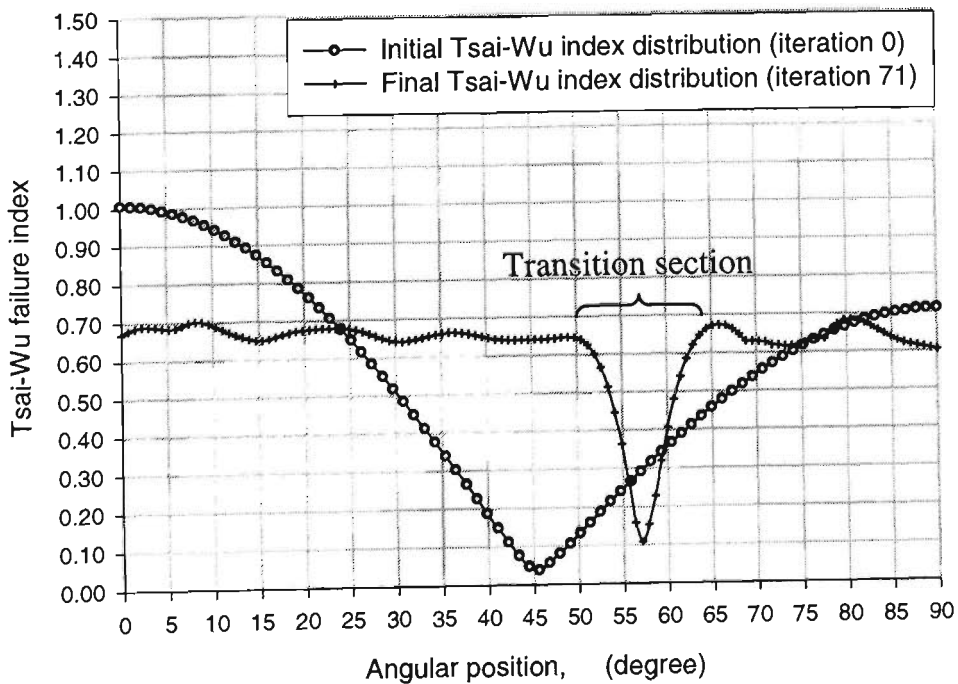
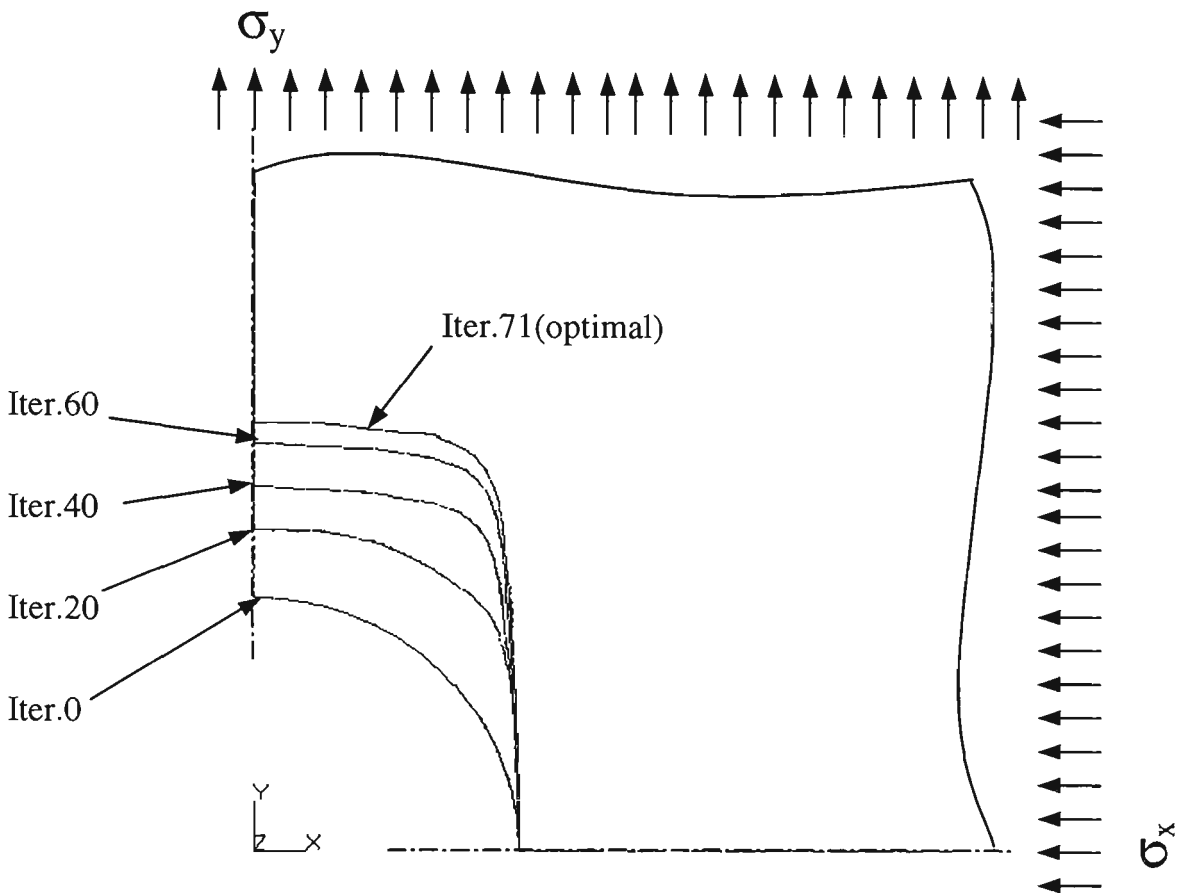


Figure 5.15: Tsai-Wu index distribution along the profile versus angular positions at iteration 0 (initial) and iteration 71 (optimal) for the case  $S_r = -1$

Figure 5.16 shows the changing hole profiles in the course of optimization (quarter model) at iterations 0 (initial), 20, 40, 60 and 71 (optimal) for the case  $S_r$  of -1. It is seen that material was removed quickly from iteration 0 (initial) to iteration 40, but at a slower rate from iteration 40 to iteration 60, then very slowly from iteration 60 to iteration 71 (optimal), reflecting the characteristics of PSM.



**Figure 5.16:** Hole profiles at iterations 0(initial), 20, 40, 60 and 71 (optimal), case  $S_r = -1$

Figure 5.17 shows the optimization history for the case  $S_r$  of -1, including the variation of the maximum Tsai-Wu index and material removal ratio  $m_r$  versus the iteration number. The minimum Tsai-Wu index on the boundary was always close to zero due to the existence of “isotropic points”, so it was not plotted on the graph. It can be seen that the maximum Tsai-Wu index keeps decreasing as the optimization proceeds. The graph of  $m_r$  indicates that a large amount of materials was removed initially, then the

rate of material removal gradually reduced until the optimization process converged, reflecting PSM's characteristics.

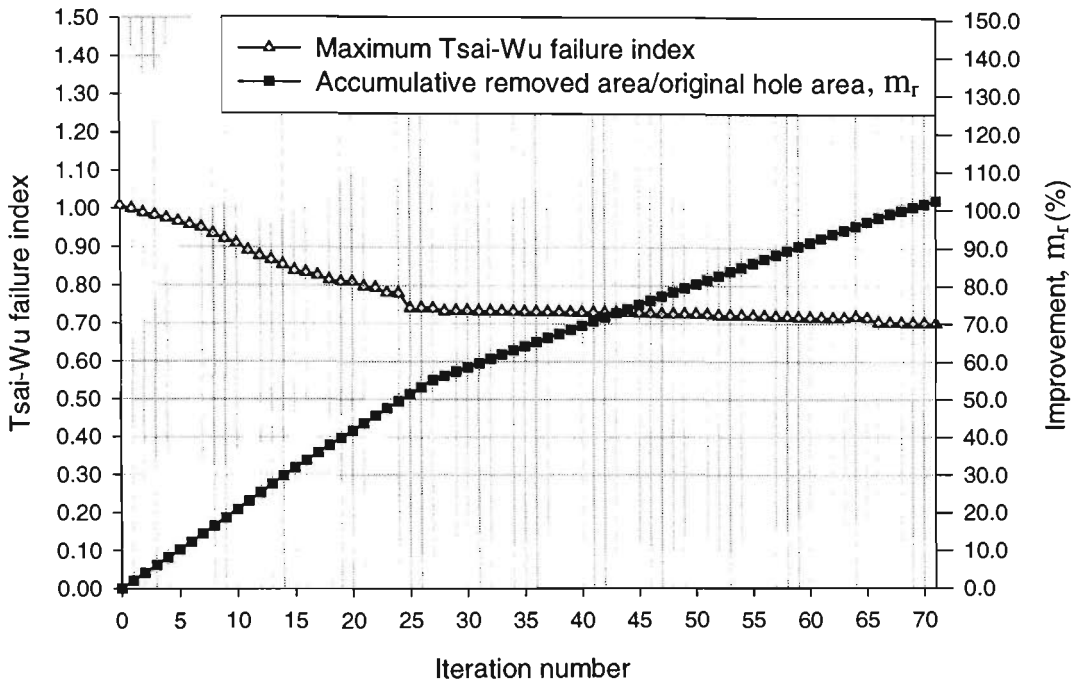


Figure 5.17: Optimization history for the case  $S_r = -1$

Figures 5.18 and 5.19 show the optimum profiles for the cases when stress ratios  $S_r$  takes values of -1.5 and -2 respectively. The optimal hole shapes obtained in three cases studied were like quadrangle holes with rounded corners as illustrated in Figures 5.14, 5.18 and 5.19. As the absolute value of the stress ratio was increased the hole became more rounded at the transition sections, and the major axes of the holes were increased or the holes became more elongated. However, the lengths of major axes did not follow a rule as was in the case for isotropic materials. The FEM simulation also required more iterations as the absolute value of the stress ratio was increased.

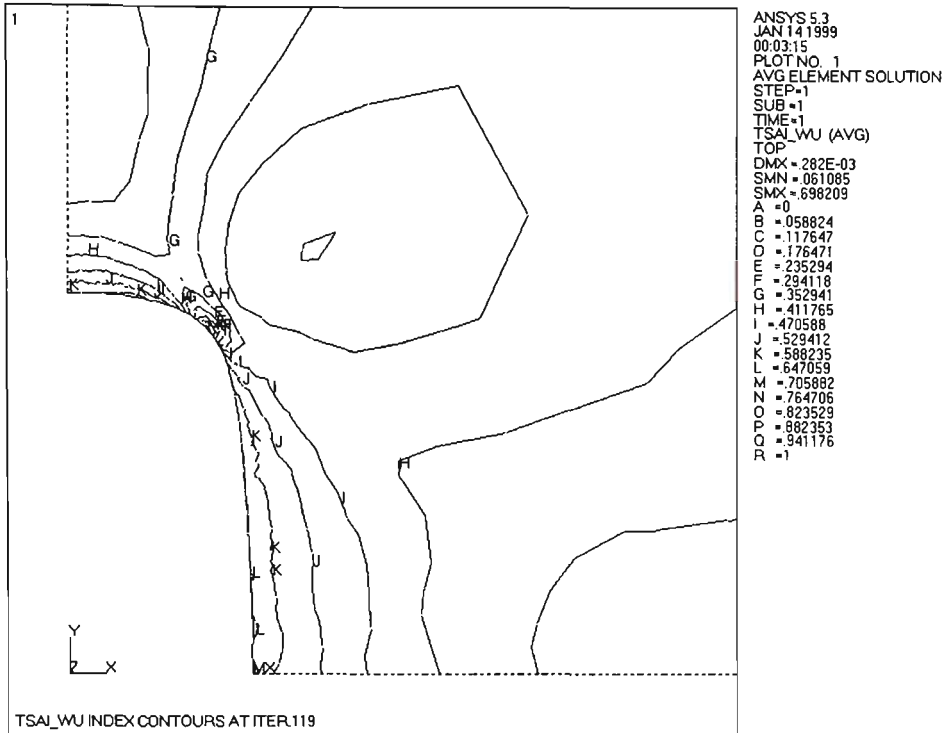


Figure 5.18: Tsai-Wu index distribution at iteration 119 (optimal), case  $S_r = -1.5$

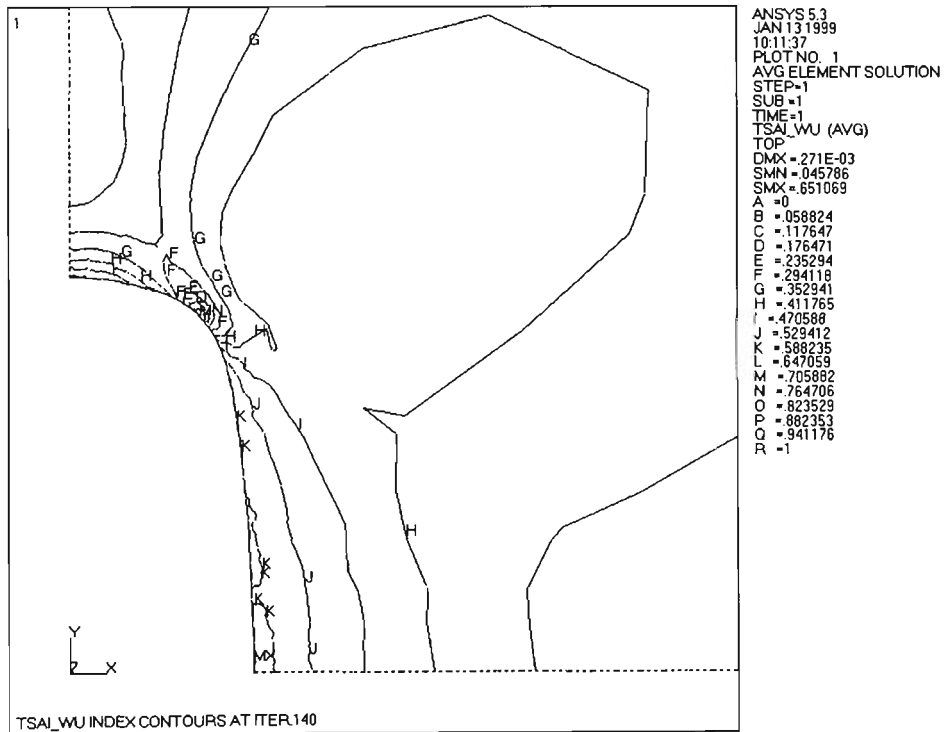


Figure 5.19: Tsai-Wu index distribution at iteration 140 (optimal), case  $S_r = -2.0$

## **5.4 Concluding remarks**

It has been shown that the FEM simulation can be extended to solve successfully the problem of stress minimization involving advanced composite laminates, employing the Tsai-Wu criterion and the first ply failure theory.

The FEM simulation has been applied to find optimal stress raiser profiles in a quasi-isotropic composite laminate plate  $[0^0, \pm 45^0, 90^0]_s$  under various biaxial stress states. While the optimal profiles in the case of the plate under biaxial tension looked identical to those of isotropic materials under the same stress ratio (Chapter 3), the optimal profiles obtained in the case of the plate under biaxial tension-compression did not. It should be noted that quasi-isotropic laminates' elastic properties are, by definition, independent of orientation, i.e. the in-plane stiffnesses and compliances and all engineering elastic constants are identical in all directions. Quasi-isotropic laminates, however, are not isotropic as far as the first ply failure is concerned according to Daniel and Ishai (1994).

In the case of the composite plate under biaxial tension-compression, the results show that there are 'isotropic points' of near zero Tsai-Wu index lying on the boundary of the discontinuity, which always exist during the course of optimization. This results in the optimized profiles, the corner regions or transition sections of which happen to be lowly stressed areas with isotropic points.

## *Chapter 6*

# **CONCLUSIONS AND RECOMMENDATIONS FOR FUTURE WORKS**

Algorithms have been proposed to simulate Durelli's PSM by FEM to solve the stress minimization problems, involving both isotropic materials and advanced fibrous composite laminates. In this chapter, conclusions drawn from this study and some recommendations for further investigations are given.

### **6.1. Conclusions**

Durelli's PSM has been successfully simulated by numerical procedures based on FEM, incorporating boundary smoothing and remeshing subroutines. The graphs of  $m_r$  versus iterations plotted in the optimization histories in all cases studied indicated that materials were at first removed quickly from the boundaries, the material removal was then controlled to be slower. This characteristic speeds up the convergence, or reduces computation costs while it still ensures the satisfaction of the optimality criteria by monitoring the maximum equivalent or Tresca stress for isotropic material, or Tsai-Wu

indices for composite material, until the processes converged.

The use of B-splines for boundary representation and primary moving control points based on a simple approximation given in Equations (3.1) and (3.2), simulates successfully the 'smooth' material removal mechanism of the PSM procedure. The boundary smoothing subroutine adopting cubic B-spline curves can produce smooth boundaries with least oscillatory shapes and thus avoids the notch-effect problems which may make the optimization process diverge as reported by Tranxuan (1998). By employing the design element concept (Section 3.2.3) with automatic mesh generators and adaptive mesh refinement, the mesh distortion problems associated with changing boundary can be avoided. It also reduces the computation efforts required in adaptive mesh refinement.

It is found that when the required uniformity of stress distribution along the stress raiser profile is not met, the use of a preset minimum number of elements to be removed at the fine tuning stage -  $\min\{nmin(K)\}$  as a termination criterion ensures the convergence of the process. The value of  $\min\{nmin(K)\}$  influences the convergence and final results significantly as presented in Section 3.3.3. It is suggested it should be set as one (asymmetrical structures) so that the process can simulate the finest cut with the preset *esize*.

A class of optimal profile problems, which were solved experimentally and explicitly by Durelli and his associates but usually overlooked by other numerical methods, were presented in this study. They are optimal profiles containing isotropic points of zero stress. It was shown in Chapters 4 and 5 that isotropic points, which always exist during the course of optimization in general, could lead to divergence from the

optimal profile. This problem was addressed by adopting a protection scheme, which takes into account the existence of isotropic points and transition sections. It was shown in Chapter 4 that results obtained by FEM simulation were further improved by the added feature of the protection scheme, and that the improved algorithm (Section 4.2.2) could handle more general classes of stress minimization problems.

The FEM simulation was also extended to solve successfully the problem of stress minimization involving advanced composite laminates, employing the Tsai-Wu criterion and the first ply failure theory as presented in Chapter 5. The optimality criterion for minimizing stress concentration in advanced composite laminates proposed in Section 5.2.2, was proved to be applicable. It should be noted that such problems cannot be easily studied by PSM since damage in the composite materials may occur when the operator files away materials from the stress raiser boundary.

It is seen that the proposed smoothing subroutine is not limited to two-dimensional structures, but can be extended to three-dimensional structures by taking into account the Z direction and employing a smooth surface function.

It was also demonstrated that the results found by the FEM simulation showed further improvement from PSM solutions by Durelli and Rajaiah (1979). This is due to the fact that FEM simulation does not experience difficulties in the practical manufacturing and optimizing process of photoelastic models. For instance, using PSM to optimize a plate with a very small hole can be quite a challenging task. This is reflected in the comparatively more rounded shapes obtained by Durelli and Rajaiah (1979). Furthermore, it is not possible to experiment freely at will and to venture too far with cuts in the photoelastic model, as models cannot be 'recut' as in cases of FEM simulation.

## 6.2. Recommendations for future works

The proposed FEM simulation algorithm has been applied to solve certain stress minimization problems found in isotropic material and advanced fibrous composite laminate structures. Further studies are however required to improve the convergence, and/or to extend the capability of the proposed algorithm to solve more technically interesting optimization problems.

- In the proposed FEM simulation, a fixed value of *esize* is used throughout the optimization process. The effects of *esize* on the convergence as outlined in Section 3.3.4 have shown that a substantial computation cost can be saved and a “less optimal” result is obtained if a larger *esize* is used. Therefore, an investigation on a FEM simulation procedure, in which large *esize* values can be used first, smaller values can be used later in the fine tuning stage, should be carried out. Such a procedure, while keeping the computation at reasonable costs, still produces acceptable results.
- As PSM, the FEM simulation only emphasizes on modifying a pre-given design so that the stress concentration is minimized and further weight savings can be obtained. However, designing a component of a given volume (weight) with stress minimization, or designing a component of a given stress constraint with volume (weight) minimization, is of more technical interest in practice. Consequently, the investigation on the problems (i) stress minimization subjected to volume (weight) constraint, or (ii) area minimization (weight) subjected to stress constraint by extending the proposed FEM simulation technique, is suggested for further studies.

- The proposed technique should be extended to three-dimensional structures.
- The optimal profiles for composite laminates have been obtained employing the Tsai-Wu and first ply failure theories. Investigation of the effects of different failure theories to the convergence and final results should also be carried out.

## REFERENCES

- Adelman, H.M. and Haftka, R.T. (1986), Sensitivity analysis of discrete structural systems, *AIAA J.I.*, Vol.24, pp.823-832.
- Arora, J.S. and Haug, E.J. (1979), Methods of design sensitivity analysis in structural optimization, *AIAA J.*, Vol.17, pp.970-974.
- ANSYS, Inc. (1996), *ANSYS theory reference*, ANSYS, Inc.
- Atrek, E. (1989), SHAPE: A program for shape optimization of continuum structures, in: Brebbia and Hernandez (eds.), *Computer Aided Optimum Design of Structures: Applications*, Computational Mechanics Publications, Southampton, pp.135-144.
- Aubert, P. and Rousselet, B. (1998), Sensitivity computation and shape optimization for a non-linear arch model with limit-points instabilities, *Int. J. Numer. Meths. Engrg.*, Vol.42, pp.15-48.
- Azegami, H. and Wu, Z.C. (1996), Domain optimization analysis in linear elastic problems (approach using traction method), *JSME Int. J., Series A, Mechanics and Material Engineering*, Vol.39, No.1, pp.272-278.
- Bäcklund, J. and Isby, R. (1988), Shape optimization of holes in composite shear panels. In: Rozvany, G.I.N., Karihaloo, B.L. (eds.), *Structural Optimization*, Kluwer Academic Publishers, pp.9-16.

- Banichuk, N.V. (1976), Optimization of elastic bars in torsion, *Int. J. Solids and Structures*, Vol.12, pp.275-286.
- Banichuk, N.V. (1989), *Problems and Methods of Optimal Structural Design*, Plenum Press, New York.
- Barthelemy, J.F.M. and Haftka, R.T. (1993), Recent advances in approximation concepts for optimum structure design, In: Rozvany, G.I.N. (ed.), *Optimization of Large Systems*, Vol.1, pp.235-256.
- Baud, R.V. (1934), Fillet profiles of constant stress, *Product Engineering*, Vol.5, pp.133-134.
- Baumgartner, A., Harzheim, L. and Mattheck, C. (1992), SKO (Soft Kill Option) The biological way to find an optimum structure topology, *Int. J. Fatigue*, Vol.14, pp.387-393.
- Bendsøe, M.P. (1995), *Optimization of Structural Topology, Shape, and Material*, Springer, Berlin.
- Bendsøe, M.P. and Kikuchi, N.V., (1988), Generating optimal topologies in structural design using a homogenization method, *Compu. Meths. Appl. Mech. Engrg.*, Vol.71, pp.197-224.
- Bennett, J.A. and Botkin, M.E. (1985), Structural shape optimization with geometric description and adaptive mesh refinement, *AIAA J.*, Vol.23, pp.458-464.
- Berke, L. and Khot, N.S. (1988), Performance characteristics of optimality criteria

methods, in: Rozvany, G.I.N. and Karihaloo, B.L. (eds.), *Structural Optimization*, Kluwer Academic Publishers, Dordrecht, pp.31-37.

Botkin, M.E. (1982), Shape optimization of plate and shell structures, *AIAA J.*, Vol.20, No.2, pp.268-273.

Braibant, V. and Fleury, C. (1984), Shape optimal design using B-Splines, *Compu. Meths. Appl. Mech. Engrg.*, Vol.44, pp.247-267.

Braibant, V. and Fleury, C. (1985), An approximation-concepts approach to shape optimal design, *Compu. Meths. Appl. Mech. Engrg.*, Vol.53, pp.119-148.

Bugeda, G. and Oliver, J. (1993), A General methodology for structural shape optimization problems using automatic adaptive meshing, *Int. J. Numer. Meths. Engrg.*, Vol.36, pp.3161-3185.

Chen, J.L. and Tsai, W.C. (1993), Shape optimization by using simulated biological growth approaches, *AIAA J.*, Vol.31, No.11, pp.2143-2147.

Chun, Y.W. and Haug, E.J. (1978), Two-dimentional shape optimal design, *Int. J. Numer. Meths. Engrg.*, Vol.13, pp.311-336.

Cook, R.D. (1995), *Finite Element Modelling for Stress Analysis*, John Wiley & Sons, New York.

Curtis, J.P. and Walpole, L.J. (1982), Optimization of the torsional rigidity of axisymmetric hollow shafts, *Int. J. Solids and Structures*, Vol.18, pp.883-887.

- Daniel, I.M. (1980), Behavior of Graphite/Epoxy plates with holes under biaxial loading, *Experimental Mechanics*, Vol. 20, pp.1-8.
- Daniel, I. M. and Ishai, O., (1994), *Engineering Mechanics of Composite Materials*, Oxford University Press, New York.
- Daniel, I.M., Rowlands, R.E. and Whiteside, J.B. (1974), Effects of material and stacking sequence on behavior of composite plates with holes, *Experimental Mechanics*, Vol. 14, pp.1-9.
- Datoo, M.H. (1991), *Mechanics of Fibrous Composites*, Elsevier Science Publishers, London.
- Dems, K. (1980), Multiparameter shape optimization, *Int. J. Numer. Meths. Engrg.*, Vol.15, pp.1517-1539.
- Dems, K. and Mróz, Z. (1978), Multiparameter structural shape optimization by the finite element method, *Int. J. Numer. Meths. Engrg.*, Vol.13, pp.247-263.
- Dhir, S.K. (1981), Optimization in a class of hole shapes in plate structures, *ASME J. Appl. Mech.*, Vol.48, pp.905-908.
- Dhir, S.K. (1982), Optimization of reinforcement for a class of openings in plate structures, *ASME J. Appl. Mech.*, Vol.49, pp.916-920.
- Dhir, S.K. (1983), Optimization of openings in plates under plane stress, *AIAA J.*, Vol.21, No.10, pp.1444-1447.

- Ding, Y. (1986), Shape optimization of structures: a literature survey, *Computers & Structures*, Vol.24, pp.985-1004.
- Durelli, A.J. and Murray, W.M. (1943), Stress distribution around an elliptical discontinuity in any two-dimensional, uniform and axial, system of combined stress, *Transactions of the Society of Experimental Stress Analysis*, pp.19-31.
- Durelli, A.J., Parks, V.J. and Uribe, S. (1968), Optimization of a slot end configuration in a finite plate subjected to uniformly distributed load, *ASME J. Appl. Mech.*, Vol.35, pp.403-406.
- Durelli, A.J., Brown, K. and Yee, P. (1978), Optimization of geometric discontinuities in stress field, *Experimental Mechanics*, Vol. 18, pp.303-308.
- Durelli, A.J. and Rajaiah, K. (1979), Optimum hole shapes in finite plates under uniaxial load, *ASME J. Appl. Mech.*, Vol.46, pp.691-695.
- Durelli, A.J. and Rajaiah, K. (1981), Minimizing stress with photoelasticity, *Machine Design*, Vol.53, No. 28, pp.125-130.
- Durelli, A.J., Erickson, M. and Rajaiah, K. (1981), Optimum shapes of central holes in square plates subjected to uniaxial uniform load, *Int. J. Solids and Structures*, Vol.17, pp.787-793.
- Erickson, P.E. and Riley, W.W. (1978), Minimizing stress concentrations around circular holes in uniaxially loaded plates, *Experimental Mechanics*, Vol. 18, pp.97-100.

- Falzon, B., Steven, G.P. and Xie, Y.M. (1996), Shape optimization of interior cutouts in composite panels, *Structural Optimization*, Vol.11, pp.43-49.
- Fancello, E.A. and Feijoo, R.A. (1994), Shape optimization in frictionless contact problems, *Int. J. Numer. Meths. Engrg.*, Vol.37, pp.2311-2335.
- Fleury, C. (1980), An efficient optimality criteria approach to the minimum weight design of elastic structures, *Computers and Structures*, Vol.11, pp.163-173.
- Francavilla, A., Ramakrishnan, C.V. and Zienkiewicz, O.C. (1975), Optimization of shape to minimize stress concentration, *J. Strain Analysis*, Vol.10, No.2, pp.63-70.
- Frocht, M.M. (1967), *Photoelasticity*, Vol. 1&2, Wiley, New York.
- Gallagher, R.H. and Zienkiewicz, O.C. (1973), *Optimum Structural Design: Theory and Applications*, John Wiley and Sons, London.
- Grunwald, J. and Schnack, E. (1997), A fatigue model for shape optimization, *Structural Optimization*, Vol.14, pp.36-44.
- Gürdal, Z. and Haftka, R.T. (1993), Optimization of composite laminates, In: Rozvany, G.I.N. (ed.), *Optimization of Large Systems*, Vol.2, pp.623-648.
- Haftka, R.T. and Adelman, H.M. (1993), Sensitivity of Discrete Systems, In: Rozvany, G.I.N. (ed.), *Optimization of Large Systems*, Vol.1, pp.289 - 312.
- Haftka, R.T. and Grandhi, R.V. (1986), *Structural Shape Optimization-A Survey*,

*Compu. Meths. Appl. Mech. Engrg.*, Vol.57, pp.91-106.

Haftka, R.T. and Gürdal, Z. (1992), *Elements of Structural Optimization*, 3<sup>rd</sup> revised and expanded edition, Kluwer Academic Publishers, The Netherlands.

Haftka, R.T. and Prasad, B. (1981), Optimum structural design with plate bending elements-A survey, *AIAA J.*, Vol.19, pp.517-522.

Haftka, R.T., Gürdal, Z. and Kamat, M.P. (1990), *Elements of Structural Optimization*, 2<sup>nd</sup> revised edition, Kluwer Academic Publishers, The Netherlands.

Hajela, P. (1990), Genetic search—an approach to the non-convex optimization problem, *AIAA J.*, Vol. 28, pp.1205-1210.

Han, C.S., Wang, B.P. (1993), Optimum design of rectangular panels with a hole, *Advances in Engineering Software*, Vol.16, pp.127-134.

Hemada, M., Seguchi, Y. and Tada, Y. (1980), Shape determination problems of structures by the inverse variational principle, *Bull. JSME*, Vol.23, pp. 1581.

Heywood, R.B. (1969), *Photoelasticity for Designers*, Pergamon, Oxford.

Hinton, E. and Sienz, J. (1995), Fully stressed topological design of structures using an evolutionary procedure, *Engineering Computations*, Vol.12, pp.229-244.

Hoà, S.V. (1995), *Computer-aided design of polymer-matrix composite structures*, Marcel Dekker, New York.

- Hoja, S.V., De Wilde, W.P., Blain W.R. (1998), *Computer methods in composite materials VI – CADCOM 98*, Computational Mechanics Publications, Southampton.
- Howland, R.C.J. (1929-30), On the stresses in the neighborhood of a circular hole in a strip under tension, *Phil. Trans. Roy. Soc. (London) A*, Vol. 229, pp. 67.
- Hull, D. (1981), *An introduction to Composite Materials*, Cambridge University Press, Cambridge.
- Hyer, M.W. and Lee, H.M. (1991), The use of curvilinear fibres format to improve buckling resistance of composite plates with central circular holes, *Composite Structures*, Vol.18, pp.239-261.
- Imam, M.H. (1982), Three-dimensional shape optimization, *Internat. J. Numer. Meths. Engrg.*, Vol.18, pp.661-673.
- Inglis, C.E. (1913), Stresses in a plate due the presence of cracks and sharp corners, *Transactions of the Institute of Naval Architects (England)*, Vol.LV, pp.219-231.
- Jenkins, W.M. (1991), Towards structural optimization via the genetic algorithm, *Computers and Structures*, Vol.40, pp.1321-1327.
- Jiang, T. and Papalambros, P. (1996), Optimal structural topology design using the homogenization method with multiple constraints, *Engineering Optimization*, Vol. 27, pp.87-108.
- Kadivar, M.H., Sensharma, K.P. and Haftka, R.T. (1994), Effect of Isotropy of

actuation strains for a plate with hole, *AIAA J.*, Vol.32, No.8, pp.1743-1745.

Kagan, P., Fischer, A. and Bar-Yoseph, P.Z. (1998), New B-Spline finite element approach for geometrical design and mechanical analysis, *Int. J. Numer. Meths. Engrg.*, Vol.41, pp.435-458.

Kamat, M.P. (1993), *Structural Optimization: Status and Promise*, Vol. 150, Progress in Astronautics and Aeronautics, AIAA, Washington.

Karihaloo, B.L. and Kanagasundaram, S. (1989), Minimum-weight design of structural frames, *Computers and Structures*, Vol.31, pp.647-655.

Kaw, A.K. (1997), *Mechanics of composite materials*, CRC Press, New York.

Khot, N.S. (1981), Algorithms based on optimality criteria to design minimum weight structures, *Engineering Optimization*, Vol.5, pp.73-90.

Kikuchi, N.V., Chung, K.Y., Torigaki, T. and Taylor, J.E. (1986), Adaptive finite element methods for shape optimization of linear elastic structures, *Compu. Meths. Appl. Mech. Engrg.*, Vol. 57, pp.67-89.

Kohli, H.S. and Carey, G.F. (1993), Shape optimization using adaptive shape refinement, *Int. J. Numer. Meths. Engrg.*, Vol.36, pp.2435-2451.

Kristensen, E.S. and Madsen, N.F. (1976), On the optimum shapes of fillets in plates subject to multiple-in-plane loading, *Int. J. Numer. Meths. Engrg.*, Vol.10, pp.1007-1019.

- Kunar, R.R. and Chan, A.S.L. (1976), A method for the configurational optimization of structures, *Compu. Meths. Appl. Mech. Engrg.*, Vol.7, pp.331-350.
- Lancaster, P., Salkauskas, K. (1986), *Curve and Surface Fitting*, Academic Press Inc.
- Le Riche, R. and Cailletaud, G. (1998), A mixed Evolutionary/Heuristic approach to shape optimization, *Int. J. Numer. Meths. Engrg.*, Vol.41, pp.1463-1484.
- Le Riche, R. and Haftka, R.T. (1993), Optimization of laminate stacking sequence for buckling load maximization by genetic algorithm, *AIAA J.*, Vol.31, pp.951-956.
- Lekhnitskii, S.G. (1963), *Theory of elasticity of an anisotropic elastic body*, Holden-Day, San Francisco.
- Lekhnitskii, S.G. (1968), *Anisotropic plates*, translated by S.W. Tsai and T. Cheron, Gordon and Breach Science publishers, New York.
- Maier, G. (1973), Limit design in the absence of a given layout: a finite element, zero-one programming problem, in: Gallagher and Zienkiewicz (eds.), *Optimum Structural Design: Theory and Applications*, John Wiley & Sons, London, pp.223-239.
- Mattheck, C. and Burkhard, S. (1990), A new method of structural shape optimization based on biological growth, *Int. J. Fatigue*, Vol.12, pp.185-190.
- Mattheck, C., Teschner, M. and Schafer, J. (1997), Mechanical control of root growth-a computer simulation, *J. Theoretical Biology*, Vol.184, pp.261-269.

- Michell, A.G.M. (1904), The limits of economy of material in frame structures, *Phil. Mag. Series 6*, Vol. 8 (47), pp. 589-597.
- Miura, H., Vanderplaats, G.N. and Kodiyalam, S. (1989), Experiences in Large Scale Structural Design Optimization, In: Brebbia, C.A. and Peters, A. (eds.), *Applications of Supercomputers in Engineering*, pp.251-268.
- Na, M., Kikuchi, N. and Taylor, J.E. (1984), Optimal shape remodeling of linearly elastic plates using finite element methods, *Int. J. Numer. Meths. Engrg.*, Vol.20, pp.1823-1840.
- Nagendra, S., Haftka, R.T. and Gürdal, Z. (1992), Stacking sequence optimization of simply supported laminates with stability and strain constraints, *AIAA J.*, Vol.30, pp.2132-2137.
- Neuber, H. (1958), *Theory of Notch Stresses: Principle for Exact Calculation of Strength with Reference to Structural Form and Material*, Oakridge, Tennessee.
- Nguyen, V. and Tran, D. (1999), Optimization of stress raiser profile in structures made of advanced composite materials, *The second Australian Congress on Applied Mechanics (ACAM 99)*, Canberra, pp.458-463.
- Oda, J. (1977), On a technique to obtain an optimum strength shape by the finite element method, *Bull. JSME*, Vol. 20, pp.160-167.
- Oda, J. and Yamazaki, K. (1977), On a technique to obtain an optimum strength shape of axisymmetric body by the finite element method, *Bull. JSME*, Vol.20, pp.1524-

1532.

- Oda, J. and Yamazaki, K. (1979), On a technique to obtain an optimum strength shape by the finite element method: Application to the problem under body force, *Bull. JSME*, Vol.22, pp.131-140.
- Olhoff, N. and Taylor, J.E. (1983), On structural optimization, *ASME J. Appl. Mech.*, Vol.50, pp.1139-1151.
- Osyczka, A. (1984), *Multicriterion Optimization in Engineering with Fortran Programs*, Ellis Horwood Limited, Chichester.
- Parks, V.J. (1975), Maximum stress in a tensile strip with a large hole, *Experimental Mechanics*, Vol.15, pp.389-391.
- Pedersen, P. (1993), Optimal orientation of anisotropic materials; Optimal distribution of anisotropic materials; Optimal shape design with anisotropic materials; Optimal design for a class of non-linear elasticity. In: Rozvany, G.I.N. (ed.), *Optimization of Large Systems*, Vol.2, pp.649-682.
- Pedersen, P. and Laursen, C.L. (1982), Design for minimum stress concentration by finite elements and linear programming, *J. Structural Mech.*, Vol.10, pp.375-391.
- Peterson, R.E. (1953), *Stress Concentration Design Factors*, John Wiley & sons, New York.
- Pilkey, W.D. (1997), *Peterson's Stress Concentration Factors*, John Wiley & Sons, New York, pp.175-256.

- Plant, R.H. and Olhoff, N. (1983), Optimal forms of shallow arches with respect to vibration and stability, *J. Structural Mech.*, Vol.11, pp.81-100.
- Prasad, B. and Emerson, J.F. (1984), Optimal structural remodeling of multi-objective systems, *Computers and Structures*, Vol.18, pp.619-628.
- Queau, J.P. and Trompette, P. (1980), Two dimensional shape optimal design by finite element method, *Int. J. Numer. Meths. Engrg.*, Vol.15, pp.1603-1612.
- Rajeev, S. and Krishnamoorthy, C.S. (1992), Discrete optimization of structures using genetic algorithms, *ASCE J. Structural Engrg.*, Vol.118, pp.1233-1249.
- Ramakrishnan, C.V. and Francavilla, A. (1975), Structural shape optimization using penalty functions, *J. Structural Mech.*, Vol.3, pp.403-432.
- Ramm, E., Bletzinger, K.-U. and Kimmich, S. (1991), Strategies in shape optimization of free form shells, In: Wriggers, P. and Wagner, W. (eds.), *Nonlinear Computational Mechanics-State of the Art*, Springer, Berlin, pp.163-192.
- Richards, R. Jr. and Bjorkman, G.S. Jr. (1980), Harmonic shapes and optimum design, *ASCE J. Engrg. Mech. Div.*, Vol.106 (6), pp.1125-1134.
- Richards, R. Jr. and Bjorkman, G.S. Jr. (1982), Neutral holes: Theory and design, *ASCE J. Engrg. Mech. Div.*, Vol.108 (5), pp.1125-1134.
- Rodriguez-Velazquez, J. and Seireg, A.A. (1985), Optimizing the shapes of structures via a rule-based computer program, *Comput. Mech. Engrg.*, Vol.4, pp.20-28.

- Roux, W.J., Stander, N. and Haftka, R.T. (1998), Response surface approximation for structural optimization, *Int. J. Numer. Meths. Engrg.*, Vol.42, pp.517-534.
- Rozvany, G.I.N., Bendøse, M.P. and Kirsh, U. (1995), Layout optimization of structures, *Appl. Mech. Review*, Vol.48, No.2, pp.41-119.
- Savin, G.N. (1961), *Stress Concentration around Holes*, Pergamon Press, New york.
- Schnack, E. (1979), An optimization procedure for stress concentrations by finite element technique, *Int. J. Numer. Meths. Engrg.*, Vol.14, pp.115-124.
- Schnack, E., and Spörl, U. (1986), A mechanical dynamic programming algorithm for structure optimization, *Int. J. Numer. Meths. Engrg.*, Vol.23, pp.1985-2004.
- Schumacher, A. and Becker, W. (1998), Optimized lay-ups of composite laminates for airframe structural design, *Proceedings of the sixth Conference on Computer Methods in Composite Materials*, Montreal, pp.13-23.
- Seireg, A.A. and Rodriguez, J. (1997), *Optimizing the Shape of Mechanical Elements and Structures*, Marcel Dekker, New York.
- Senocak, E. and Waas, A.M. (1993), Neutrally designed cutouts for laminated shells, In: Hyer, M.V. (ed.), *Mechanics of Composite Materials-nonlinear Effects*, AMD-Vol.159, ASME, New York, pp.29-38.
- Sivakumar, K., Iyengar, N.G.R. and Deb, K. (1998), Optimum design of laminated composite plates with cutouts using a genetic algorithm, *J. Compo. Structures*, Vol.42, Iss.3, pp.265-279.

- Smith, D.R. (1974), *Variation Methods in Optimization*, Prentice Hall, Eaglewood Clifts, NT.
- Soares, C.A.M., Rodrigues, H.C., Faria, L.M.O. and Haug, E.J. (1984), Optimizatiuon of the geometry of shafts using boundary elements, *ASME J. Transmissions and Automation in Design*, Vol.106, pp.199-203.
- Spillers, W.R., Asce, M. and Singh, S. (1981), Shape optimization: Finite element example, *ASCE J. Structural Division*, Vol.107, pp.2015-2025.
- Steven, G.P., Querin, O.M., Guan, H., Xie, Y.M. (1998), *Structural Optimisation- Proceedings of the Australian Conference on Structural Optimisation*, Oxbridge, Melbourne.
- Suzuki, K. and Kikuchi, N. (1993), Layout optimization using the homogenization method, In: Rozvany, G.I.N. (ed.), *Optimization of Large Systems*, Vol.1, pp.157-176.
- Tada, Y., Matsumoto R. and Imagura, O. (1991), Optimum design of structures under uncertain loading by Boundary Element Method, *JSME Int. J., Series A, Mechanics and Material Engineering*, Vol.34, No.1, pp.23-29.
- Tan, S.C. (1987), Laminated composites containing an elliptical opening. I. Approximate stress analyses and fracture models, *J. Compo. Mater.*, Vol.21, pp.925-948.
- Tauchert, T.R. and Adibhatla, S. (1984), Design of laminated plates for maximum

stiffness, *J. Compo. Mater.*, Vol.18, pp.58-69.

Tekkaya, A.E. and Güneri, A. (1996), Shape optimization with the Biological Growth method: a parameter study, *Engineering Computations*, Vol.13, No.8, pp.4-18.

Thierauf, G. (1996), Optimal topologies of structures; Homogenization; Pseudo-Elastic Approximation and the Bubble-Method, *Engineering Computations*, Vol.13, No.1, pp.86-102.

Thomas, H.L. and Vanderplaats, G.N. (1993), The state of the art of approximation concepts in structural optimization, In: Rozvany, G.I.N. (ed.), *Optimization of Large Systems*, Vol.1, pp.257-270.

Timoshenko, S. and Goodier, J.N. (1970), *Theory of Elasticity*, McGraw-Hill, New York.

Topping, B.H.V. (1983), Shape optimization of skeletal structures: A review, *ASCE J. structural Engrg.*, Vol.109, pp.1933-1951.

Tran, D. and Nguyen, V. (1999), Optimal hole profile in a finite plate under uniaxial stress by finite element simulation of Durelli's photoelastic stress minimization method", *Finite Elements in Analysis and Design*, Vol.32, pp.1-20.

Tran, D. and Nguyen, V. (1998a), Finite element simulation of the photoelastic stress minimization to find optimal hole profile in a plate under axial stress, in: Steven, G.P. et.al. (eds.), *Proceedings of the First Australian Conference on Structural Optimization*, Sydney, pp.499-506.

- Tran, D. and Nguyen, V. (1998b), Optimal hole profile in a composite material plate under biaxial tension by finite element simulation”, in: Hoa, S.V. *et.al.* (eds.), *Proceedings of the Sixth International conference on Computer Methods in Composite Materials (CADCOM 98)*, Montreal, pp. 45-54.
- Tran, D., Do, T. and Nguyen, V. (1997), Layout optimization by photoelastic model and by finite element analysis simulation, in: Zayegh, A. (ed.), *Proceedings of the Third International Conference on Modelling and Simulation*, Melbourne, pp. 368-373.
- Tranxuan, D. (1998), Finite element simulation of a layout optimization technique by photoelastic stress minimization, *Finite Elements in Analysis and Design*, Vol.28, pp.277-292.
- Tsai, S.W. and Hahn, H.T. (1980), *Introduction to Composite Materials*, Technomic, Lancaster, PA.
- Tsai, S.W. and Wu, E.M. (1971), A general theory of strength for anisotropic materials, *J. Compo. Mater.*, Vol.5, pp.58-80.
- Tsangarakis, N. (1984), Fatigue failure of an orthotropic plate with a circular hole, *J. Compo. Mater.*, Vol.18, pp.47-57.
- Umetani, Y. and Hirai, S. (1978), Shape optimization of beams subject to displacement restrictions on the basis of the growing-reforming procedure, *Bull. JSME*, Vol.21, pp.1113-1119.

- Vanderplaats, G.N. (1982), Structural optimization-Past, Present and Future, *AIAA J.*, Vol.20, No.7, pp.992-1000.
- Vanderplaats, G.N. (1984), *Numerical Optimization Techniques for Engineering Design: with Application*, Mc Graw-Hill, New York.
- Vanderplaats, G.N. (1993), Mathematical programming methods for constraint optimization: Primal methods, in: Kamat M.P. (ed.), *Structural Optimization: Status and Promise*, Progress in Astronautics and Aeronautics, AIAA, Washington, Vol.150, pp.29-49.
- Vanderplaats, G.N. and Miura, H. (1989), Computational Trends in Large Scale Engineering Optimization, In: Brebbia, C.A. and Peters, A. (eds.), *Applications of Supercomputers in Engineering*, pp.269-283.
- Vanderplaats, G.N. and Weisshaar, T.A. (1989), Optimum design of composite structures, *Int. J. Numer. Meths. Engrg.*, Vol.27, pp.437-448.
- Velleichamy, S., Prakash, B.G., and Brun, S. (1990), Optimum design of cutouts in laminated composite structures, *Computers and Structures*, Vol.37, pp.241-246.
- Venkayya, V.B. (1978), Structural Optimization: a review and some recommendations, *Int. J. Numer. Meths. Engrg.*, Vol.13, pp.203-228.
- Venkayya, V.B. (1993a), Introduction: Historical perspective and future directions, in: Kamat M.P.(ed.), *Structural Optimization: Status and Promise*, Progress in Astronautics and Aeronautics, AIAA, Washington, Vol.150, pp.1-10.

- Venkayya, V.B. (1993b), Generalized optimality criteria methods, in: Kamat M.P. (ed.), *Structural Optimization: Status and Promise*, Progress in Astronautics and Aeronautics, AIAA, Washington, Vol.150, pp.151-182.
- Walker, T. R. and Hoff, R. (1988), Two dimensional shape optimization with application to the plate hole problem, *Engineering Optimization*, Vol.14, pp.39-52.
- Weck, M. and Steinke, P. (1983-1984), An efficient technique in shape optimization, *J. Structural Mech.*, Vol.11, pp.433-449.
- Wheeler, L.J. (1976), On the role of constant stress surfaces in the problem of minimizing elastic stress concentration, *Int. J. Solids and Structures*, Vol.12, pp.779-789.
- Wheeler, L.J. and Kunin, I.A. (1982), On voids of minimum stress concentration, *Int. J. Solids and Structures*, Vol.18, pp.85-89.
- Xie, Y.M. and Steven, G.P. (1993), A simple evolutionary procedure for structural optimization, *Computers and Structures*, Vol.49, No.5, pp.885-896.
- Xie, Y.M. and Steven, G.P. (1994), Optimal design of multiple load case structures using an evolutionary procedure, *Engineering Computations*, Vol.11, pp.295-302.
- Xie, Y.M. and Steven, G.P. (1997), *Evolutionary Structural Optimisation*, Springer-Verlag, Heidelberg.
- Zhou, M. and Rozvany, G.I.N. (1993), Iterative COC Methods, In: Rozvany, G.I.N.

(ed.), *Optimization of Large Systems*, Vol.1, pp.27-76.

Zienkiewicz, O.C. and Campbell, J.S. (1973), Shape optimization and sequential programming. In: R.H. Gallagher and O.C. Zienkiewicz (eds.) *Optimum Structural design*, Wiley, New York, pp.109-126.

## Appendix A

### ANALYTICAL SOLUTION FOR DETERMINING A POINT SUCH THAT THE SUM OF SQUARES OF THE DISTANCES FROM IT TO A GIVEN SET OF NODES IS MINIMIZED

Given a set of  $N$  nodes,  $i = 1, \dots, N$ . The task is to find a point  $P_k$  such that the sum of squares of distances from it to those points is minimized.

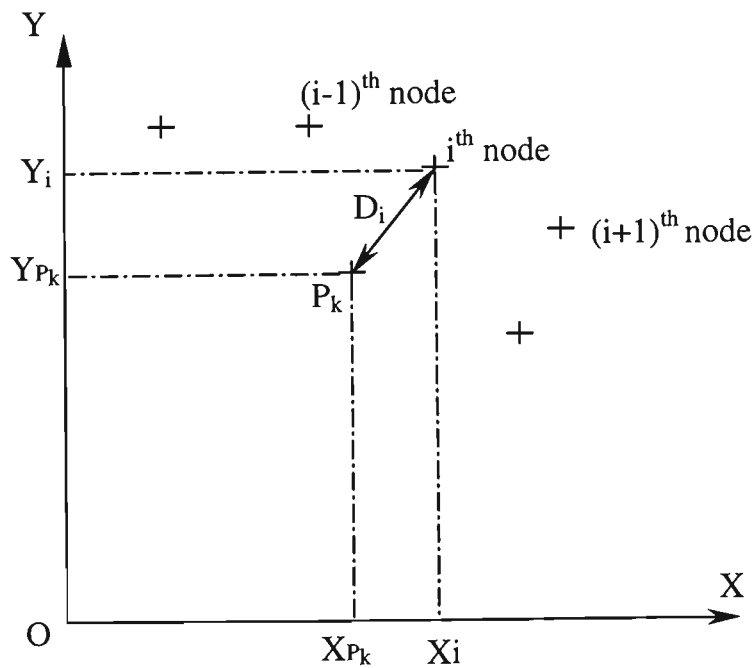


Figure A.1: Diagram of minimization of  $\sum_{i=1}^N D_i^2$

Let

$X_{P_k}, Y_{P_k}$  be Cartesian coordinates of  $P_k$ ;

$X_i, Y_i$  be Cartesian coordinates of the  $i^{\text{th}}$  node; and

$D_i$  be the distance from  $P_k$  to the  $i^{\text{th}}$  node.

From Figure A.1, we have

$$D_i^2 = (X_i - X_{P_k})^2 + (Y_i - Y_{P_k})^2 \quad (\text{A-1})$$

Sum of squares of distances from  $P_k$  to the given  $N$  nodes:

$$\sum_{i=1}^N D_i^2 = \sum_{i=1}^N (X_i - X_{P_k})^2 + \sum_{i=1}^N (Y_i - Y_{P_k})^2 \quad (\text{A-2})$$

It can be seen that  $\sum_{i=1}^N D_i^2$  is minimized if both  $\sum_{i=1}^N (X_i - X_{P_k})^2$  and  $\sum_{i=1}^N (Y_i - Y_{P_k})^2$  are minimized simultaneously.

Let

$$G(X_{P_k}) = \sum_{i=1}^N (X_i - X_{P_k})^2 \quad (\text{A-3})$$

$G(X_{P_k})$  has a minimum or maximum at  $X_{P_k}$ , if

$$\frac{\partial G(X_{P_k})}{\partial X_{P_k}} = 0 \quad (\text{A-4})$$

From Equation (A-3) and (A-4), we obtain:

$$X_{P_k} = \frac{1}{N} \sum_{i=1}^N X_i \quad (\text{A-5})$$

Hence  $G(X_{P_k})$  has a minimum or maximum at  $X_{P_k}$  determined by Equation (A-5).

Furthermore,

$$\frac{\partial^2 G(X_{P_k})}{\partial X_{P_k}^2} = 2 \tag{A-6}$$

Thus  $G(X_{P_k})$  is concave and has a minimum at  $X_{P_k}$ .

Similarly, we proved that

$$Y_{P_k} = \frac{1}{N} \sum_{i=1}^N Y_i \tag{A-7}$$

is the condition for  $\sum_{i=1}^N (Y_i - Y_{P_k})^2$  to have a minimum at  $Y_{P_k}$ .

Hence, point  $P_k$  having Cartesian coordinates  $X_{P_k}$ ,  $Y_{P_k}$  determined by Equations (A-5) and (A-7) satisfies the least square condition, i.e. the sum of squares of distances from it to the given  $N$  nodes is minimized.

## ***Appendix B***

### **CHECKING OPTIMAL SOLUTIONS WITH FINER MESHES FOR CASES: $S_r$ OF 1.5, -1 FOR ISOTROPIC MATERIAL; AND $S_r$ OF 1.5 FOR COMPOSITE LAMINATES**

The optimal solutions for three cases:  $S_r$  of 1.5, -1 for isotropic material; and  $S_r$  of 1.5 for composite laminates were presented in sections: 3.3.2, 4.2.1 and 5.3.2.1 respectively. They are further checked against those with finer meshes in this appendix. For each case, the FEM mesh of the optimal solution produced by the programs is refined. Since the element sizes on the hole boundaries are very small (e-size = 0.3 mm), only meshes in areas 1 and 2 are refined (figure 3.7).

#### **B.1 Case $S_r$ of 1.5 for isotropic material**

Figure B.1a and B.1b show the FEM models before and after mesh refinement. Figures B.2a and B.2b illustrate the Tresca stress distribution in the models before and after refining mesh. The results are tabulated in Table B.1. It can be seen that a larger number of elements were used for the refined FEM model, which results in the reduction of SEPC. However the magnitude of the maximum Tresca stress occurs on the boundary of interest still remains the same.

**Table B.1: Case  $S_r$  of 1.5 for isotropic material**

FEM model	esize (mm)	No. of elements	$\sigma_{\max}$ (MPa)	SEPC (%)
Algorithm produced	0.3	1408	17.57	0.0834
Mesh refined	0.3	3536	17.57	0.0474

**B.2 Case  $S_r$  of -1 for isotropic material**

Figures B.3a and B.3b show the FEM models before and after mesh refinement. Figures B.4a and B.4b illustrate the Tresca stress distribution in the models before and after refining mesh. The results are tabulated in Table B.2. As the previous case, a larger number of elements were used for the refined FEM model, which results in the reduction of SEPC. However the magnitude of the maximum Tresca stress occurs on the boundary of interest after mesh refinement is 0.32 % higher than that originally produced by the optimization program.

**Table B.2: Case  $S_r$  of -1 for isotropic material**

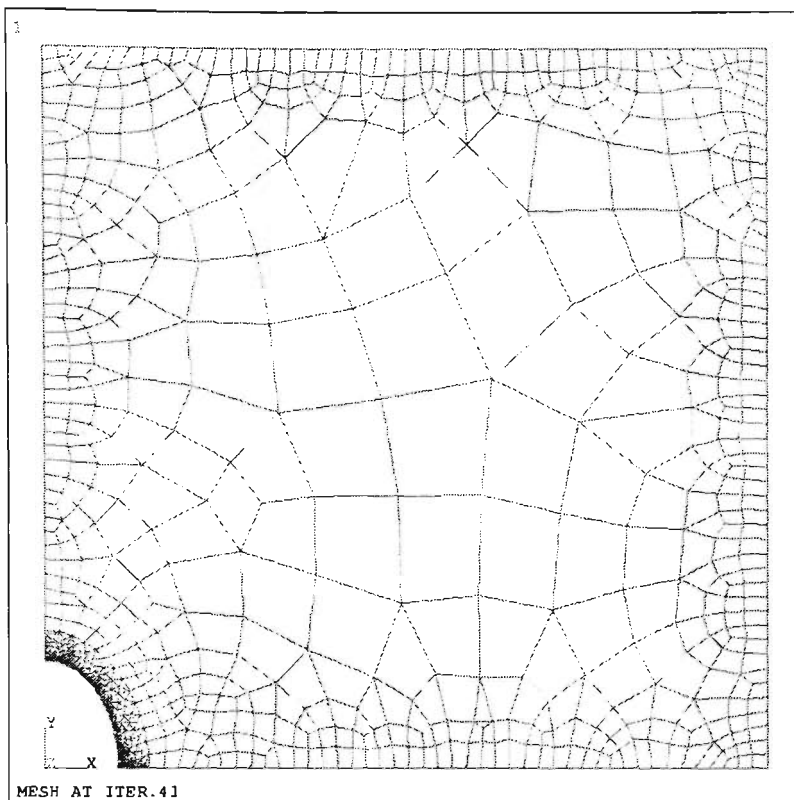
FEM model	esize (mm)	No. of elements	$\sigma_{\max}$ (MPa)	SEPC (%)
Algorithm produced	0.3	1168	30.613	0.479
Mesh refined	0.3	3290	30.712	0.215

### B.3 Case $S_r$ of 1.5 for composite laminates

Figures B.5a and B.5b show the FEM models before and after mesh refinement. Figures B.6a and B.6b illustrate the Tsai-Wu indices distribution in the models before and after refining mesh. The results are tabulated in Table B.3. For SHELL99-100 layer structural shell elements, the calculation of SEPC is not available by ANSYS 5.3 software. However, no errors were detected when checking the distortion of element shapes. The difference between the magnitudes of the maximum Tsai-Wu indices occur on the boundary of interest before and after mesh refinement is unnoticeable.

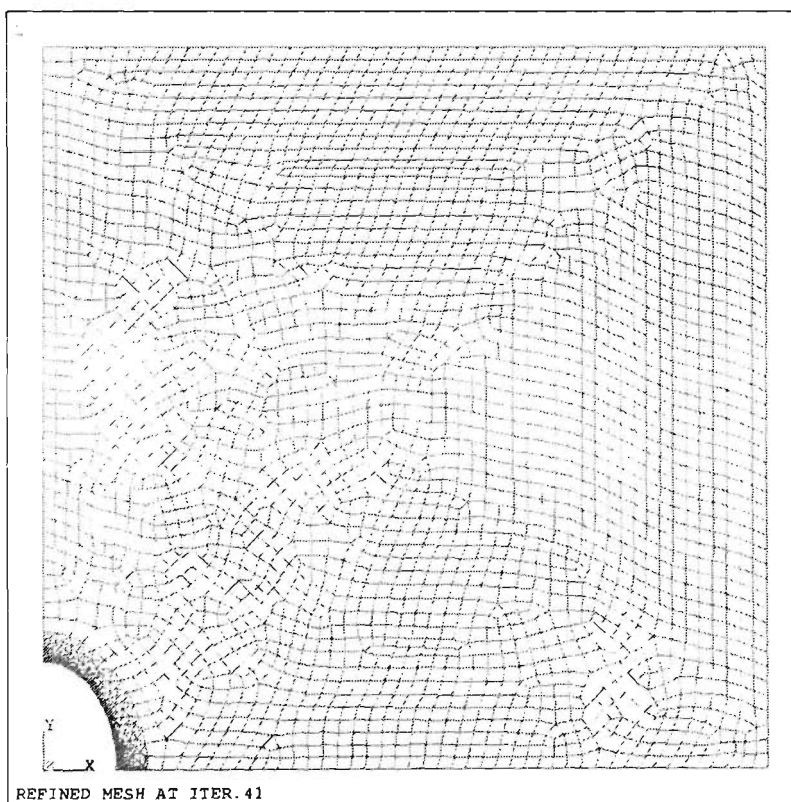
**Table B.3: Case  $S_r$  of 1.5 for composite laminates**

FEM model	esize (mm)	No. of elements	Max. Tsai-Wu index	SEPC (%)
Algorithm produced	0.3	1771	0.78613	nil
Mesh refined	0.3	3475	0.78612	nil



ANSYS 5.3  
 NOV 27 1996  
 20:32:29  
 PLOT NO. 1  
 ELEMENTS  
 TYPE NUM  
  
 ZV =1  
 DIST=.0825  
 XF =.075  
 YF =.075

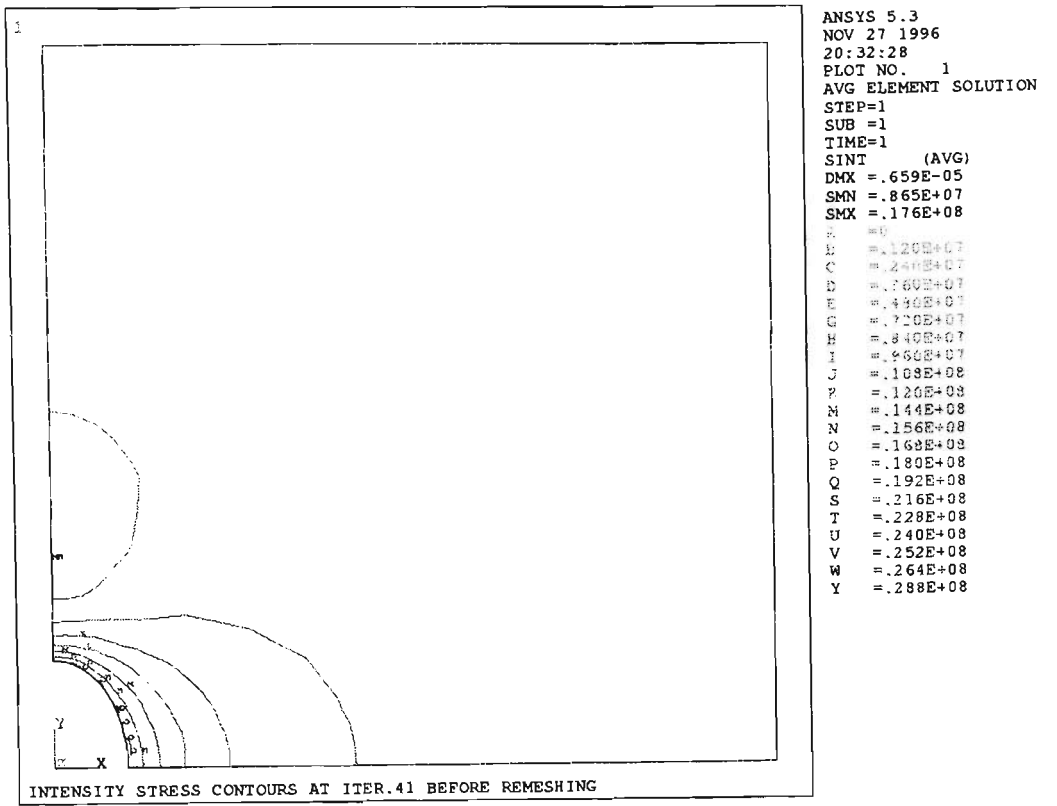
(a)



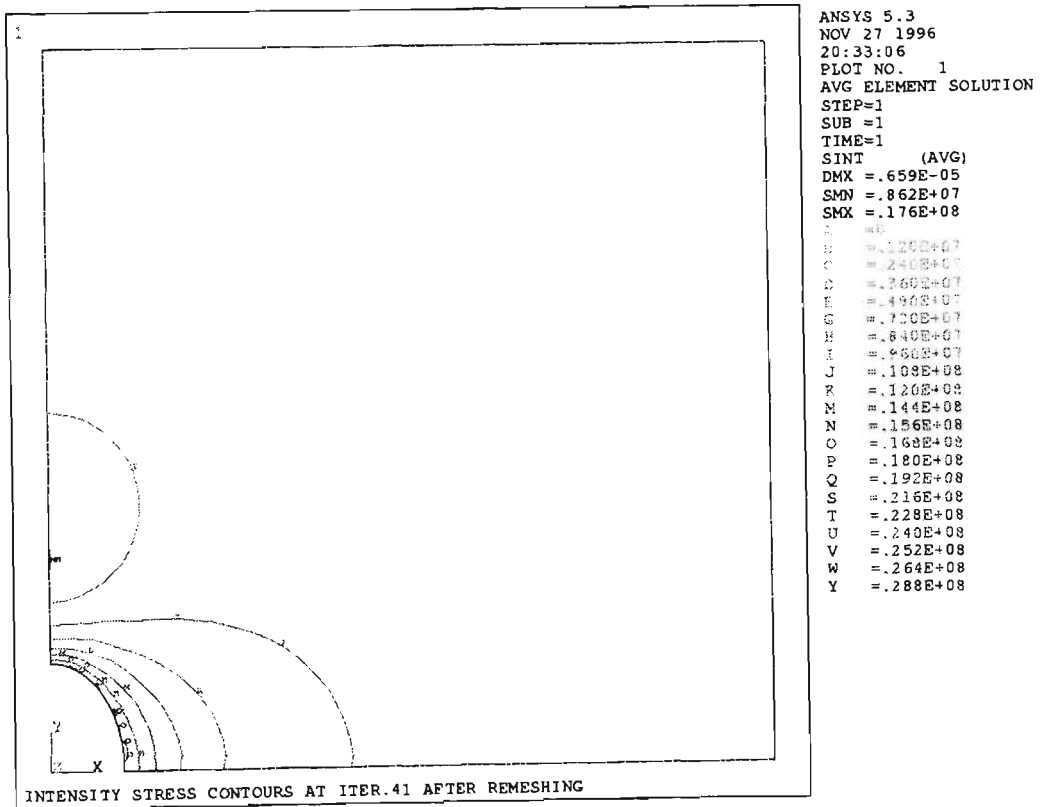
ANSYS 5.3  
 NOV 27 1996  
 20:32:40  
 PLOT NO. 1  
 ELEMENTS  
 TYPE NUM  
  
 ZV =1  
 DIST=.0825  
 XF =.075  
 YF =.075

(b)

**Figure B.1:** (a) FEM mesh produced by the optimization program;  
 (b) FEM mesh after mesh refinement.

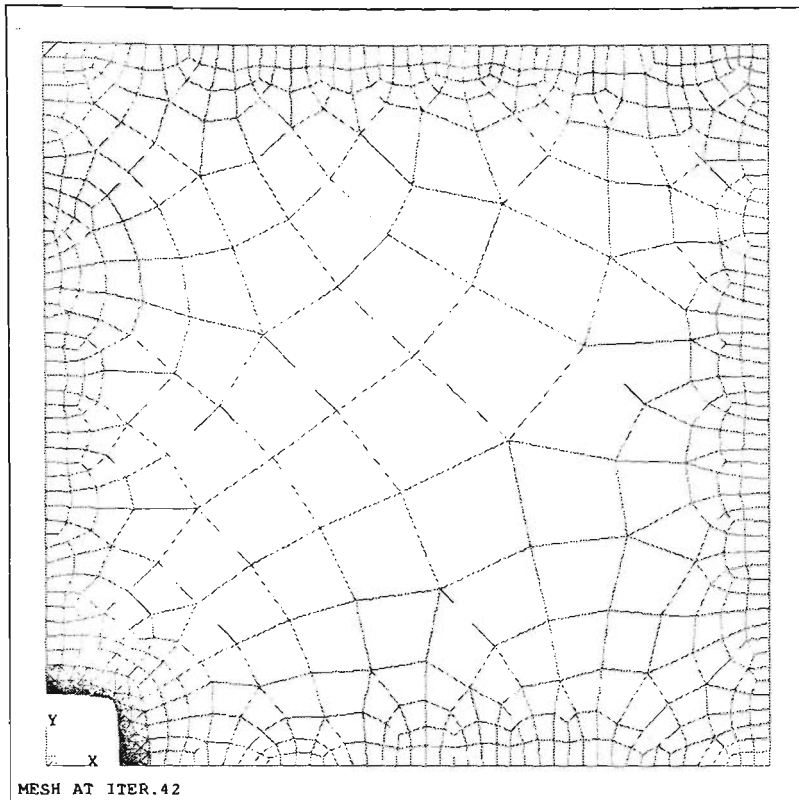


(a)



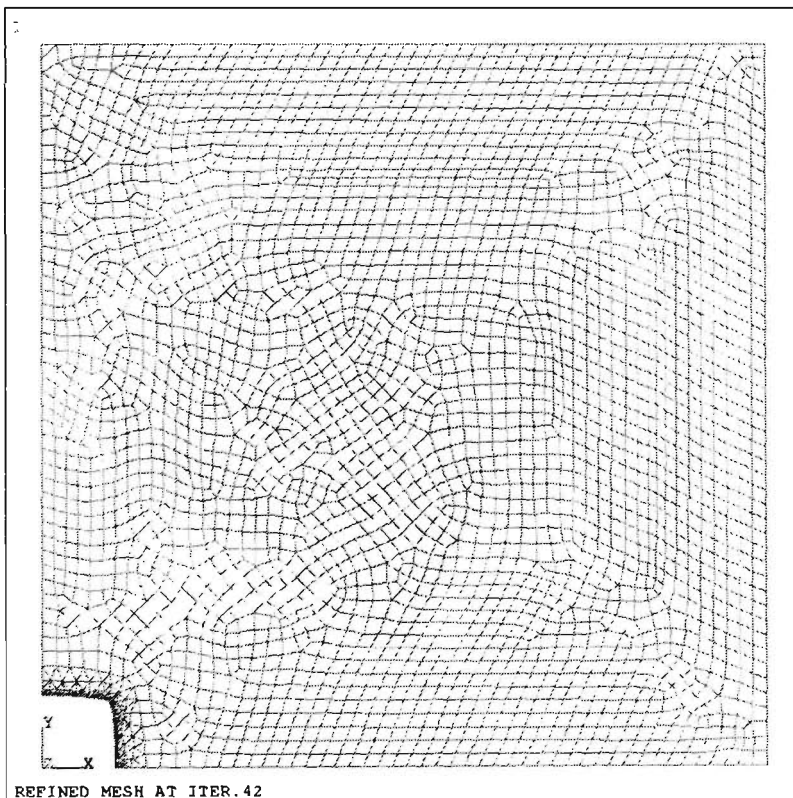
(b)

Figure B.2: (a) Optimal Tresca stress distribution before mesh refinement;  
 (b) Optimal Tresca stress distribution after mesh refinement.



ANSYS 5.3  
NOV 27 1996  
18:28:36  
PLOT NO. 1  
ELEMENTS  
TYPE NUM  
ZV =1  
DIST=.0825  
XF =.075  
YF =.075

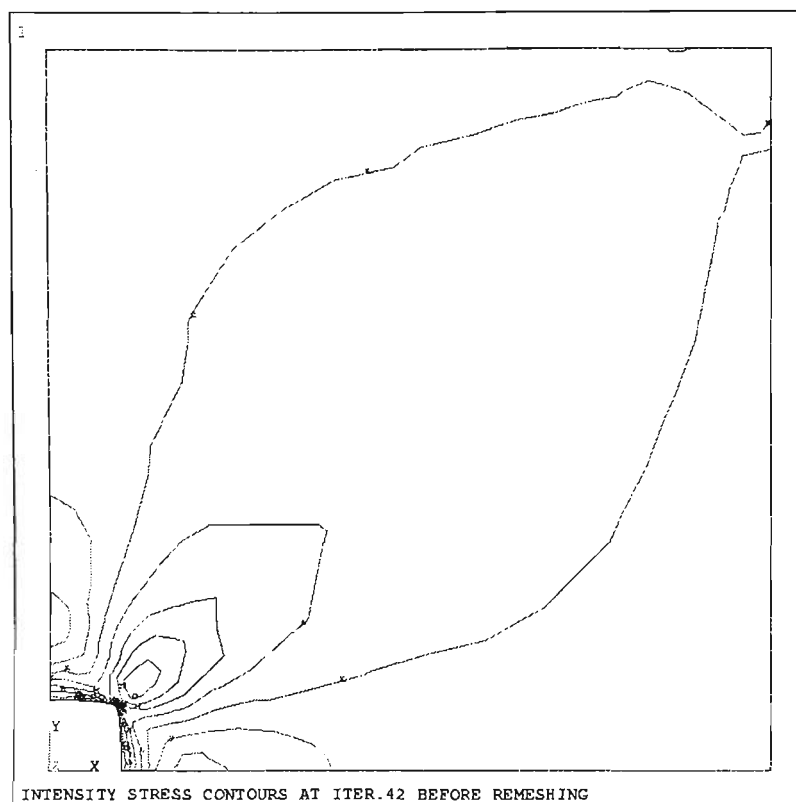
(a)



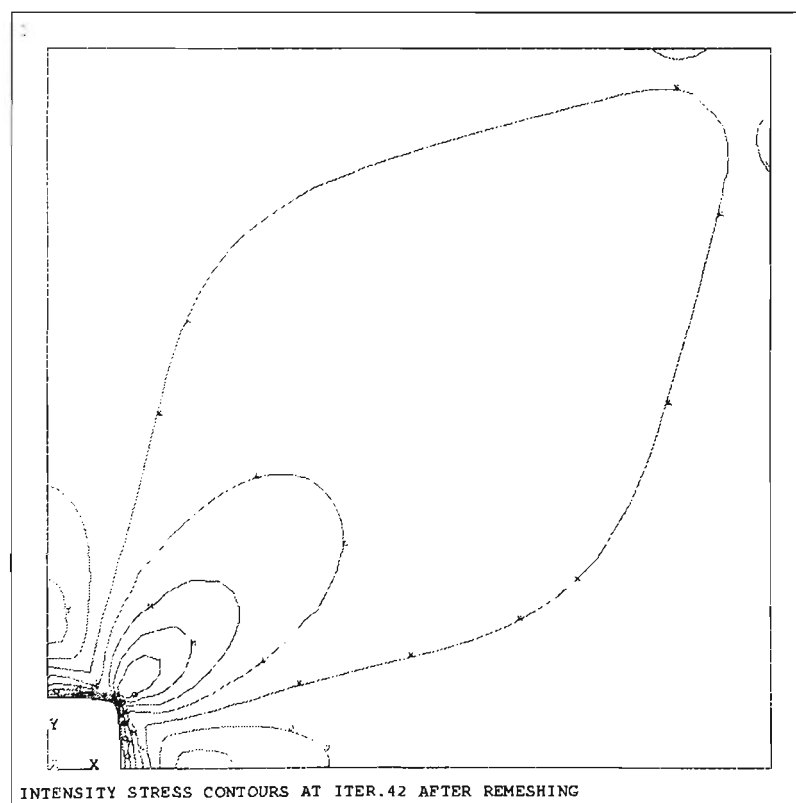
ANSYS 5.3  
NOV 27 1996  
18:28:49  
PLOT NO. 1  
ELEMENTS  
TYPE NUM  
ZV =1  
DIST=.0825  
XF =.075  
YF =.075

(b)

Figure B.3: (a) FEM mesh produced by the optimization program;  
(b) FEM mesh after mesh refinement.

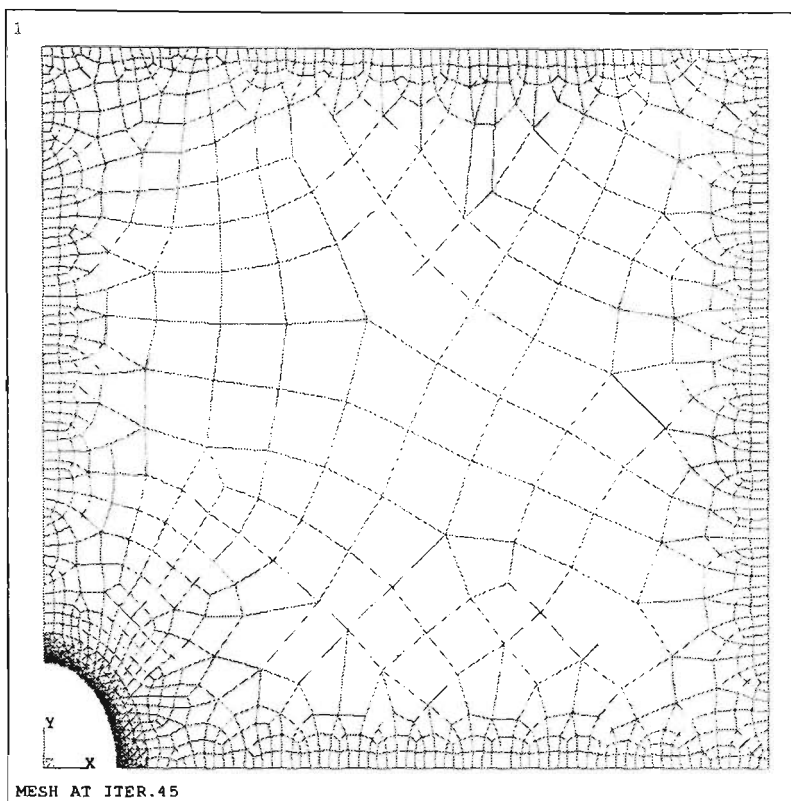


(a)



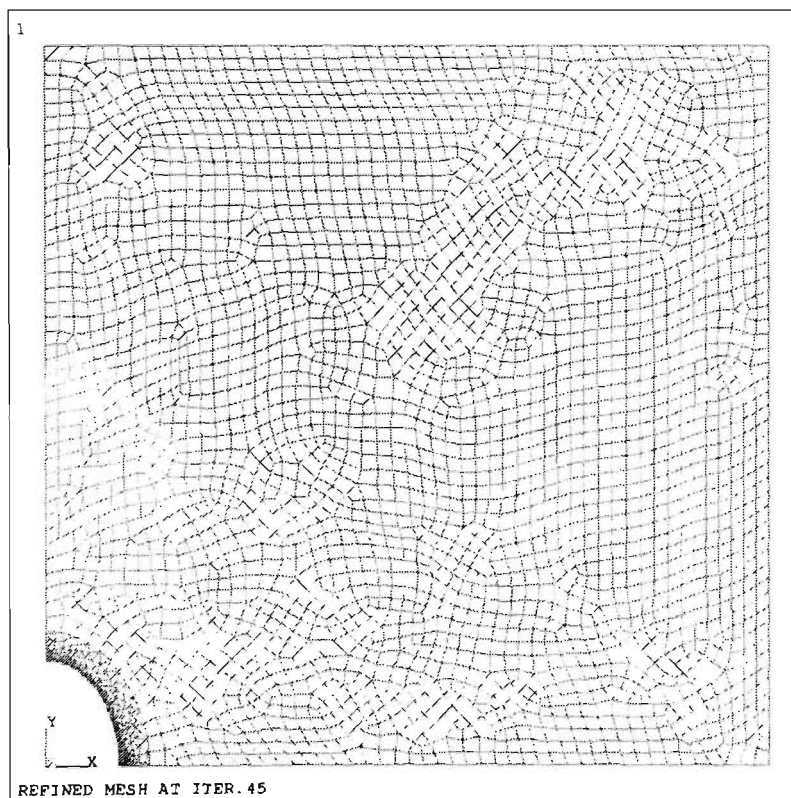
(b)

Figure B.4: (a) Optimal Tresca stress distribution before mesh refinement;  
 (b) Optimal Tresca stress distribution after mesh refinement.



ANSYS 5.3  
 NOV 27 1996  
 21:11:21  
 PLOT NO. 1  
 ELEMENTS  
 TYPE NUM  
  
 ZV =1  
 DIST=.0825  
 XF =.075  
 YF =.075

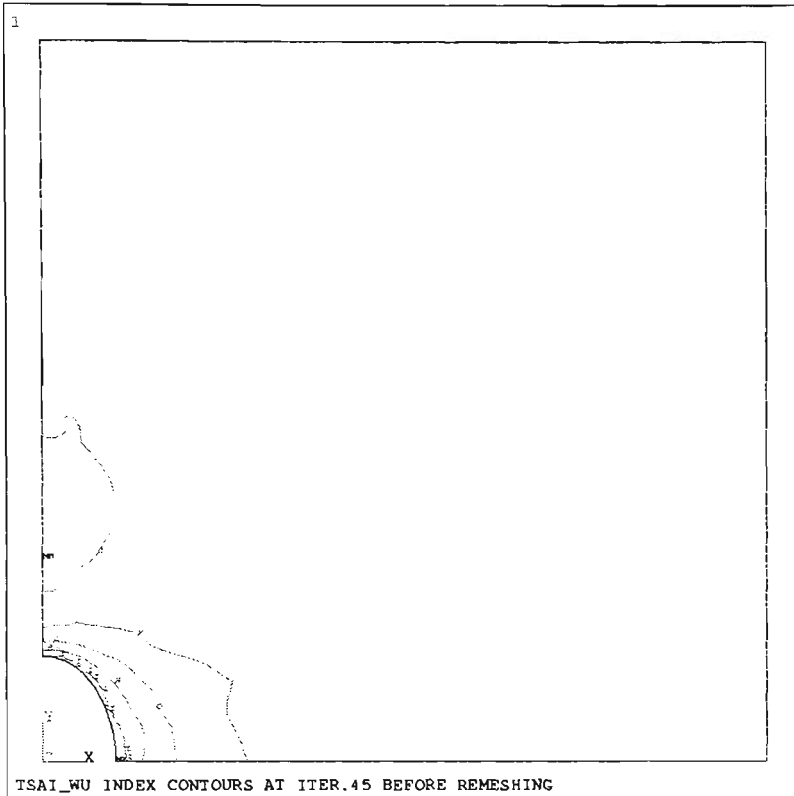
(a)



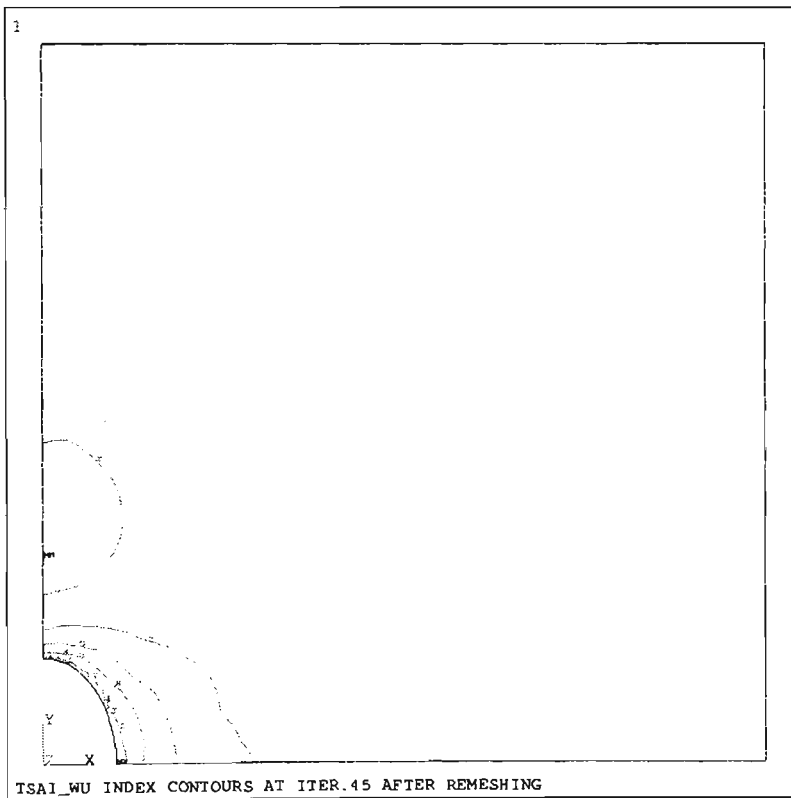
ANSYS 5.3  
 NOV 27 1996  
 21:18:56  
 PLOT NO. 1  
 ELEMENTS  
 TYPE NUM  
  
 ZV =1  
 DIST=.0825  
 XF =.075  
 YF =.075

(b)

Figure B.5: (a) FEM mesh produced by the optimization program;  
 (b) FEM mesh after mesh refinement.



(a)



(b)

Figure B.6: (a) Optimal Tsai-Wu index distribution before mesh refinement;  
 (b) Optimal Tsai-Wu index distribution after mesh refinement.